

Fracture of Anisotropic Rock

E. Hoek

South African Council for Scientific and Industrial Research

Journal of the South African Institute of Mining and Metallurgy
Volume 64, Pages 501-518, No. 10, May 1964

Introduction

Due to their disposition, most rocks of sedimentary origin which occur in the upper layers of the earth's crust exhibit some degree of anisotropy when subjected to stress. Since the deformation and fracture of these rocks is of importance to engineers concerned with the design of shallow mining excavations or of foundations for civil engineering structures, it is obvious that research into the effects of anisotropy on rock behaviour is necessary.

Most of the published research on anisotropic rock is of an experimental nature^{1, 2, 3} and in this paper an attempt is made to formulate a theoretical explanation for the observed fracture behaviour. This theoretical approach is based upon Griffith's postulate that fracture initiates from existing cracks and flaws inherent in any brittle material^{4, 5, 6}. In the case of an anisotropic rock, these cracks are assumed to be oriented preferentially along bedding planes. The effect of anisotropy on the deformation and stress distribution prior to fracture is not considered in this paper.

Results of triaxial strength tests on a South African slate are in good agreement with the theoretical predictions.

Griffith's theory of brittle fracture

The currently accepted interpretation of Griffith's theory of brittle fracture^{4, 5} is that fracture initiates when the molecular cohesive strength of the material is exceeded by the tensile stresses at the tips of inherent cracks and flaws in the material^{6, 7}. If it is assumed that these cracks and flaws are elliptical in shape, then the results presented by Inglis⁸ can be used to calculate the stresses induced around the boundary of these very flat elliptical cracks.

The stress system acting upon an elliptical crack is illustrated Figure 1. The ellipse and the surrounding stress field are related to the elliptical coordinates η and ε which are defined by the following equations of transformation of a rectangular system of coordinates x and z :

$$\begin{aligned}x &= c \sinh \varepsilon \sin \eta, \\z &= c \cosh \varepsilon \cos \eta\end{aligned}$$

The stress system acting on the crack is given by two normal components σ_{xx} and σ_{zz} and a shear component τ_{xz} . The stress σ_{zz} , which acts parallel to the major axis of the crack, has a negligible influence upon the stresses induced near the crack tip and need not be considered in the following analysis. The stresses σ_{xx} and τ_{xz} are related to the principal stresses σ_1 and σ_3 by the following equations:

$$2\sigma_{xx} = (\sigma_1 + \sigma_3) - (\sigma_1 - \sigma_3)\cos 2\psi \quad (1)$$

$$2\tau_{xz} = (\sigma_1 - \sigma_3)\sin 2\psi \quad (2)$$

Where ψ is the angle between the major axis of the elliptical crack and the direction of the major principal stress σ_1 . Note that σ_1 is defined as the algebraically largest and σ_3 the algebraically smallest of the three principal stresses. The sign convention used in this paper is such that *compressive* stresses are taken as *positive*.

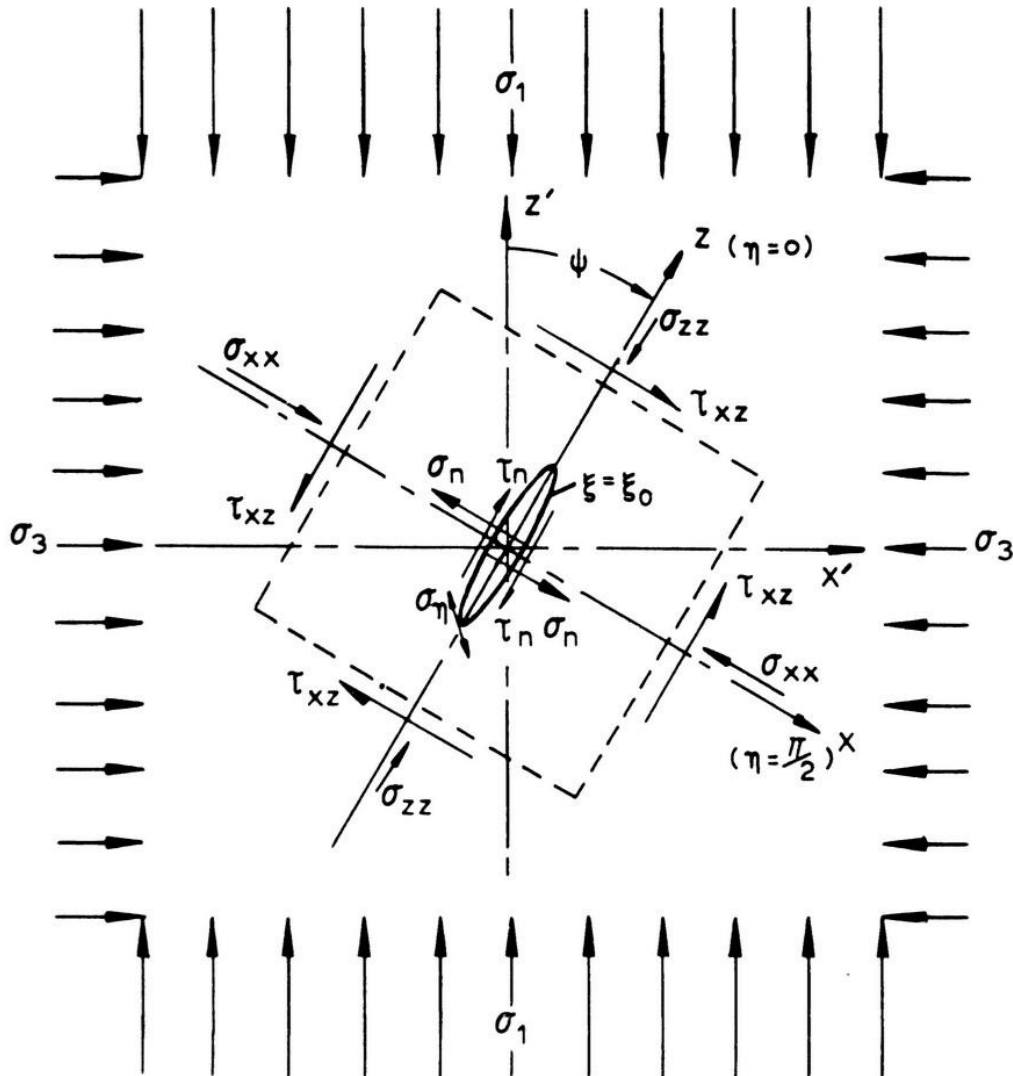


Figure 1. Stresses acting upon a crack which is inclined at an angle ψ to the direction of the major principal stress σ_1

The stresses σ_n and τ_n which act on the surface of the crack as shown in Figure 1 exist only when closure of the crack has occurred and their influence is considered in a later section of this paper which deals with the effects of crack closure.

The tangential stress σ_n at the boundary of an open elliptical crack, due to the applied stresses σ_{xx} and τ_{xz} , neglecting σ_{zz} is given by the following equation ⁸:

$$\sigma_\eta = \frac{\sigma_{xx}(\sinh 2\xi_0 + e^2 \xi_0 \cdot \cos 2\eta - 1) + 2\tau_{xz} \cdot e^2 \xi_0 \cdot \sin 2\eta}{\cosh 2\xi_0 - \cos 2\eta} \quad (3)$$

Where ξ_0 is the value of the elliptical coordinate ξ on the crack boundary.

The maximum tangential stresses, both tensile and compressive, occur near the ends of the crack, i.e. when the value of η is small. Since the value of ξ_0 is also small for a very flat ellipse, equation (3) may be simplified by series expansion in which terms of the second order and higher which appear in the numerator are neglected. This simplification results in the following equation, valid only for the stresses near the crack tip:

$$\sigma_\eta = 2 \left\{ \frac{\sigma_{xx} \cdot \xi_0 + \tau_{xz} \cdot \eta}{\xi_0^2 + \eta^2} \right\} \quad (4)$$

Differentiation of equation (4) with respect to η and equating $\partial\sigma_\eta/\partial\eta$ to zero results in a quadratic equation in η from which the positions on the crack boundary at which the maximum and minimum stresses occur can be determined. Substituting these values of η into equation (4) gives the maximum and minimum stresses on the crack boundary as

$$\sigma_N \cdot \xi_0 = \sigma_{xx} \pm \sqrt{\sigma_{xx}^2 + \tau_{xz}^2} \quad (5)$$

Where σ_N is the maximum value of σ_η .

Expressing equation (5) in terms of the principal stresses σ_1 and σ_3 from equations (1) and (2) gives

$$\sigma_N \cdot \xi_0 = \frac{1}{2} [(\sigma_1 + \sigma_3) - (\sigma_1 - \sigma_3) \cos 2\psi] \pm \sqrt{\frac{1}{2} [(\sigma_1^2 + \sigma_3^2) - (\sigma_1^2 - \sigma_3^2) \cos 2\psi]} \quad (6)$$

The critical crack orientation ψ_c at which the maximum and minimum stresses are induced at or near the crack tip is found by differentiating equation (6) with respect to ψ and letting $\partial\sigma_\eta/\partial\psi = 0$. This gives

$$\cos 2\psi_c = \frac{\sigma_1 - \sigma_3}{2(\sigma_1 + \sigma_3)} = \frac{1 - k}{2(1 + k)} \quad (7)$$

Where $k = \sigma_3/\sigma_1$.

Note that equation (7) is only meaningful if $k \geq -0.33$. When $k = -0.33$ then $\cos 2\psi_c = 1$. Substituting this value into equation (6) gives

$$\sigma_c \cdot \xi_0 = 2\sigma_3 \quad (8)$$

Where σ_c is the maximum value of the tangential stress σ_η at the critical crack orientation ψ_c .

In other words, for $k \leq -0.33$ the maximum tensile stress at the crack tip depends upon the magnitude of the minor principal stress σ_3 only and, since this stress is tensile because k is negative, fracture occurs when the minor principal stress attains the uniaxial tensile strength of the material. Since the strength of a material cannot be lower than its uniaxial tensile strength, the fracture condition expressed in equation (8) holds for the entire range $-\infty < k \leq -0.33$. The critical crack orientation ψ_c remains unchanged at zero ($\cos 2\psi_c = 1$).

Denoting the uniaxial tensile strength of the material by σ_t , equation (8) can be re-written as

$$\sigma_c \cdot \xi_0 = 2\sigma_t \quad (9)$$

The term $\sigma_c \cdot \xi_0$ which appears in equations (8) and (9) is a product of the cohesive strength σ_c of the material and the parameter ξ_0 which defines the shape of the crack. Both of these parameters are difficult to evaluate under practical conditions but equation (9) offers the opportunity of determining their product fairly readily.

Substituting equation (9) into equation (6) gives the following relationship between the stresses required to initiate fracture from a crack inclined at the angle ψ to the direction of σ_1 and the uniaxial tensile strength of the material.

$$2\sigma_t = \frac{1}{2} [(\sigma_1 + \sigma_3) - (\sigma_1 - \sigma_3) \cos 2\psi] \pm \sqrt{\frac{1}{2} \left[(\sigma_1^2 + \sigma_3^2) - (\sigma_1^2 - \sigma_3^2) \cos 2\psi \right]} \quad (10)$$

In the case of a homogeneous, isotropic material, it is normally assumed that the inherent cracks are randomly distributed throughout the specimen and that fracture will initiate from those cracks which are inclined at the angle ψ_c defined by equation (7).

Substituting equation (7) into equation (10) results in the following fracture criterion for such a material:

$$\sigma_1 = \frac{-8\sigma_t(1+k)}{(1-k)^2} \quad (11)$$

In the case of an anisotropic material where the weakest cracks are assumed to lie in the bedding planes, it is necessary to consider the orientation of these cracks in relation to the applied stress system in order to determine the fracture conditions. In this case, the fracture criterion is expressed by equation (10) where ψ is the orientation of the weakest cracks to the direction of the major principal stress σ_1 . A graphical representation of this equation is given in Figure 2.

Modified fracture criterion for closed cracks

In deriving the fracture criterion outlined above, it has been assumed that the shape of the crack does not change until fracture occurs. In other words, the elliptical crack remains open under all conditions of applied stress. While this may be true for predominantly tensile stress fields, it certainly does not hold for the case of very flat cracks which are subjected to compressive stress. Consequently, it is necessary to consider the effects of crack closure upon the Griffith's fracture criterion.

In the following analysis, based upon the modification to Griffith's theory by McClintock and Walsh⁹, it is assumed that the initial crack in an unstressed body is uniformly closed over its entire length. If the normal stress σ_{xx} is tensile, the crack opens and the Griffith's criterion holds. If the normal stress σ_{xx} is compressive (positive) then a stress $\sigma_n = \sigma_{xx}$ results from the reaction between the crack surfaces. Under these conditions, the stress σ_{xx} is transmitted across the crack without influencing the stresses induced at the crack tips and, hence, it plays no direct part in the fracture process.

In addition, however, a frictional shear resistance τ_n occurs parallel to the crack as a result of the contact pressure between the crack surfaces. Denoting the coefficient of friction between these surfaces by μ ;

$$\tau_n = \mu\sigma_n = \mu\sigma_{xx} \quad (12)$$

The shear stress τ_{xz} can only induce tensile stresses at the crack tip when this frictional resistance has been overcome and when relative movement between the crack surfaces can occur. Consequently, the net shear stress which is effective in inducing tensile stresses at the crack boundary is $\tau_{xz} - \tau_n$ or $\tau_{xz} - \mu\sigma_{xx}$.

From Equation (4), the tangential stress σ_η on the boundary of a closed crack due to the net shear stress $\tau_{xz} - \mu\sigma_{xx}$ is

$$\sigma_\eta = \frac{2\eta(\tau_{xz} - \mu\sigma_{xx})}{\xi_0^2 + \eta^2} \quad (13)$$

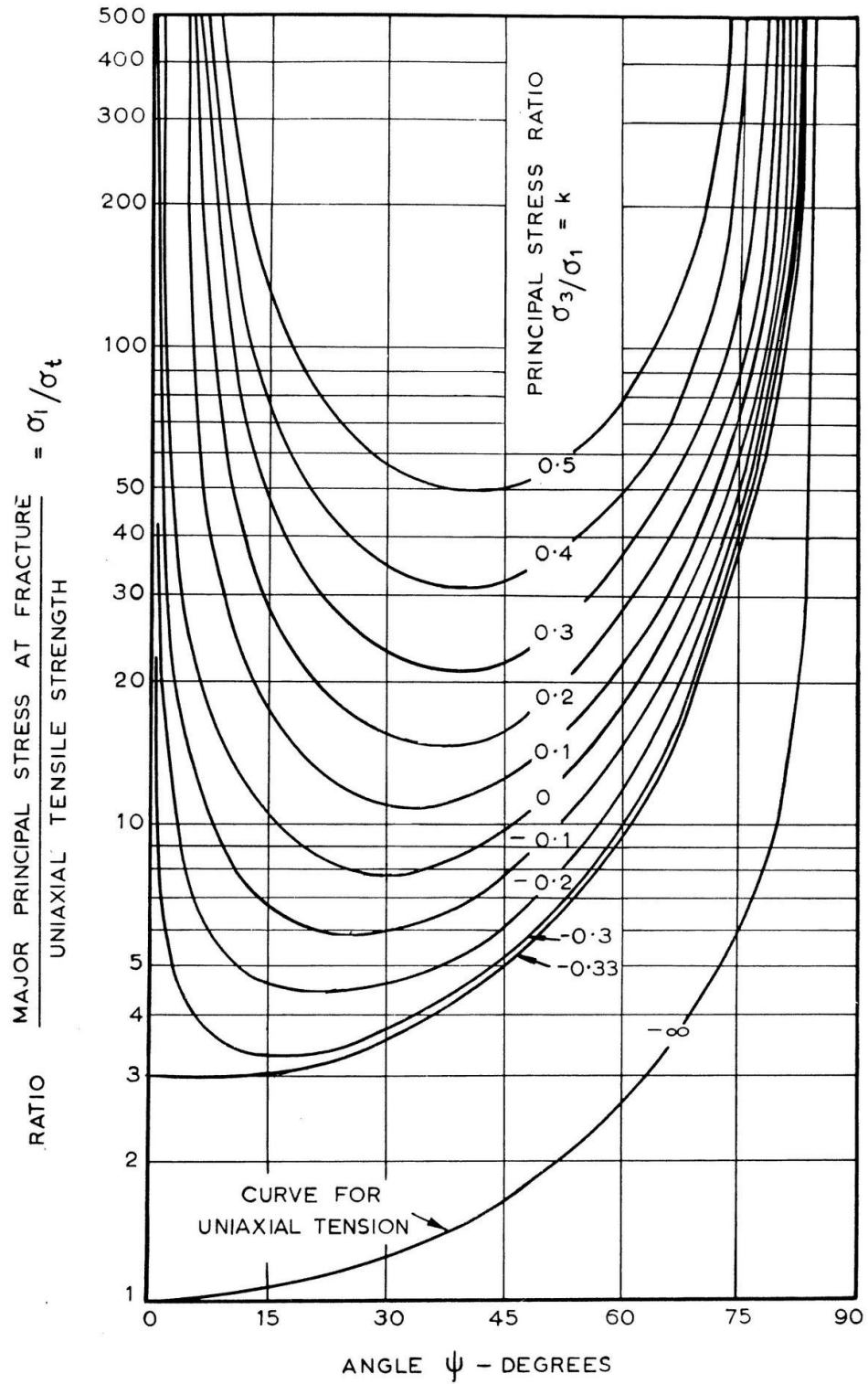


Figure 2. Fracture initiation from a single open Griffith crack inclined at an angle ψ to the major principal stress σ_1 .

Differentiating equation (13) with respect to η and equating $\partial\sigma_\eta/\partial\eta$ to zero gives the position on the crack boundary at which the maximum and minimum stresses occur as $\eta = \pm\xi_0$. Substituting these values into equation (13) gives the maximum and minimum tangential stresses on the crack boundary as

$$\sigma_N \cdot \xi_0 = \pm(\tau_{xz} - \mu\sigma_{xx}) \quad (14)$$

Since crack propagation occurs as a result of tensile stress, only the negative value given by this equation need be considered.

Expressing equation (14) in terms of the principal stresses and the uniaxial tensile strength of the material:

$$2\sigma_t = -\frac{1}{2}\{(\sigma_1 - \sigma_3)\sin 2\psi - \mu[(\sigma_1 - \sigma_3) - (\sigma_1 - \sigma_3)\cos 2\psi]\} \quad (15)$$

Differentiating equation (15) with respect to ψ and equating $\partial\sigma_N/\partial\psi$ to zero gives the critical crack orientation at which the highest tensile stresses are induced at the tip of a closed crack as

$$\tan 2\psi_c = \frac{1}{\mu} \quad (16)$$

Substituting this critical crack orientation into equation (15) gives the fracture criterion for a material in which the highest tensile stresses are induced at the tip of a closed crack as

$$\sigma_1 = \frac{-4\sigma_t}{(1-k)\sqrt{1+\mu^2} - \mu(1+k)} \quad (17)$$

Where k is the principal stress ratio σ_3/σ_1 .

As in the case of the original Griffith criterion, it is generally assumed that the specimen contains a sufficient number of randomly oriented cracks for fracture to initiate from those cracks which are inclined at an angle defined by equation (16). If, however, the cracks are oriented preferentially as in the case of a highly anisotropic material, it is necessary to consider the inclination of the cracks with respect to the applied stress system. In this case the conditions for fracture are determined from equation (15).

In using the modified criterion outlined above, it must be remembered that equations (15) and (17) apply only when the normal stress σ_{xx} is compressive. When σ_{xx} is tensile the original Griffith theory must be applied. A detailed discussion on the transition from the

original to the modified fracture criteria has been given by the author in a previous paper⁶.

Mohr envelopes for original and modified Griffith Theories

Murrell¹⁰ has shown that the original Griffith theory can be represented by a Mohr fracture envelope which is defined by the following equation:

$$\tau^2 = 4\sigma_t(\sigma_t - \sigma) \quad (18)$$

Brace¹¹ has shown that the fracture criterion, modified to account for the effects of crack closure in compression, can be represented by a limiting Mohr envelope which is a straight line having the equation

$$\tau = \mu\sigma - 2\sigma_t \quad (19)$$

Fracture criterion for anisotropic rock

Brace¹² has presented evidence which indicates that the cracks, from which the fracture of rock propagates, probably lie within the grain boundaries of the material. Even in rocks of sedimentary origin which exhibit marked foliation and planar anisotropy, the constituent lamellae are made up of grains which are cemented together and hence randomly oriented grain boundary cracks are likely to be present.

In the case of an anisotropic rock, two distinct systems of inherent cracks can be visualized:

- a) A set of relatively large preferentially oriented cracks which lie along bedding planes and which may sometimes be in the form of mica flakes;
- b) A randomly oriented matrix of grain boundary cracks which are probably several times smaller than the bedding plane cracks.

In the following analysis, the preferentially oriented bedding plane cracks will be referred to as the *primary* crack system while the grain boundary cracks will be termed *secondary* cracks.

In deciding upon the stress required to cause fracture of a particular specimen, it is necessary to consider the inclination of the primary cracks to the applied stress system and to determine whether the tensile stresses induced at the tips of these primary cracks are higher than those which occur at the tips of the most favourably oriented secondary cracks. If the primary cracks are oriented at an angle approaching the critical angle ψ_c , defined by equation (7) or (16), then fracture will generally initiate at the tips of these cracks. If, on the other hand, the primary cracks are parallel or perpendicular to the

direction of the major principal stress σ_1 , then the tensile stresses induced at the tips of these cracks will be relatively low and very high applied stresses will be necessary to initiate fracture from these cracks (see Figure 2). In this case, fracture will initiate at the tips of the most favourably oriented secondary cracks.

Obviously, the transition from fracture initiation from primary cracks to the propagation of secondary cracks depends upon the physical characteristics of the material, particularly upon the relative crack lengths (ξ_0) and upon whether either or both of the crack systems close under compressive stress (μ). These details are best illustrated by means of a practical example.

A study of the fracture of a South African slate

In order to illustrate the application of the theoretical considerations proposed in this paper and to check their validity, a series of strength determination was carried out on a sample of slate obtained from the Pretoria area. These tests included uniaxial tensile tests parallel to and perpendicular to the bedding planes as well as triaxial compression tests on samples in which the bedding plane orientation was varied, in steps of 15° , from $\psi = 0^\circ$ to $\psi = 90^\circ$.

Details of the test procedures used by the National mechanical Engineering Research institute for determining the strength of rock materials have not been published previously and a brief description of these techniques is included as an appendix to this paper.

Results of the tests on the slate material are given in Table I. Note that, wherever possible, two specimens were tested for each applied stress condition.

The uniaxial tensile strength of the material perpendicular to the bedding planes can be assumed to be predominantly influenced by the primary crack system (bedding plane cracks). Consequently, this value of tensile strength is denoted by σ_{tp} . The tensile strength parallel to the bedding planes will not be influenced by the primary cracks and fracture can be assumed to initiate at secondary cracks, hence this value of tensile strength is denoted by σ_{ts} .

In order that the results of these tests may readily be compared with the theoretical predications (see Figure 2 for example), the strength values are reduced to dimensionless form by dividing each by the uniaxial tensile strength perpendicular to bedding planes σ_{tp} .

Table 1. Fracture data for a South African slate

1. Uniaxial tensile tests

- a) Tensile strength perpendicular to bedding planes ($\psi = 0^\circ$), $\sigma_{tp} = 660$ and 570 lb/sq.in., average 615 lb/sq.in.
- b) Tensile strength parallel to bedding planes ($\psi = 90^\circ$), $\sigma_{ts} = 2,780$ and 3,000 lb/sq.in., average 2,880 lb/sq.in.

2) Triaxial compression tests

$k = \sigma_3/\sigma_1$	$k = 0$ (uniaxial)		$k = 0.113$		$k = 0.171$	
ψ	σ_1 lb/sq.in.	σ_1/σ_{tp}	σ_1 lb/sq.in.	σ_1/σ_{tp}	σ_1 lb/sq.in.	σ_1/σ_{tp}
0	17,600	28.6	39,200	63.7	55,700	90.8
	21,600	35.2	36,000	59.5	49,300	80.0
15	6,900	11.2	18,300	29.8	34,200	55.6
	8,700	14.2	30,000	48.0	39,000	63.4
30	4,500	7.3	7,300	11.8	8,730	14.2
	4,150	6.8	--	--	7,840	12.8
45	5,540	9.0	13,900	22.6	15,000	24.4
	6,560	10.7	11,000	17.9	16,300	26.7
60	11,850	19.3	24,600	40.0	29,600	48.2
	11,600	18.8	19,400	31.6	32,400	52.6
75	16,000	26.0	31,200	50.7	41,400	67.2
	16,600	27.0	31,900	52.0	42,900	69.7
90	15,600	25.3	30,600	49.8	41,700	68.0
	16,100	26.2	--	--	39,300	64.0

From the results presented in Table 1, the behaviour of the primary and secondary crack systems of the slate can be approximated.

In the case of the primary cracks, the compressive fracture behaviour of the specimen will be most strongly influenced by these cracks when they are oriented at between 30° and 35° if the cracks remain open (equation (7)). If the cracks close under compression, they will exert their strongest influence when inclined at an angle defined by equation (16).

Examination of the experimental results reveals that the compressive strength of the slate is lowest when the bedding planes are inclined at approximately 30° to the direction of the major principal stress. Consequently, it can be concluded that the cracks have either remained open or that, if they have closed, the coefficient of internal friction μ has a value of approximately 0.6.

In an attempt to establish which of these two possibilities is most likely, a Mohr fracture diagram for the primary crack system was plotted and is illustrated in Figure 3. In plotting the Mohr circles, the tensile strength used is that obtained from tests perpendicular to the bedding planes. The Mohr circles for uniaxial and triaxial compressive values are taken as those given for tests in which the bedding planes were inclined at 30° to the direction of the major principal stress.

On the basis of the limited number of test results available, the indications are that the primary cracks have remained open and that the original Griffith fracture criterion can be applied to them. However, caution must be exercised in drawing definite conclusions from so few results and, in the following analysis, both possibilities outlined above will be explored.

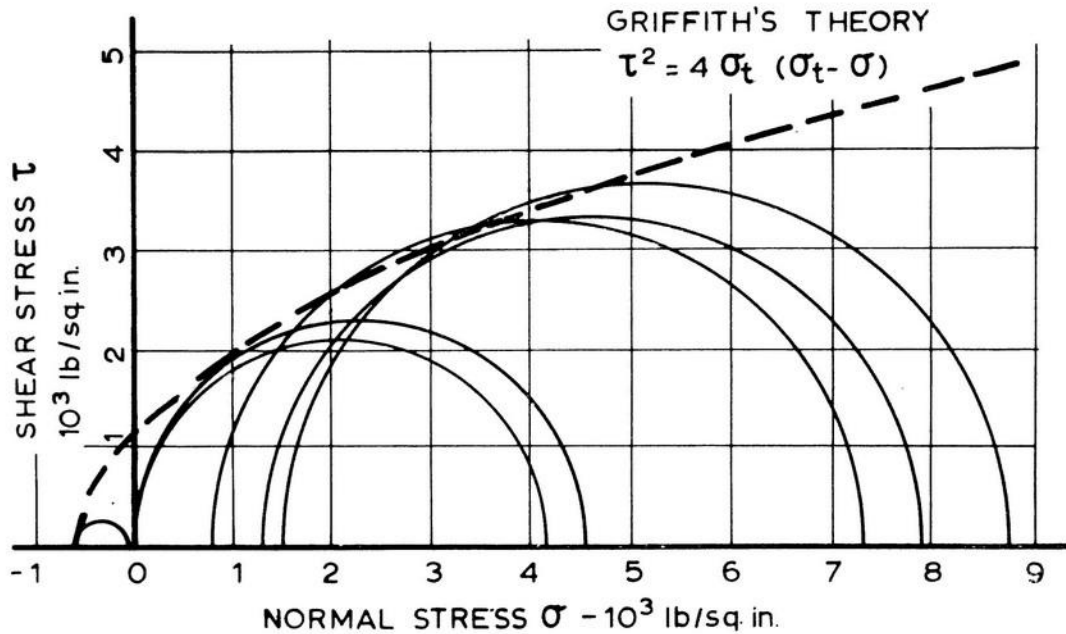


Figure 3. Mohr fracture diagram for primary crack system of slate

Behaviour of the secondary crack system is fairly clearly defined by the Mohr fracture diagram presented in Figure 4. In this case, it can be anticipated that the cracks will be initially closed and it will be seen that the modified Griffith fracture criterion offers a reasonably good prediction of the observed behaviour. In plotting the Mohr diagram illustrated in Figure 4, the tensile strength parallel to the bedding planes (σ_{ts}) has been used. Compressive fracture data for specimens tested at $\psi = 0^\circ$ and $\psi = 90^\circ$ are included since these values should not be influenced by the primary cracks.

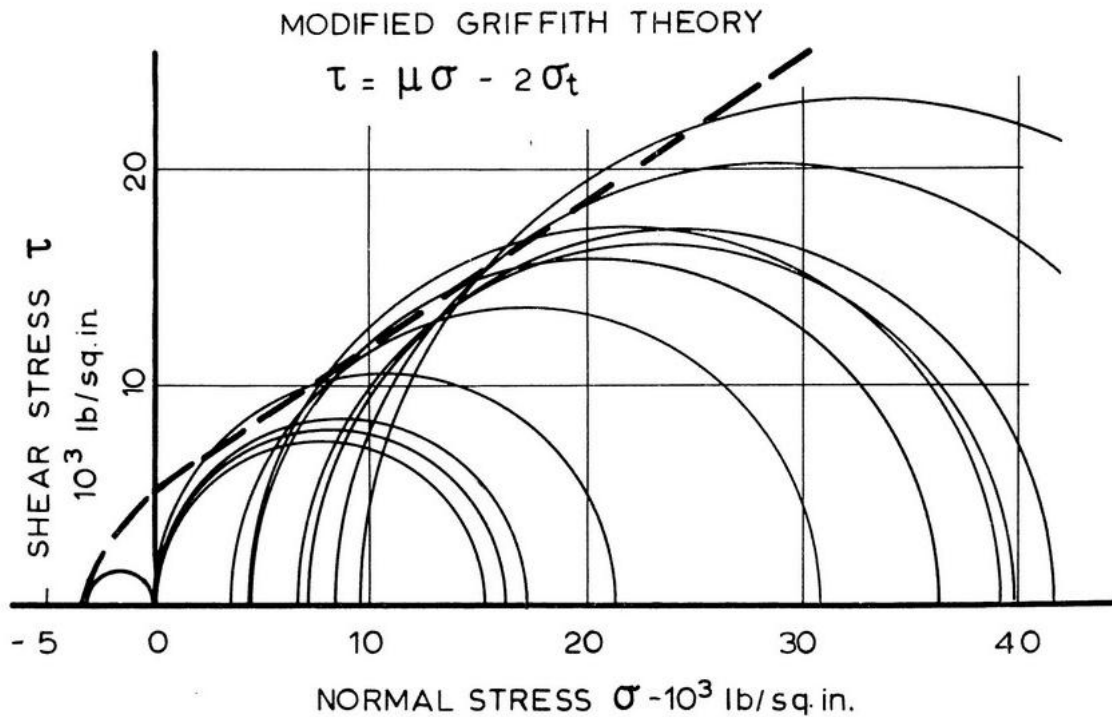


Figure 4. Mohr fracture diagram for secondary crack system of slate

The influence of the bedding plane orientation upon the uniaxial compressive strength and upon the strength of the slate, when subjected to triaxial stress conditions in which the principal stress ratio $k = 0.171$, is illustrated in Figures 5 and 6. In these graphs, the experimental results are compared with the behaviour predicted by both the original Griffith theory and by the modified fracture criterion.

The dipping portions of the theoretical curves are obtained by solving equation (10) for the original Griffith theory and equation (15) for the modified fracture theory. In both cases σ_t is taken as $\sigma_{tp} = 615$ lb/sq.in. The value of the coefficient of internal friction μ substituted into equation (15) is 0.6 as deduced above.

The straight line portions of the theoretical curves are obtained from equation (17), substituting $\sigma_t = \sigma_{ts} = 4.7\sigma_{tp}$. The coefficient of internal friction used in this case was determined from the slope of the Mohr envelope presented in Figure 4 and was found to be 0.61.

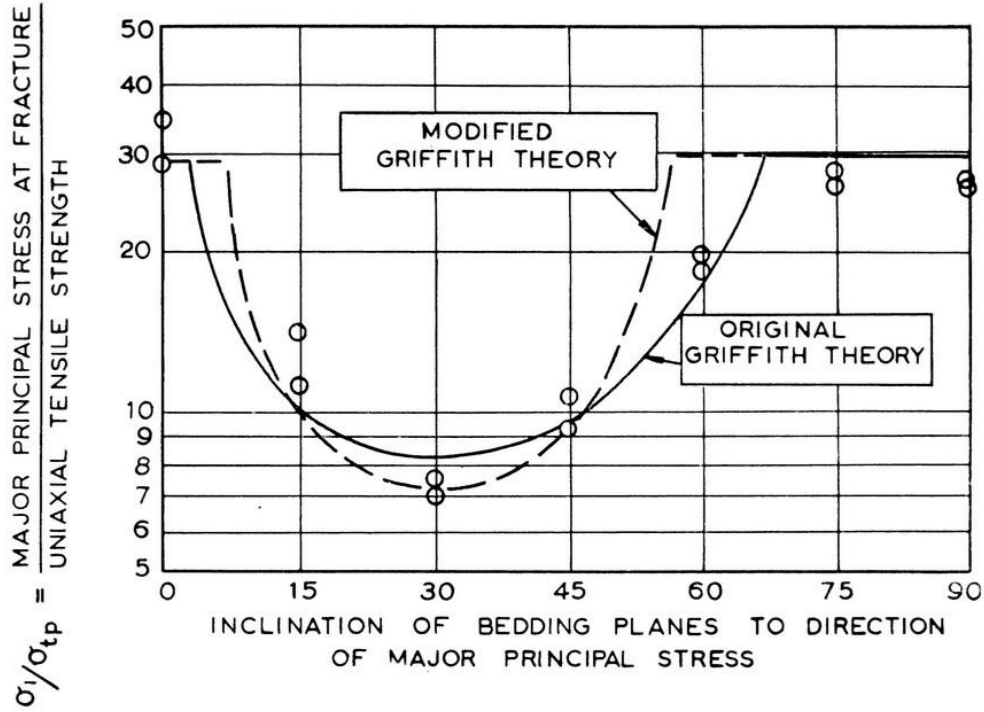


Figure 5. Influence of bedding plane orientation on the uniaxial compressive strength of South African slate

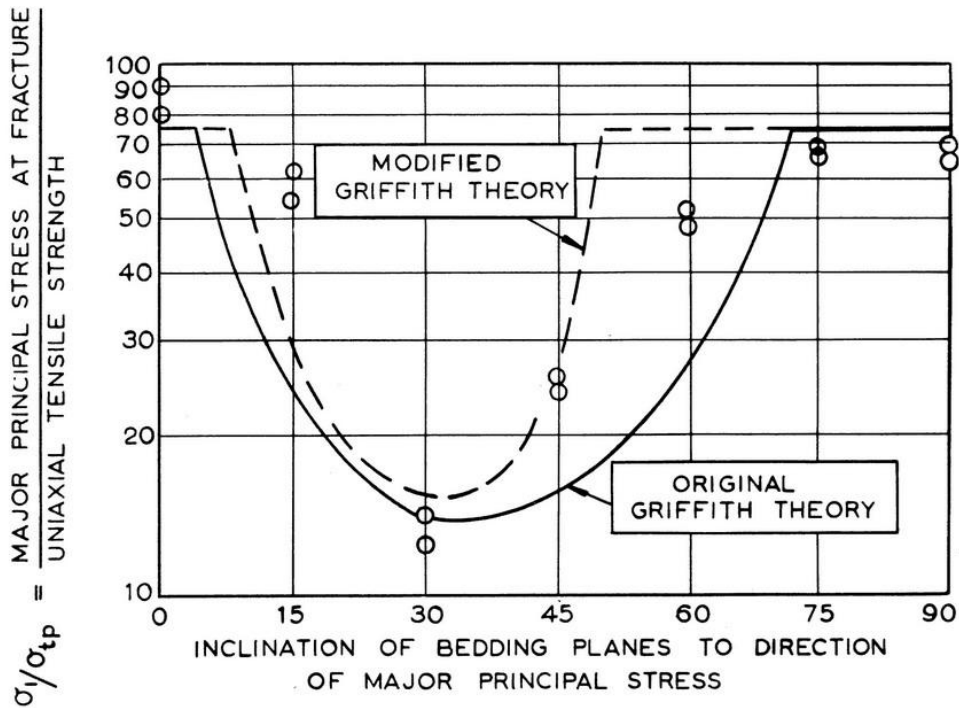


Figure 6. Influence of bedding plane orientation on triaxial compressive strength ($K = 0.171$) of South African slate

Discussion of results

The primary purpose of attempting to formulate a theoretical fracture criterion such as that outlined in this paper is to facilitate the interpretation and rationalisation of experimental results. Unless such a fundamental theory exists, the results presented in Table 1 are merely an interesting example of material behaviour which applies to this particular sample of slate only. If, however, the experimental results can be compared with and are found to substantiate the theoretical predictions, then they become part of a rational behaviour pattern which can be extended to cover other materials.

Note that equations (10), (15) and (17), which have been used to predict the theoretical fracture behaviour of this sample of slate, depend only upon two material constants, namely the uniaxial tensile strength and the coefficient of internal friction. If these equations are found to be generally applicable to materials of this type, a reliable prediction of their fracture behaviour could be made on the basis of a few simple physical tests.

In spite of the approximations which have been made in deriving this theory the agreement between the predicted and observed fracture behaviour of slate is encouraging. Results of similar tests on Martinsburg slate from Pennsylvania in the United States of America have been presented by Donath^{1, 2}. Although the results have been presented in a form which makes a complete analysis difficult, a number of approximate checks have indicated that Donath's results would also be in good agreement with the theory.

Considering the present empirical nature of the science of rock mechanics, the accuracy of prediction offered by these theoretical considerations is adequate for most practical purposes. It is believed that more detailed experiments as well as more sophisticated mathematical treatment could be used to refine the existing theory, if and when an improvement in accuracy becomes necessary.

Although the present theory is based upon the assumption that only two distinct crack systems are present in an anisotropic material, it is obvious that these arguments can be extended to the case where two or more major crack systems are superimposed upon the randomly distributed grain boundary cracks. Such an extension would probably prove useful in the analysis of fracture of coal where cleats as well as bedding planes are present.

An important conclusion which can be drawn from the results presented in this paper is that compression tests parallel to and perpendicular to the bedding planes are not sufficient to define the fracture behaviour of an anisotropic material. There is a tendency to conclude that a material is isotropic with respect to strength if its compressive strength perpendicular and parallel to the bedding planes is the same. Examination of Figures 5 and 6 reveals that this deduction can be grossly in error.

The simplest test for strength isotropy is to compare the uniaxial tensile strength parallel to and perpendicular to the bedding planes. Failing this, a compression test in which the

bedding planes are included at approximately 30° to the major principal stress direction should be included in the test programme.

The author wishes to avail himself of this opportunity to emphasize the importance of choosing the correct specimen geometry and test conditions for strength determination of rock materials. If the calculated stress at fracture requires anything more than a simple division of applied load by cross-sectional area, the results of strength tests will probably be unreliable. This is particularly true of an anisotropic material where not only the strength but also the stress distribution in the specimen are markedly influenced by anisotropy.

As an example of an uncertainty involved in indirect strength tests, the case of the uniaxial tensile strength of the specimen of slate discussed in this paper is quoted.

Direct tensile tests on carefully designed and prepared specimens (see Appendix) gave the tensile strength perpendicular to the bedding planes as 615 lb/sq.in. and that parallel to the bedding planes as 2,880 lb/sq.in..

Indirect tests in which a tensile stress is induced in the centre of a disc subjected to diametral compression³ gave values of 438 lb/sq.in. perpendicular to the bedding planes and 1,310 lb/sq.in. in parallel to the bedding planes.

Correct specimen design is equally important for compression specimens and the same laws apply whether the specimen being tested is a single rock grain or a block of rock of 10 ft cube. Only if the stress conditions in the specimen are accurately known can the results be interpreted with any degree of certainty.

Conclusions

It has been shown that Griffith's theory of brittle fracture, modified where necessary to account for the effects of crack closure in compression, can be used to predict the fracture behaviour of a material such as slate which exhibits a high degree of planar anisotropy.

It is suggested that this theory could be extended to the case of a material such as coal which may have several major weakness planes oriented at various angles to each other.

While the accuracy of the present theory is regarded as adequate for most practical purposes, it is believed that, if necessary, refinements to this theory are possible.

As a result of this study, it is concluded that special care should be exercised in planning strength tests on anisotropic material. It is particularly important that deductions should not be made unless adequate experimental data is available.

Acknowledgements

The author wishes to express his appreciation to the owners of the Elliot Slate Quarries in Pretoria for supplying the sample of slate used in these tests, to Mr. J.B. Kennard for his careful preparation of the specimens and to Mr. U.W.O.L. Vogler and Mr. H.K. van der Merwe for carrying out the tests.

The permission of the South African Council for Scientific and Industrial Research to publish the material contained in this paper is acknowledged.

Appendix – Equipment and experimental techniques used for the determination of strength of rock materials

Experimental verification of the theoretical postulates contained in this and in a previous paper⁶, necessitates the loading of specimens of rock to fracture under various accurately known and controlled stress conditions. This appendix contains a brief description of the triaxial test apparatus, designed by the author and used by the Rock Mechanics division of the National Mechanical Engineering Research Institute for compressive tests on rock material. Details of the specimens used for the determination of tensile strength are also given.

Triaxial test apparatus

The triaxial test apparatus, illustrated diagrammatically in Figure 7, is designed to apply a constant ratio of lateral hydraulic pressure to axial stress in the specimen. This is achieved by loading the specimen in series with a piston and cylinder unit which generates the hydraulic pressure.

If the diameters of the loading piston, specimen and pressure piston are denoted by D_L , D_S and D_p respectively, then the lateral stress σ_3 , which is equal to the hydraulic pressure acting on the specimen, is given by

$$\sigma_3 = \frac{4L}{\pi D_p^2} \quad (1A)$$

Where L is the total load applied to the loading and pressure pistons.

The axial stress σ_1 in the specimen is given by the following equation

$$\sigma_1 = \frac{4L}{\pi D_S^2} \left\{ 1 - \frac{D_L^2 - D_S^2}{D_p^2} \right\} \quad (2A)$$

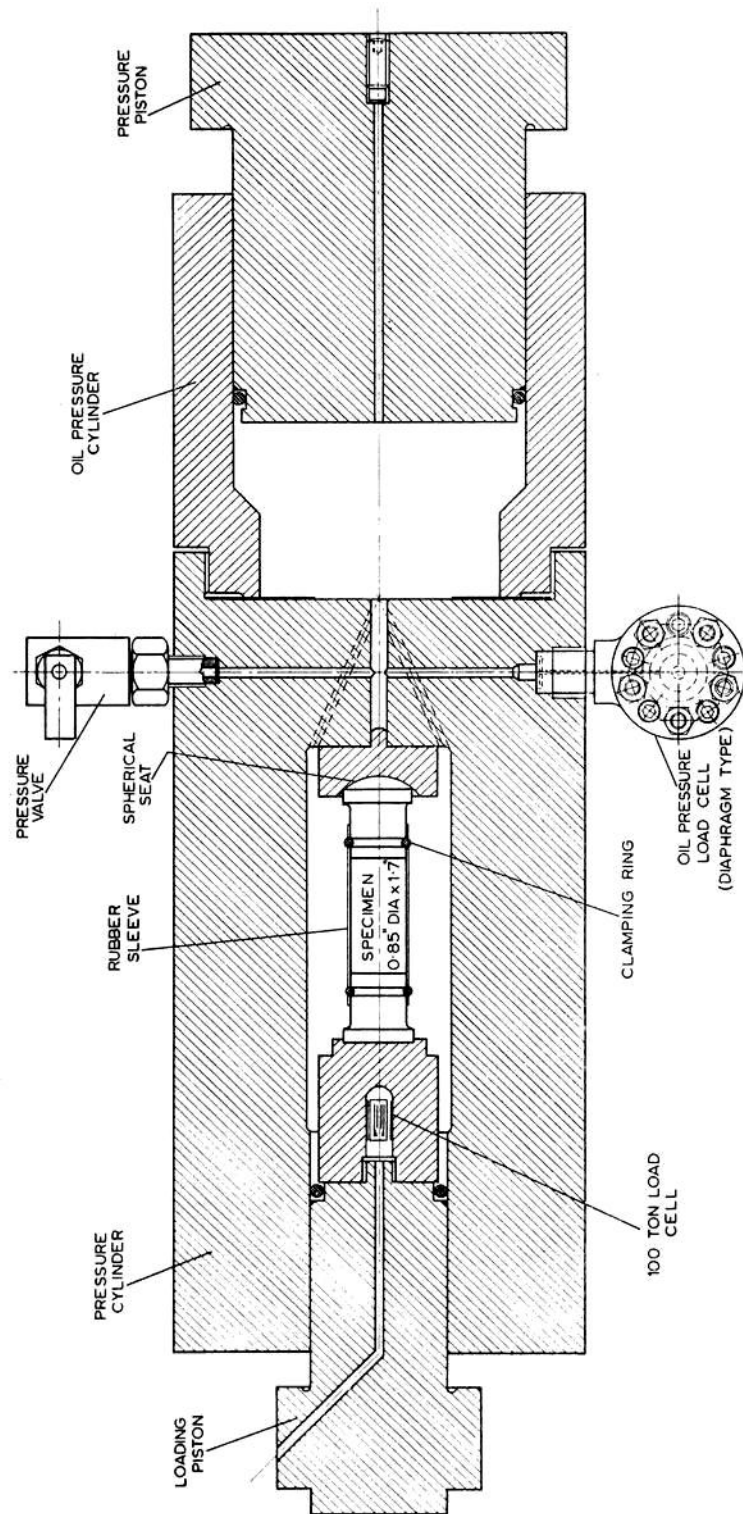


Figure 7. Triaxial test apparatus

The apparatus, illustrated in Figure 7, for testing EX core specimens (0.85 in. diameter) has been designed for applying axial stresses (σ_1) of up to 350,000 lb/in.² and lateral stresses (σ_3) of up to 35,000 lb/in.². The ratio of σ_3/σ_1 , which is chosen for any particular test depends upon the diameter of the pressure piston D_p which is used.

Changes in the stress ratio σ_3/σ_1 are achieved by replacing the entire oil pressure cylinder and piston unit with another of a different diameter. Sealing between the oil pressure cylinder and the body of the test cell is achieved by a method which was originally suggested to the author by Professor G.T. van Rooyen at Pretoria University. The principal features of this method are illustrated in Figure 8.

The oil pressure cylinder is attached to the test cell body by means of a loosely fitting thread – designed to provide location and initial sealing only. A thin deformable gasket of the impregnated paper type is placed between the sealing faces and serves to compensate for any irregularities of these faces and to provide initial sealing.

Once the oil pressure is generated by the application of load, the thread load is relieved and the gasket is acted upon by a force which is directly proportional to the oil pressure. Since the area A of the sealing face is smaller than the area B of the step in the cylinder wall, the sealing pressure on the gasket is always greater than the pressure of the oil trying to escape and hence the device is self-sealing.

The moving seals on the loading and pressure pistons are a combination of neoprene rubber ‘O’-rings and brass anti-extrusion rings as illustrated in Figure 9. At the high pressures dealt with in this application, extrusion of the rubber rings into the clearance gap between piston and cylinder becomes a serious problem unless special steps are taken to prevent it. The provision of an anti-extrusion ring of the type illustrated ensures that there is virtual metal to metal contact between this ring and the cylinder wall and extrusion of the rubber is thereby prevented. The anti-extrusion ring is made from a softer metal than the cylinder to prevent scoring of the ground cylinder wall.

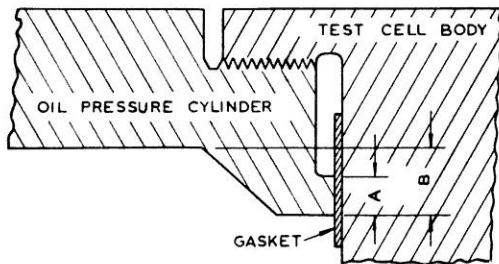


Figure 8. Detail of self-sealing joint between oil pressure and test cell body.

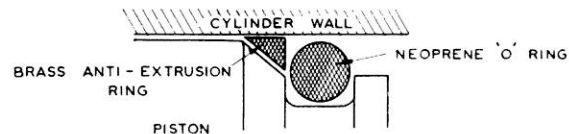


Figure 9. Detail of high pressure moving seal.

These sealing devices have proved to be completely reliable for the range of pressures generated in this apparatus. Measurements have shown that the frictional resistance due to the moving seals is very low – of the order of 1 per cent of the hydraulic pressure.

Although the neoprene rings and anti-extrusion rings are regarded as expendable items and can easily be replaced, it has not been found necessary to replace the original sealing units in spite of the fact that several hundred triaxial tests have already been completed.

The specimens used for the triaxial tests described in this paper consist of 1.7 in. length of standard EX diamond drill core (0.85 in. diameter). The ends of the specimen are ground flat and parallel but no additional grinding of the cylindrical surface is necessary. The specimen is loaded between hardened steel platens as illustrated in Figure 7. A spherical seat at the base of one of these platens eliminates bending in the specimen.

The specimen is sheathed in a thin rubber sleeve as illustrated and this effectively prevents ingress of the pressurized hydraulic fluid.

The load applied to the specimen is measured by means of a strain gauge type load cell which is loaded in series with the specimen. Provision is also made of measurement of the hydraulic pressure. The deformation of the specimen is measured by means of a linear potentiometer which measures the displacement between the loading piston and the test cell body.

During a test, the electrical outputs of the load cell (or pressure gauge) and the linear potentiometer are plotted automatically on an X-Y recorder. The resulting load-deformation graph is then converted to a stress-strain graph by applying experimentally determined calibration factors.

The triaxial test apparatus together with its loading frame and the X-Y recorder are shown in the photograph which is reproduced in Figure 10.

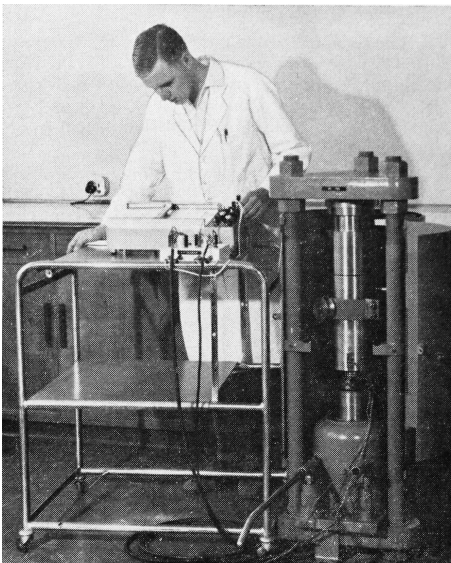


Figure 10. Triaxial compression test apparatus set up in a 100 ton loading frame.

Tensile test specimens

Tensile testing of rock materials is generally regarded as difficult because of the problem of gripping the specimen. After a great deal of unsuccessful effort had been devoted to devising methods for gripping specimens, the author came to the conclusion that, if the results of tensile tests are to have any meaning, correctly shaped tensile specimen are essential.

The shape of the tensile specimen which is used by the Rock Mechanics Division of the national mechanical Engineering Research institute is illustrated in Figure 11.

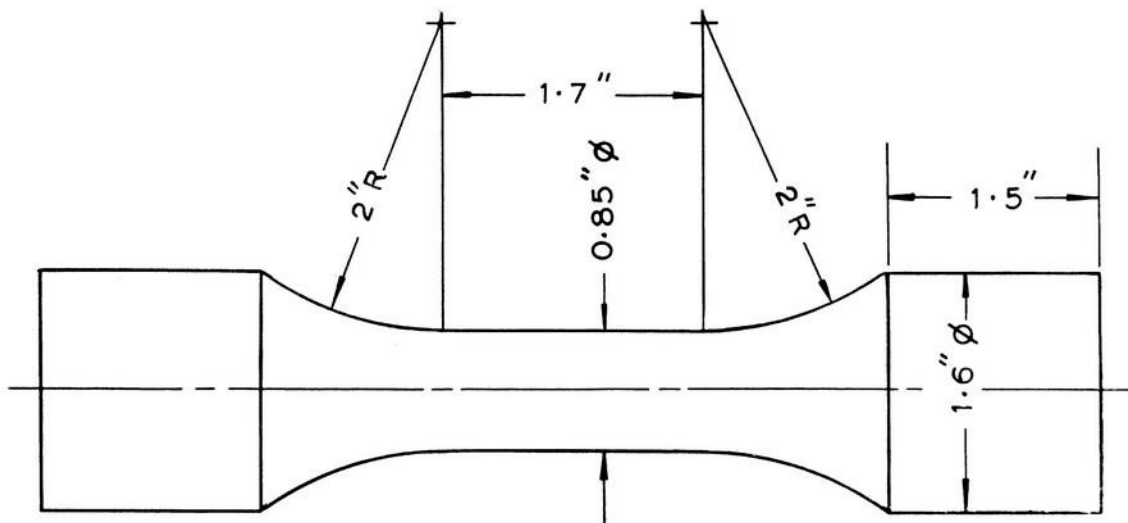


Figure 11. Detail of tensile specimen

Note that the actual 'test section' is 0.85 in. diameter by 1.7 in. long, in other words, it has the same dimensions as the compression specimen. The fillets forming the transition between the test section and the gripping section are designed to reduce the stress concentration at this transition to a minimum. The specimen is gripped by means of conventional wedge type grips and the tests which have been carried out on such specimens are regarded as completely successful.

The specimens are prepared by grinding with a high speed water-cooled diamond wheel. The grinding attachment is carried on the tool post of a lathe and the profile of the specimen is generated by a profile and follower device which is actuated by the lead screw of the lathe. This grinding attachment, illustrated in Figure 12, was designed by Mr. J. B. Kennard of the rock Mechanics Division of the National Mechanical Engineering Research Institute.

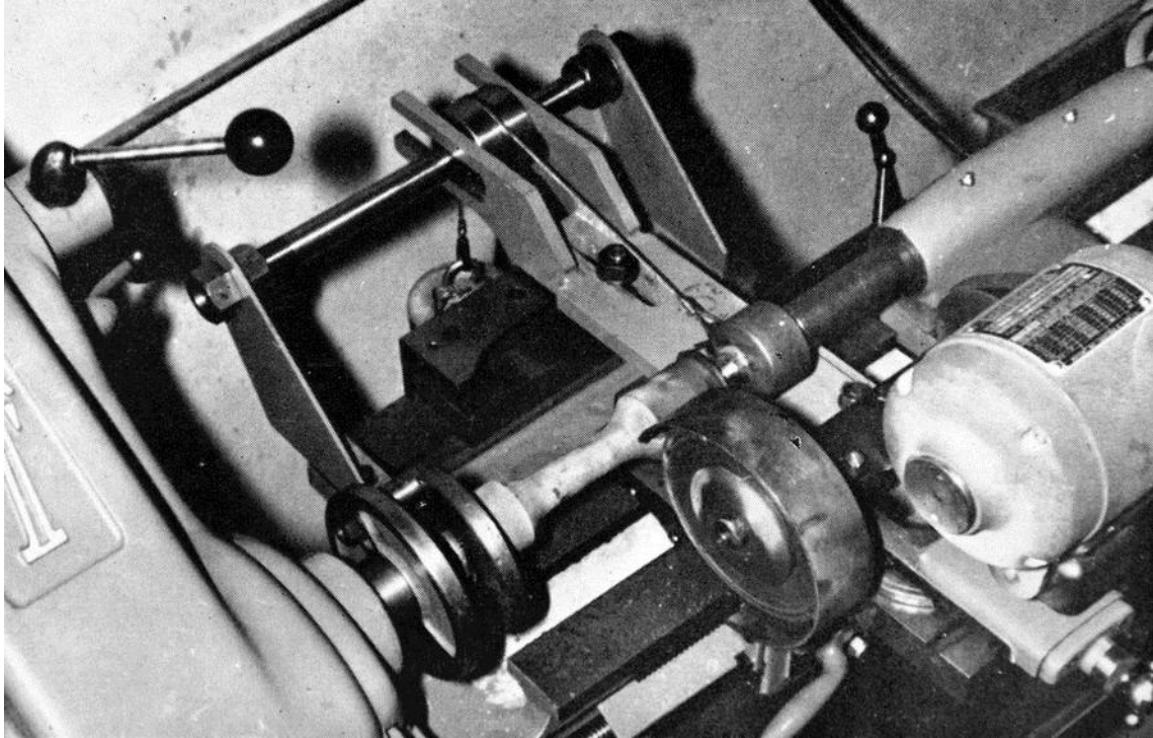


Figure 12. Grinding attachment for the preparation of tensile specimens of rock materials

References

1. Donath, F.A. (1961). "Experimental study of shear failure in anisotropic rocks." *Geophysical Society of America Bulletin*. Vol. 72, June, pp. 985-990.
2. Donath, F.A. (1963). "Strength variation and deformation behaviour of anisotropic rock." Preprints of papers. International Conference on the State of Stress in the Earth's crust, Santa Monica, June 1963. *The Rand Corporation Memorandum RM-3583*, pp. 5/1-9.
3. Berenbaum, R. and Brodie, I. (1958). Measurement of the tensile strength of coal: A critical assessment and the application of a new technique." *National Coal Board Scientific Department, Mining Research Establishment*, Report No. 2109, 1958.
4. Griffith, A.A. (1921). "The phenomena of rupture and flow in solids." *Philosophical Transactions of the Royal Society, London, A*. Vol. 221, pp. 163-197.
5. Griffith, A.A. (1924). "Theory of rupture." *Proceedings of the First International Congress for Applied Mechanics, Delft*,. J. Waltman Jr., 1255, pp. 55-63.

6. Hoek, E. (1963). "Rock fracture around mine excavations.: CSIR Rock Mechanics Special Report No. 38". To be presented to International Conference on Strata control and Rock Mechanics, New York, 1964.
7. Orowan, E. (1949). "Fracture and strength of solids." *Reports on Progress in Physics*, Vol. 12. The Physical Society, pp. 182-232..
8. Inglis, C.E. (1913). "Stresses in a plate due to the presence of cracks and sharp corners." *Institution of Naval Architects*, London, pp. 219-230.
9. McClintock, F.A. and Walsh, J.B. (1962). "Friction on Griffith cracks in rocks under pressure." *International Congress on Applied Mechanics*, Berkeley, in Press.
10. Murrell, S.A.F. (1958). "The strength of coal under triaxial compression." *Mechanical properties of non-metallic Brittle Materials, Butterworth Scientific Publications*, pp. 123-145.
11. Brace, W.F. (1960). "An extension of Griffith theory of fracture to rocks." *Journal of Geophysical Research*, Vol. 65, No. 10, pp. 3477-3480.
12. Brace, W.F. (1961). "Dependence of fracture strength of rocks on grain size." *Bulletin of Mineral Industries Experimental Station*. Penn. State University, No. 76, pp.99-103.

**Brittle Rock Fracture
Propagation in Rock Under
Compression**

E. Hoek and Z.T. Bieniawski
South African Council for Scientific and Industrial Research
Pretoria

International Journal of Fracture Mechanics
1(3), 137-155

1965

Brittle Rock Fracture Propagation in Rock Under Compression

E.Hoek and Z. T. Bieniawski

Members of the Rock Mechanics Division,

National Mechanical Engineering Research Institute,

South African Council for Scientific and Industrial Research, Pretoria.

Abstract

The results of studies of the initiation and propagation of fracture from a single Griffith crack in a biaxial compressive stress field are reported. It is concluded that Griffith's theory of brittle fracture offers a reliable prediction of the fracture initiation stress but that the resulting fracture propagation from a single crack cannot account for the macroscopic fracture of a specimen. Some preliminary results of studies on crack arrays and on the effects of crack closure in compression are presented. The applicability of these results to the prediction of rock fracture in predominantly compressive stress fields is discussed.

Introduction

One of the most serious problems encountered in deep-level gold mining in South Africa is the sudden and violent fracture of rock, known in the mining industry as a rockburst. Seismic location of the foci of these rock-bursts (Cook, 1963) has established that they occur most frequently in the zones of high compressive stress which surround the working faces of the mining excavations. Since the mining industry is constantly striving to minimize the hazards created by these rockbursts, an understanding of the mechanism of rock fracture under compressive stress conditions is of vital interest.

Previous research (Brace, 1964; Hoek, 1964) has shown that Griffith's brittle fracture theory (Griffith, 1924) modified to account for the effects of crack closure in compression (McClintock and Walsh, 1962), is a useful basis for the study of the fracture of hard rock. Brace (Brace, 1964), in discussing the nature of the pre-existing cracks in rock, suggests that the grain boundaries act as or contain micro-cracks while joints and faults can be regarded as macro-cracks.

An analysis of the stress distribution around a crack (Erdogan and Sih, 1963) indicates the points of fracture initiation as well as the initial direction of crack propagation. As a result of the change in stress distribution associated with fracture propagation it is, however, impossible to predict the final path of the propagating crack. Consequently, a serious limitation of the Griffith theory lies in the fact that it can only be used to predict fracture initiation. In its usual form, it yields no information on the rate or direction of fracture propagation.

In studying the fracture of brittle materials subjected to tension, fracture is normally expected in a direction perpendicular to the applied tension, in other words, in the plane of the critically oriented crack. In the case of a brittle material subjected to compressive stress, one might therefore expect that fracture propagation will also follow the direction of the most critically oriented crack, i.e. the one which is inclined at 20-30° to the major principal field stress direction. It will be shown in this paper that this anticipated result is incorrect and that there is no simple relationship between the critical orientation of the original "Griffith crack" and the orientation of the macroscopic fracture surface of a specimen.

Theoretical conditions for fracture initiation

Griffith's original postulate on fracture initiation was based on energy considerations and his equations contained a surface energy term (Griffith, 1924). Because of the difficulty of evaluating experimentally the surface energy of a material, an alternative approach, which considers the stress concentration at the crack tip, has been adopted by most workers in rock mechanics.

The current interpretation (Orowan, 1949) of Griffith's theory is that fracture initiates when tensile stress induced at or near the tip of an inherent crack exceeds the molecular cohesive strength of the material. Since the molecular cohesive strength is difficult to determine by direct measurement, the fracture criterion is expressed in terms of the uniaxial tensile strength of the material (Hoek, 1964).

In order that the reader may readily follow the equations which are used in this paper, a brief derivation of these equations, based upon the work by Griffith and McClintock and Walsh, follows.

It is assumed that the crack from which the fracture of a brittle rock originates can be regarded as a flat elliptical opening in a two-dimensional body which is subjected to a stress system¹ as illustrated in Figure 1.

The stress field around an elliptical opening is related to the elliptical coordinates ε and η which are defined by the following equations of transformation of a rectangular system of coordinates x and z :

$$\begin{aligned}x &= c \sinh \varepsilon \sin \eta \\y &= c \cosh \varepsilon \cos \eta\end{aligned}$$

¹ Because of the predominance of compressive stress in rock mechanics problems, compressive stress is taken as positive.

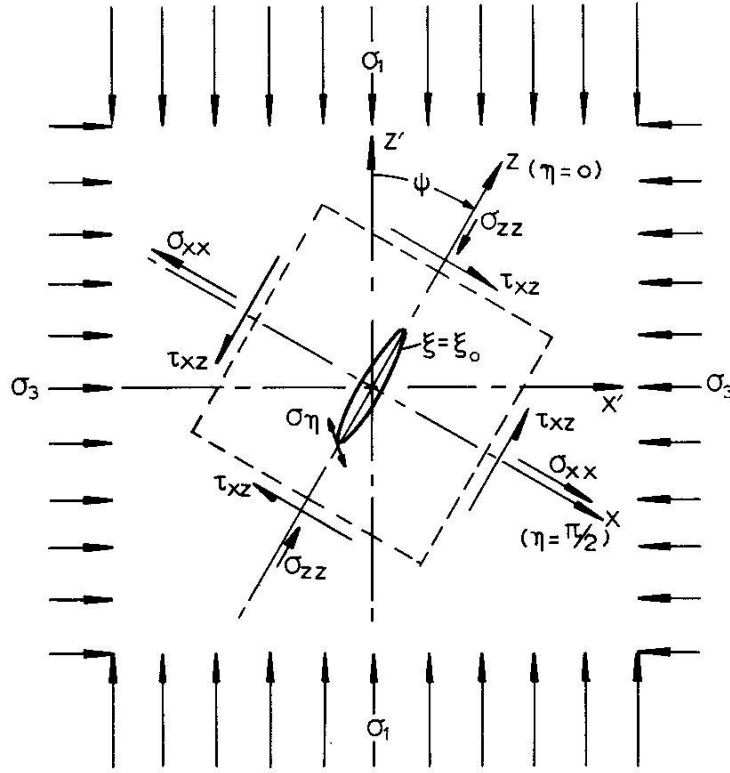


Figure 1. Stresses acting upon a crack which is inclined at an angle ψ to the direction of the major principal stress σ_1 .

In Figure 1, the system of rectangular coordinates x, z is parallel to the axes of the elliptical opening: it is inclined at an angle ψ with respect to the system of rectangular coordinates x', z' which is parallel to the directions of the principal stresses σ_1 and σ_3 . Of these, σ_1 is algebraically largest and σ_3 algebraically smallest of the three principal stresses².

The normal stress σ_{xx} and the shear stress τ_{xz} are related to the principal stresses σ_1 and σ_3 by the following equations:

$$2 \sigma_{xx} = (\sigma_1 + \sigma_3) - (\sigma_1 - \sigma_3) \cos 2\psi \quad (1)$$

$$2\tau_{xz} = (\sigma_1 - \sigma_3) \sin 2\psi \quad (2)$$

The stress σ_{zz} , parallel to the major axis of the crack, has a negligible influence upon

² In this analysis, the intermediate principal stress σ_3 is assumed to have a negligible influence upon fracture.

the stresses induced near the crack tip and need not be considered in the following analysis.

The stresses σ_η and τ_η which act on the surface of the crack as shown in Figure 1, exist only when closure of the crack has occurred and their influence was considered by McClintock and Walsh (1963) in deriving their modification to Griffith theory.

The tangential stress σ_η around the boundary of an open elliptical crack, due to the stresses σ_{xx} and τ_{xz} can be calculated from the results presented by Inglis (1913) and is found to be:

$$\sigma_\eta = \frac{\sigma_{xx} \left(\sinh 2\varepsilon_o + e^{2\varepsilon_o} \cos 2\eta - 1 \right) + 2\tau_{xz} e^{2\varepsilon_o} \sin 2\eta}{\cosh 2\varepsilon_o - \cos 2\eta} \quad (3)$$

where ε_o is the value of the elliptical coordinate ε on the crack boundary. The maximum boundary stresses, both tensile and compressive, occur near the ends of the crack (i.e., when the value of η is small). Since the value of ε_o is also small for a flat ellipse, (3) may be simplified by series expansion in which terms of the second order and higher which appear in the numerator are neglected. This simplification results in the following equation, valid only for the stresses near the crack tip:

$$\sigma_\eta = \frac{2(\sigma_{xx}\varepsilon_o + \tau_{xz}\eta)}{\cosh 2\varepsilon_o - \cos 2\eta} \quad (4)$$

Differentiation of (4) with respect to η and equating $\partial\sigma_\eta/\partial\eta$ to zero results in a quadratic equation in η from which the positions on the crack boundary at which the maximum and minimum stresses occur can be determined. Substituting these values of η into (4) gives the maximum and minimum stresses on the boundary of the crack as:

$$\sigma_N\varepsilon_o = \sigma_{xx} \pm \left(\sigma_{xx}^2 + \tau_{xz}^2 \right)^{1/2} \quad (5)$$

where σ_N is the maximum or minimum value of the tangential stress σ_η of the ellipse boundary.

Expressing equation (5) in terms of the principal stresses σ_1 and σ_3 from equations (1) and (2) gives

$$\sigma_N\varepsilon_o = \frac{1}{2} \left[(\sigma_1 + \sigma_3) - (\sigma_1 - \sigma_3) \cos 2\psi \right] \pm \left[\frac{1}{2} \left\{ (\sigma_1^2 + \sigma_3^2) - (\sigma_1^2 - \sigma_3^2) \cos 2\psi \right\} \right]^{1/2} \quad (6)$$

The critical crack orientation ψ_c at which the maximum and minimum stresses are induced near the crack tip is found by differentiating equation (6) with respect to ψ and letting $\partial\sigma_N / \partial\psi = 0$. This gives:

$$\cos 2\psi_c = \frac{\sigma_1 - \sigma_3}{2(\sigma_1 + \sigma_3)} \quad (7)$$

Note that this equation is only meaningful for values of $\sigma_3 / \sigma_1 \geq -0.33$ and the critical crack orientation for smaller values of σ_3 / σ_1 must be determined from other considerations.

The maximum and minimum stresses at the boundary of a crack oriented at the critical angle ψ_c under conditions where $\sigma_3 / \sigma_1 \geq -0.33$ are found by substituting ψ_c from equation (7) for ψ in equation (6). If it is accepted that fracture occurs as a result of tensile stress at or near the crack tip, only the minimum (negative) stress given by this substitution need be considered. Hence,

$$\sigma_o \cdot \varepsilon_o = \frac{-(\sigma_1 - \sigma_3)^2}{4(\sigma_1 + \sigma_3)} \quad (8)$$

where σ_o denotes the minimum (algebraically smallest) value of the tangential stress on the boundary of the ellipse.

If it is postulated that the fracture of a brittle material initiates when the maximum tensile stress at the crack tip is equal to the molecular cohesive strength of the material (Orowan 1949), then equation (8) expresses a fracture criterion for a brittle material under conditions where $\sigma_3 / \sigma_1 \geq -0.33$, if σ_o is taken as the molecular cohesive strength of the material.

The molecular strength, σ_o , and the crack geometry, ε_o , cannot be determined by direct physical measurements. However, their product can be expressed in terms of the uniaxial tensile strength, σ_t , determined on a laboratory specimen. Since, for uniaxial tension ($\sigma_3 < 0$, $\sigma_1 = 0$), $\sigma_3 / \sigma_1 = -\infty$ equations (7) and (8), which are only valid for $\sigma_3 / \sigma_1 \geq -0.33$, cannot be used to find a relationship between σ_o , ε_o and σ_t and equation (6) must be resorted to for finding this relationship.

If the plane body containing the crack, illustrated in Figure 1, is subjected to a uniaxial tensile stress (i.e. $\sigma_3 < 0$, $\sigma_1 = 0$), the maximum stress at the crack tip (σ_N) is dependent upon the minor principal stress σ_3 only. Hence, equation (6) simplifies to

$$\sigma_N \cdot \varepsilon_o = \sigma_3 \left[\frac{1}{2}(1 + \cos 2\psi) \pm \left[\frac{1}{2}(1 + \cos 2\psi) \right]^{\frac{1}{2}} \right] \quad (9)$$

The maximum tensile stress at the crack tip occurs when the bracketed term on the right hand side of equation (9) is a maximum. This occurs when $\cos 2\psi = 1$ or when $\psi = 0$, giving

$$\sigma_o \cdot \varepsilon_o = 2\sigma_3 \quad (10)$$

$$(\sigma_1 = 0, \quad \psi = 0)$$

If the minor principal stress σ_3 is tensile (negative), equation (10) defines the fracture criterion for uniaxial tensile stress conditions in terms of the molecular cohesive strength of the material (σ_o) and the crack geometry (ε_o). Denoting the uniaxial tensile strength of the material, measured on a laboratory specimen, as σ_t ⁽³⁾, equation (10) may, with $\sigma_3 = \sigma_t$, be re-written as:

$$\sigma_o \cdot \varepsilon_o = 2\sigma_1 \quad (11)$$

Equation (8), which is valid for $\sigma_3 / \sigma_1 \geq -0.33$, is of limited practical use because the term $\sigma_o \cdot \varepsilon_o$ cannot be evaluated in the laboratory. If, however, this term is expressed in terms of the uniaxial tensile strength of the material (σ_t), according to equation (11), the fracture criterion becomes

$$\frac{(\sigma_1 - \sigma_3)^2}{(\sigma_1 + \sigma_3)} = -8\sigma_1 \quad (12)$$

The authors have found that the most useful interpretation of this equation is in expressing the major principal stress (σ_1), at fracture, in terms of the principal stress ratio σ_3 / σ_1 and the uniaxial tensile strength (σ_t) or the uniaxial compressive strength (σ_c).

Thus:

$$\sigma_1 = \sigma_3 - 4\sigma_t \left[1 + \left(1 - \frac{\sigma_3}{\sigma_1} \right)^{\frac{1}{2}} \right] \quad (13)$$

or

³ Note that the uniaxial tensile strength is negative by definition. Hence, in substituting a numerical value for σ_t , the negative sign must be shown; e.g. $\sigma_t = -100$ lb/sq. in.

$$\sigma_1 = \sigma_3 + \sigma_c \left(2 \frac{\sigma_3}{\sigma_c} + \frac{1}{4} \right)^{\frac{1}{2}} + \frac{1}{2} \sigma_c \quad (14)$$

Equation (14) is obtained by putting $\sigma_3 = 0$ and $\sigma_1 = \sigma_c$ in equation (12) and substituting thus obtained result ($\sigma_c = -8 \sigma_t$) in equation (13).

Equations (7), (13) and (14) are valid only when the principal stress ratio $\sigma_3 / \sigma_1 \geq -0.33$. For, $\sigma_3 / \sigma_1 < -0.33$ fracture occurs when the minor principal stress equals the uniaxial tensile strength of the material, i.e. when $\sigma_3 = \sigma_t$.

The Griffith fracture theory can also be represented by a parabolic Mohr envelope defined by the following equation:

$$\tau^2 = 4 \sigma_t (\sigma_t - \sigma) \quad (15)$$

where τ is shear stress acting along the fracture surface; σ is normal stress perpendicular to the fracture surface.

Studies of rock fracture suggest that the inherent cracks from which fracture propagates are contained within grain boundaries (Brace, 1961) and can be simulated by very long elliptical openings. Under compressive stress conditions, closure of these cracks can occur before the tensile stress at the crack tip is high enough to initiate fracture. When crack closure has occurred, the shear resistance resulting from the contact pressure between the crack faces has to be overcome before propagation of the crack can occur.

McClintock and Walsh (1962) modified Griffith's original theory to account for the effects of crack closure in compression. If it is assumed that the inherent cracks are initially closed, the relationship between the principal stresses required to initiate fracture is

$$\sigma_1 = \sigma_3 \frac{\left(1 + \mu^2\right)^{\frac{1}{2}} + \mu}{\left(1 + \mu^2\right)^{\frac{1}{2}} - \mu} + \sigma_c \quad (16)$$

where μ is the coefficient of friction between the crack faces and σ_c is the uniaxial compressive strength of the material.

The critical orientation of a closed crack is given by

$$\tan 2 \sigma_c = \frac{1}{\mu} \quad (17)$$

Equations (16) and (17) are valid when the normal stress σ_n acting across the crack is compressive, i.e. when

$$\sigma_n = \frac{1}{2} [(\sigma_1 + \sigma_3) - (\sigma_1 - \sigma_3) \cos 2\psi] > 0 \quad (18)$$

When σ_n is tensile, the original Griffith theory, defined by equations (7) and (12) is applicable.

The modified Griffith theory can be represented by a straight-line Mohr envelope having the following equation:

$$\tau = \mu\sigma - 2\sigma_t \quad (19)$$

In order to establish whether the original and modified Griffith theories are applicable to the prediction of rock fracture behaviour, a survey of published rock fracture data was undertaken. To facilitate comparison of the results, they were reduced to a dimensionless form by dividing each strength value of a particular rock by its uniaxial compressive strength. These dimensionless strength values are plotted in Figure 2 together with the original and modified Griffith fracture loci derived from equations (14) and (16).

It is evident from Figure 2 that, in spite of the wide variety of materials included (listed in Table 1), there is a remarkable agreement between the experimental results and the fracture initiation behaviour predicted by the modified Griffith theory. Detailed examination of the results reveals that the coefficient of internal friction, μ , given by the slope of the modified Griffith fracture locus, is closely related to the rock type tested. The igneous and metamorphosed sedimentary rocks (granites, dolerite, quartzites) are characterized by coefficients of friction of greater than 1.0; the sedimentary rocks (sandstones, limestones and shales) have coefficients of friction between 1.0 and 0.5.

A coefficient of internal friction of greater than unity implies that the shear resistance is greater than the normal stress acting across the crack. This apparent anomaly is probably due to interlocking of surface irregularities or, carrying the thought to the extreme, due to the fracture initiating from an elastic discontinuity rather than an actual crack.

It must be emphasized that both the original and modified fracture theories predict fracture initiation from a single crack and that, strictly, they cannot be applied to the fracture of a specimen as a whole. It has already been suggested by Brace and Bombolakis (1963) that a fracture propagation from a single crack follows a more complex path than is generally assumed and that it is the presence of favourable crack arrays which coalesce to form the macroscopic fracture surface that make the Griffith theory applicable to predicting fracture of rock and rock specimens.

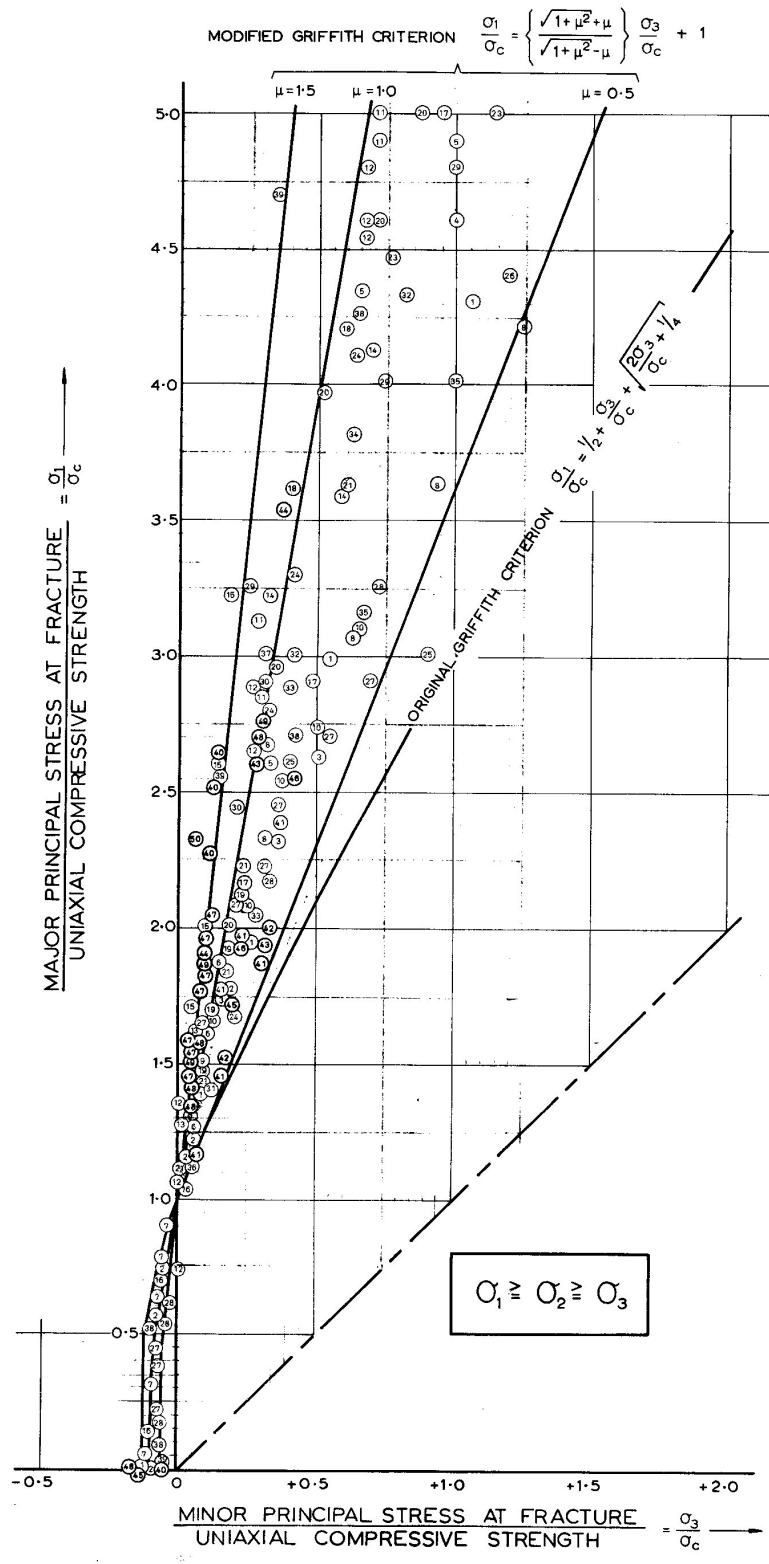


Figure 2. Triaxial fracture data for rock materials.

Table 1. Summary of triaxial test results on rock and concrete.

Graph Point	Material	σ_c lb/sq. in	Tested by
1	Marble	13 700	Ros. and Eichinger
2	Marble	18 000	Ros and Eichinger
3	Marble	20 000	Von Karman
4	Carthage Marble	10 000	Bredthauer
5	Carthage Marble	7 500	Bredthauer
6	Wombeyan Marble	10 000	Jaeger
7	Concrete	2 380	McHenry and Kami
8	Concrete	3 200	Akroyd
9	Concrete	6 000	Jaeger
10	Concrete	5 700	Fumagalli
11	Concrete (28 day)	3 510	Balmer
12	Concrete (90 day)	4 000	Balmer
13	Granite Gneiss	25 500	Jaeger
14	Barre Granite	24 200	Robertson
15	Granite (slightly alt)	10 000	Wreuker
16	Westerly Granite	33 800	Brace
17	Iwaki Sandstone	1 780	Horibe & Kobayashi
18	Rush Springs Sandstone	26 000	Bredthauer
19	Pennant Sandstone	22 500	Price
20	Darley Dale Sandstone	5 780	Price
21	Sandstone	9 000	Jaeger
22	Oil Creek Sandstone	**	Handin
23	Dolomite	24 000	Bredthauer
24	White Dolomite	12 000	Bredthauer
25	Clear Fork Dolomite	*	Handin
26	Blair Dolomite	**	Handin
27	Blair Dolomite	75 000	Brace
28	Webtuck Dolomite	22 000	Brace
29	Chico Limestone	10 000	Bredthauer
30	Virginia Limestone	48 000	Bredthauer
31	Limestone	20 000	Jaeger
32	Anhydrite	6 000	Bredthauer
33	Knippa Basalt	38 000	Bredthauer
34	Sandy Shale	8 000	Bredthauer
35	Shale	15 000	Bredthauer
36	Porphyry	40 000	Jaeger
3-7	Sioux Quartzite	**	Handin
38	Frederick Diabase	71 000	Brace
39	Cheshire Quartzite	68 000	Brace
40	Chert dyke material	83 000	Hoek
41	Quartzitic Shale (Dry)	30 900	Colback and Wiid
42	Quartzitic Shale (Wet)	17 100	Colback and Wiid
43	Quartzitic Sandstone (Dry)	9 070	Colback and Wiid
44	Quartzitic Sandstone (Wet)	4 970	Colback and Wiid
45	Slate (primary cracks)	4 300	Hoek
46	Slate (secondary cracks)	15 900	Hoek
47	Dolerite	37 000	CSIR
48	Quartzite (ERPM Footwall)	31 000	CSIR
49	Quartzite (ERPM Hanging wall)	43 200	CSIR
50	Glass	91 000	CSIR

* Uniaxial compressive strength

** Presented in dimensionless form by McClintock and Walsh

Fracture propagation from a single crack

In order to study the propagation of fracture from a single crack, 6 inch square by $\frac{1}{4}$ inch thick plates of annealed glass were carefully prepared. Open “Griffith cracks” were ultrasonically machined into these plates. The length of the crack was kept constant at $\frac{1}{2}$ inch and its axis ratio at 25:1. The cracks were oriented at their critical angles as determined by Equation (7).

The plates were subjected to uniformly distributed edge loading in the tension and compression loading devices described in the Appendix to this paper. The specimens were studied photo-elastically while under load and the stress at which fracture initiated as well as the direction of crack propagation was noted. A typical isochromatic pattern obtained in a plate subjected to the uniaxial compression is reproduced in Figure 3.

The stresses at which fracture is initiated are plotted in terms of the major and minor principal stresses, in Figure 4 and as Mohr circles in Figure 5. The theoretical fracture loci according to the original Griffith fracture initiation criterion, defined by equations (13) and (15), are given by the curves in Figures 4 and 5. The agreement between these and the experimental plots is considered satisfactory.

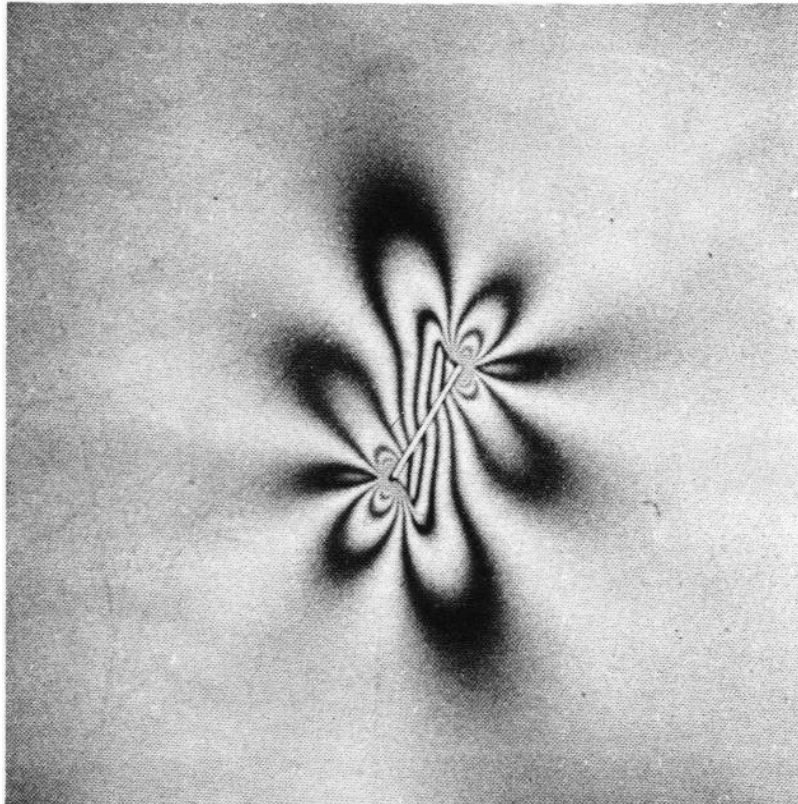


Figure 3. Photo-elastic pattern in a glass plate containing elliptical crack from which fracture has propagated.

In uniaxial tension, fracture initiation and fracture of the specimen occurred in the period of a few milliseconds. As can be expected, the fracture propagated in a direction normal to the direction of applied tension.

In biaxial compression, the fracture propagation followed a consistent pattern. Fracture initiated at a point on the crack boundary near, but not at the crack tip, (Ode, 1963) and followed a curved path (e.g. Figure 6, or upon careful observation, Figure 3). Generally, fracture propagation ceased when the crack path had become parallel to the major principal stress direction. In all cases, the applied stress was increased to at least three times the fracture initiation stress and, if the cracks showed no tendency to propagate further, the test was discontinued on the assumption that fracture of the specimen would not occur except at much higher stress levels.

The lengths of the stable cracks were found to be related to the ratio of the applied principal stresses as illustrated in Figure 6. This finding is similar to that previously reported by Hoek (1965) for the propagation of cracks from a circular hole in a biaxial compressive stress field.

Under uniaxial compressive stress conditions, fracture propagation commenced with the sudden appearance of a small cracks of approximately 0.2 times the original crack length. Normally a crack would appear at only one end of the initial crack but would be followed, within a period of a few seconds⁴ and at the same applied stress level, by a mirror image crack at the other end of the initial crack. Further propagation of these cracks required increased applied stress and this is plotted against crack length in Figure 7.

In the case of biaxial compression, insufficient information is available to permit plotting graphs similar to that shown in figure 7. From examination of available records, however, it appears that the length of the initial and final cracks did not differ by more than a few percent. This implies that, if the crack can be propagated, the stress required to do so would be as much as about ten times greater than the initiation stress and, as such, ceases to be of practical interest.

From these results, it can be concluded⁵ that a single Griffith crack cannot account for the failure of a specimen in a compressive field unless the ratio of applied principal stress is less than or equal to zero i.e. in uniaxial compression or when one principal stress is tensile. It is also suggested that, where failure of the specimen originates from a single crack, the direction of macroscopic fracture is normal to the minor (algebraically smallest) principal stress direction, i.e. in uniaxial compression parallel to the compressive stress direction.

⁴ In many of these tests fracture initiation was observed to be significantly time-dependent but no conclusions can be drawn from the present results because of a lack of adequate records in this respect.

⁵ Somewhat similar conclusions have been reached by Brace and Bombolakis (1963).

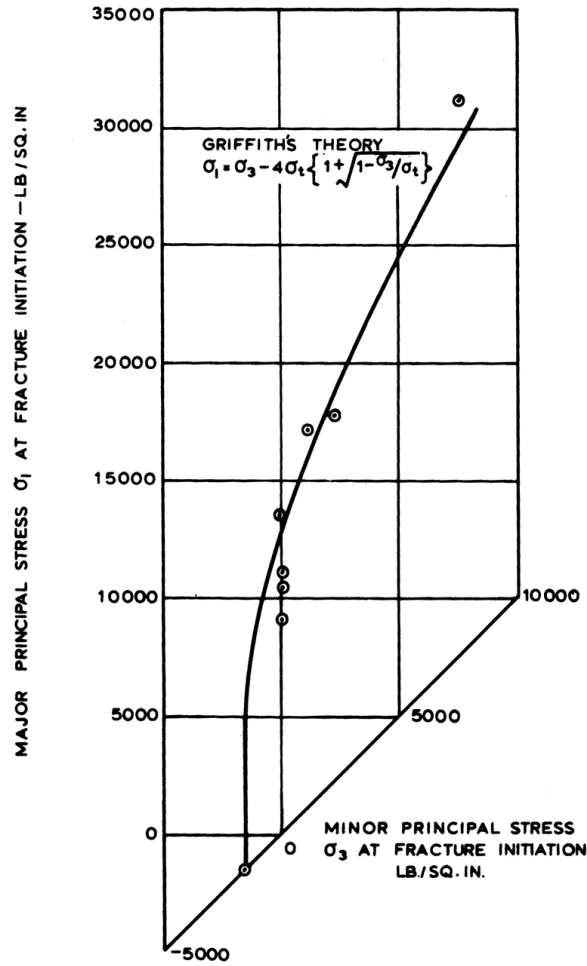


Figure 4. Relationship between principal stresses at fracture initiation at the boundary of an open crack.

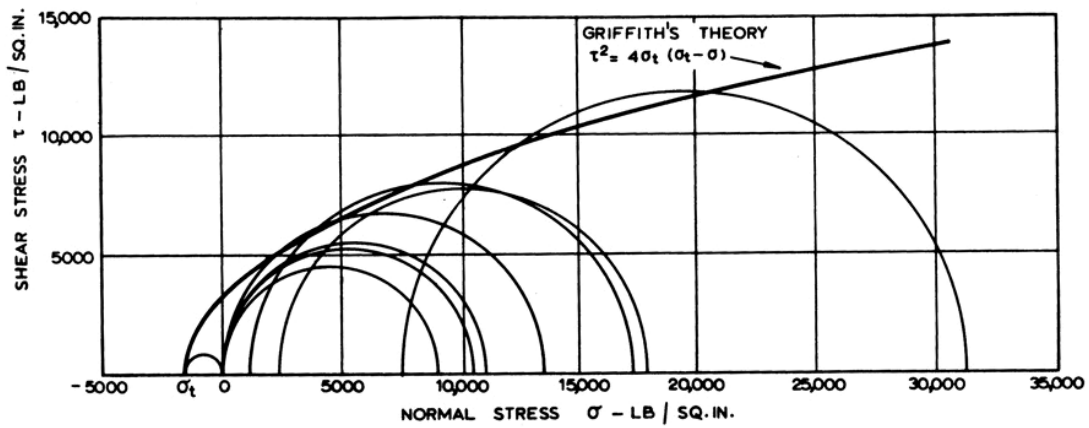


Figure 5. Mohr circles for fracture initiation at the boundary of an open crack.

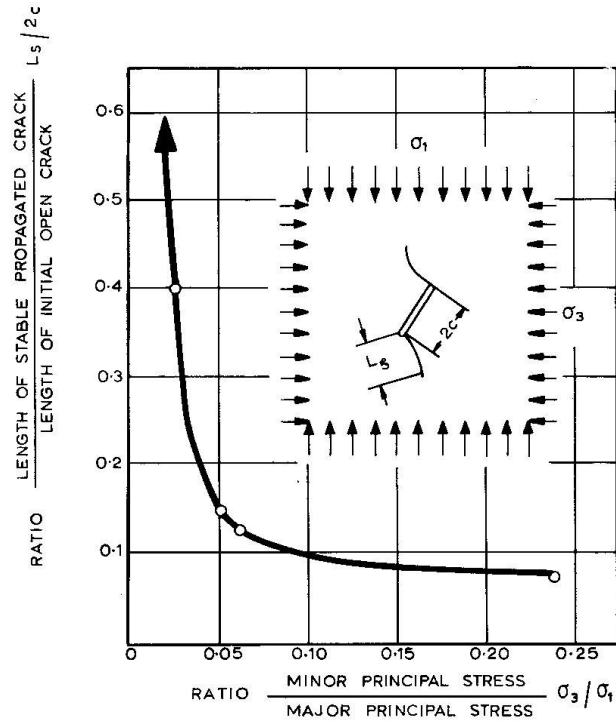


Figure 6. Relationship between stable crack length and ratio of applied principal stresses.

Since it appears reasonable to assume that the inherent cracks form which the fracture of hard rock initiates are initially closed (Brace and Bombolakis, 1963), an attempt was made to produce initially closed cracks in annealed glass plates.

The method used to produce these cracks involves inducing a hairline crack of the required length on the surface of the glass plate. A hardened roller type glass tool which induces this crack as a result of the stress distribution under the contact point has been found preferable to a diamond tool which scores the glass surface. The shallow hairline crack is propagated throughout the thickness of the plate by reflected tensile stress waves generated by impacting the plate on the face opposite to that containing the crack.

At the time of writing it has not been possible to produce closed cracks of the same length in sufficient quantity to permit similar tests to those described in the previous section to be carried out. However, the authors feel that precise control of the main parameters involved in the process of closed crack formation, namely the quality of the initial hairline crack and the magnitude of the impact required to propagate it through the plate, will ultimately enable them to reproduce these cracks as required.

A few of the better quality cracks which have been obtained were tested in uniaxial compression and a typical result obtained is illustrated in Figure 8.

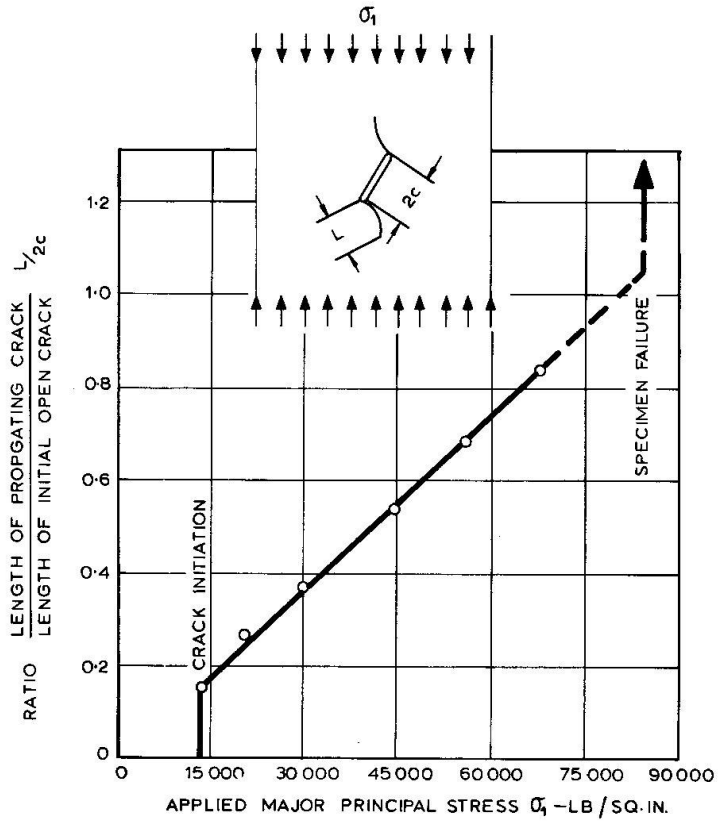


Figure 7. Relationship between propagating crack length and applied uniaxial compressive stress.

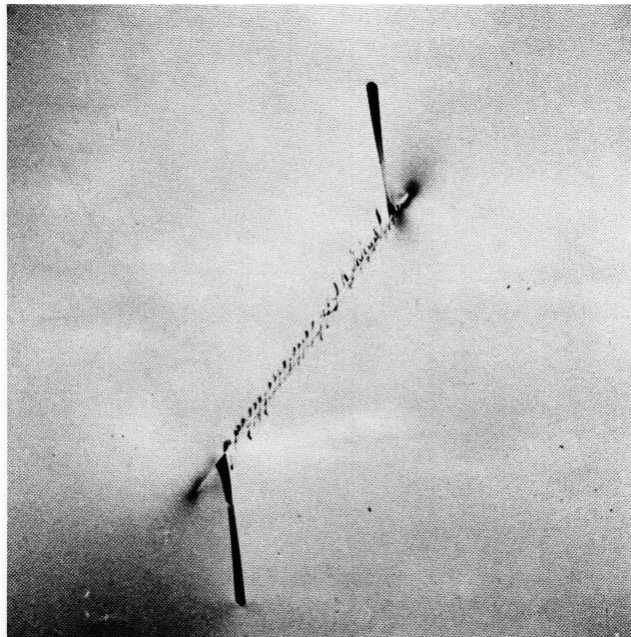


Figure 8. Fracture propagation from a closed crack in glass.

This photograph suggests some modification of the mechanism of fracture propagation assumed by McClintock and Walsh (1962). In their study of the friction effects on closed cracks, they postulated that the shear stress acting parallel to the crack surfaces exceeds the shear resistance due to friction, relative movement of the crack faces will occur and fracture will propagate from the crack tip.

The authors' observations of fracture propagation from closed cracks in glass leads to the conclusion that the crack tip itself plays a very minor role in the fracture process. The primary factor responsible for fracture initiation is the relative movement of the crack faces. Slight irregularities in the crack surface result in an uneven stress distribution along the crack surfaces and tensile fracture initiates in the tensile stress zones which occur at points where the crack surface is relatively free to move. The formation of these tensile cracks is clearly illustrated in Figure 8.

In all the tests carried out by the authors it was found that these short tensile cracks formed at regular intervals over a fairly wide stress range. Fracture propagation occurred which the cracks closest to the tips of the initial crack propagated as illustrated in Figure 8. Once this state of fracture propagation had commenced, initiation and propagation of the other short tensile cracks ceased. While the actual fracture initiation process may differ from that postulated by McClintock and Walsh, the authors feel that it may eventually be possible to express the fracture initiation criterion by means of an equation very similar in form to equation (16).

Once sufficient experimental evidence is available, the theoretical conditions for fracture initiation will be re-examined and, if necessary, modified.



Figure 9. Reflected light photoelastic pattern showing strain distribution in a large grained granite plate subjected to uniaxial compression.

Preliminary studies of crack arrays

It is evident from the results presented in this paper that fracture of a specimen is unlikely to occur unless a large number of cracks are present. Obviously, the spatial distribution of the cracks will influence the mechanism of fracture initiation and propagation and it is considered essential that this aspect of the problem be investigated if the fracture mechanism of rock is to be fully understood.

The results of a preliminary study of arrays of open cracks are included in Table 2. It is evident from these results that the interaction of cracks within the array influences both the initiation stress and the mechanism of crack propagation. The future research problem calls for a detailed study of the various parameters which influence the behaviour of crack arrays.

In addition to the tests on glass plates described above, the authors are also studying the mechanism of crack initiation and propagation in plates of rock. The plates, measuring 6 inches square by $\frac{1}{4}$ inch thick, have a dish-shaped central portion ground out of each face, giving a three inch diameter section of $\frac{1}{8}$ inch thickness. One side of this reduced section is covered with a birefringent layer and the strain pattern associated with fracture initiation is studied by means of reflected polarised light (Hoek and Bieniawski, 1963). A typical photoelastic pattern obtained in these studies is illustrated in Figure 9 which shows stress concentrations around individual grains and the point of fracture initiation.

A study of the reverse side of the plates used for these tests permits detailed examination of the crack path. A low magnification micrograph of a typical crack in quartzite is reproduced in Figure 10. The stepped path followed by the propagation crack is evident in this photograph and the authors hope that, by studying the fracture paths in such specimens, a rational picture of rock fracture can be built up.

Conclusions

The results presented in this paper have shown that the Griffith theory offers a reliable basis for the prediction of fracture initiation from a single open crack. It is concluded, however, that a single crack cannot account for the failure of a specimen unless one of the applied principal stresses is zero or tensile. The effects of crack closure in compression have been shown to differ from those assumed by McClintock and Walsh but it is anticipated that this difference will not significantly influence the final fracture criterion.

Examples have been given of studies of crack arrays and of fracture propagation in rock which indicate the direction of future research.

Table 2. Preliminary study of arrays of open cracks.

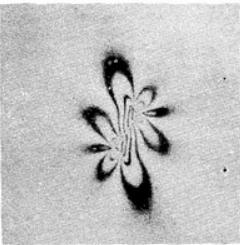
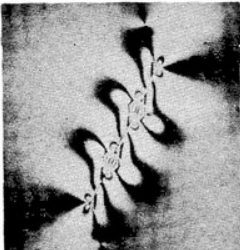
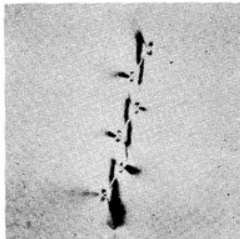
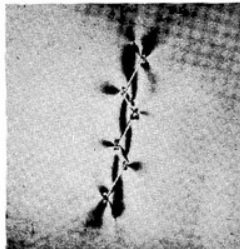
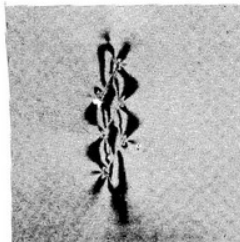
Array	Fracture Initiation	Remarks
	<p>11 180 lb/sq. in</p>	<p>Fracture propagation occurred with increasing applied stress as illustrated in Figure 7</p>
	<p>8 750 lb/sq. in</p>	<p>Fracture initiation at lower stress than single crack due to greater "crack length". Individual cracks do not join.</p>
	<p>11 590 lb/sq. in</p>	<p>Individual cracks do not join. Array does not appear to influence initiation or propagation.</p>
	<p>9 900 lb/sq. in</p>	<p>Crack array influences propagation so that centre cracks tend to move together.</p>
	<p>13 420 lb/sq. in</p>	<p>Cracks join although initiation stress is higher.</p>



Figure 10. Crack path in a quartzite specimen subjected to uniaxial compression.

Acknowledgements

This work forms part of an extensive research program being carried out by the South African Council for Scientific and Industrial Research on behalf of the Transvaal and Orange Free State Chamber of Mines. The authors are indebted to these organizations for permission to publish the material contained in this paper.

The authors wish to thank Mr. M.N. Marais for his assistance in carrying out the tests and to Mr. J. B. Kennard for preparing the specimens.

Appendix: Apparatus for the application of uniformly distributed edge loads to plate models

Tensile apparatus

The apparatus for applying uniformly distributed uniaxial tension to 6 inch square by ¼ inch thick plate models is illustrated in Figure 11. Load distribution is achieved by means of a “whipple tree” arrangement of pinjointed segments. The eight small segments which transmit the load to the model itself are bonded onto the model edge with epoxy resin.

Loading of the model and the photoelastic study of the stress distribution around the crack is carried out on the 12 inch diameter lens polariscope which has been described elsewhere by Hoek (1965).

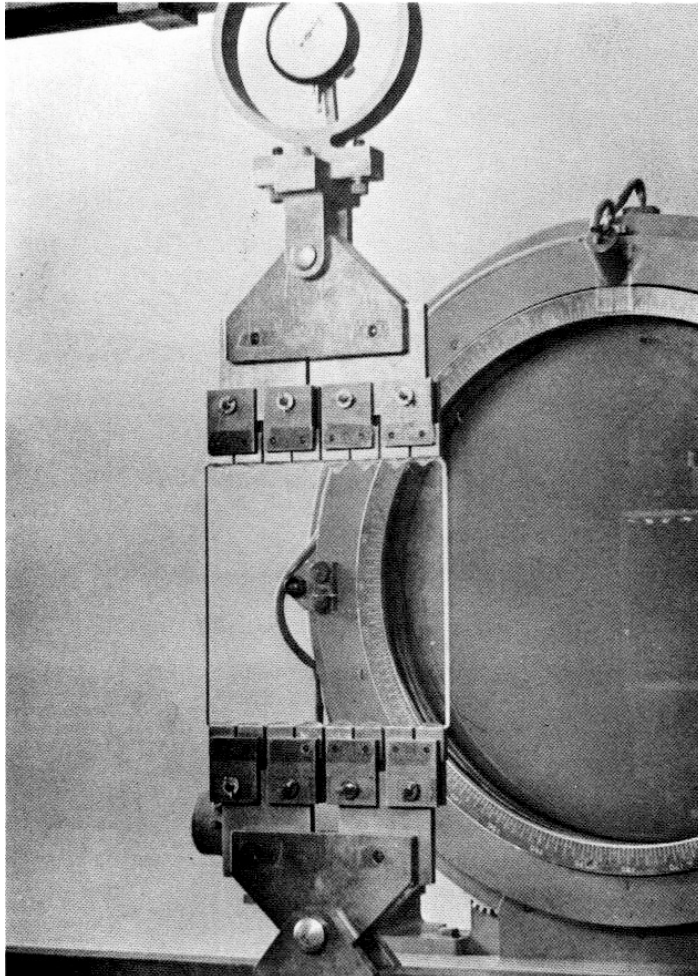


Figure 11. Apparatus for subjecting plate models to uniaxial tension.

Biaxial compression loading apparatus

The biaxial compression loading apparatus which was used in the tests described in this paper was designed for general rock mechanics model studies and extreme care was taken to ensure uniformity of the load distribution.

The load is applied to the accurately ground edges of the model through stacks of semi-circular segments. These segments are held in alignment by means of a set of copperberyllium leaf springs. The photograph of the partially dismantled load distribution frame reproduced in Figure 12 shows the arrangement of these segments and springs.

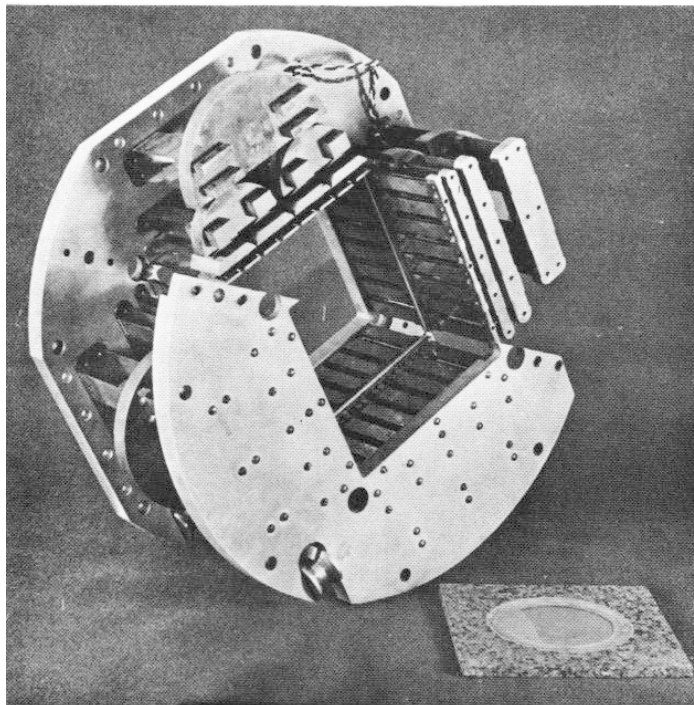


Figure 12. Partially dismantled biaxial loading frame showing details of the load distribution mechanism.

The load is applied onto the large segments by means of 4 hydraulic jacks, designed to exert a thrust of 100 tons each. These jacks are located in a circular frame illustrated in Figure 13. All the jacks are interconnected and fed by a single variable volume high pressure hydraulic pump.

Load control is achieved by means of a needle bleed-off valve in the hydraulic circuit. The horizontal jacks can be isolated to allow the application of uniaxial compression in the vertical direction. Alternatively, different diameter pistons can be fitted into the horizontal jacks to give a constant ratio of vertical to horizontal load.

The applied load is measured by means of strain gauges bonded onto the four large segments onto which the jacks act. The signals from these gauges are displayed on a digital voltmeter which permits direct load read-out in tens of pounds.

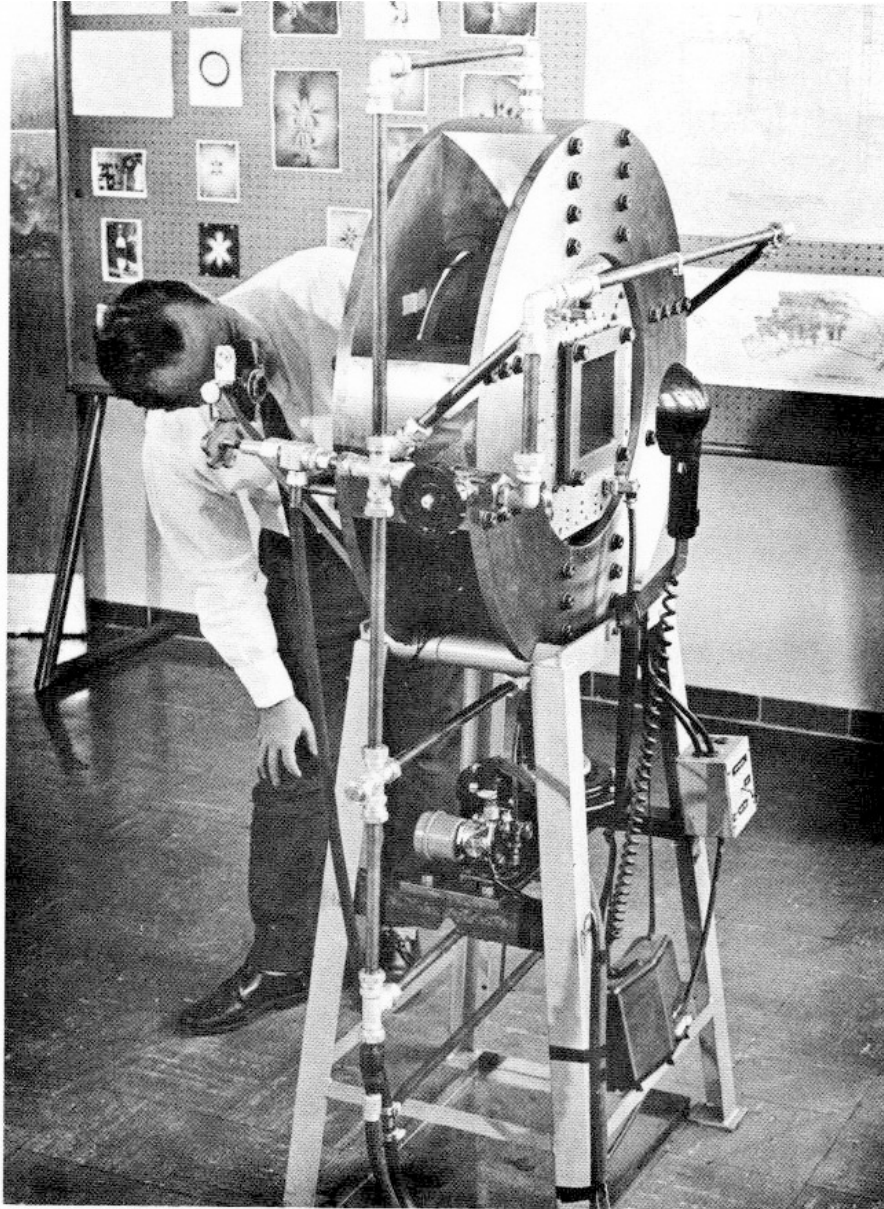


Figure 13. Apparatus for subjecting plate models to biaxial compression.

Submitted June 14, 1965.

References

- Brace, W.F. 1964. Brittle fracture of rocks. In *State of Stress in the Earth's Crust*. (ed Judd), 111-180. New York: American Elsevier Publishing Co.
- Brace, W.F. 1961. Dependence of fracture strength of rocks on grain size. *Penn. State Univ Mineral Exp. Station Bulletin* **76**, 99-103.
- Brace, W.F. and E.G. Bombolakis 1963. A note on brittle crack growth in compression. *J. Geophys. Res.* **68**(12), 3709-3713.
- Cook, N.G.W. 1963. The seismic location of rockbursts. In *Rock Mechanics* (ed Fairhurst) 493-516. New York: Pergamon Press.
- Ergodan, F. and Sih, G.C. 1963. * *TransAmerican Society of Mechanical Engineers, Series D., J. Basic Engineering* **85**(4). 519-27.
- Hoek, E. 1965. Rock fracture around mining excavations. *Proc. Fourth Int. Conf. on Strata Control and Rock Mechanics* 335-348. New York: Columbia University Press.
- Hoek, E. 1963. Experimental study of rock stress problems in deep level mining. In *Experimental Mechanics* (ed. Rossi) 177-194. New York: Pergamon Press.
- Hoek, E. and Z.T. Bieniawski 1963. Application of the photoelastic coating technique to the study of the stress redistribution associated with plastic flow around notches. *S. Afr. Mech. Eng.* **12**(8). 222-226.
- Griffith, A.A. 1924. Theory of rupture. *Proc. First Int. Cong. Applied Mech* (eds Bienzo and Burgers). 55-63. Delft: Technische Boekhandel and Drukkerij.
- Inglis, C.E. 1913. Stresses in a plate due to the presence of cracks and sharp corners. *Trans. Instn. Nav. Archet. London.* **55**, 219-230.
- McClintock, F.A. and J.B. Walsh 1962. Friction of Griffith cracks in rock under pressure. *Proc. Fourth U.S. Congr. Appl. Mech.* 1015-21. Berkeley: American Society of Mechanical Engineers.
- Ode, H. 1963. * In *Rock Deformation* (eds Handin and Griggs) 517-535. New York: Geological Society of America.
- Orowan, E. 1949. Fracture and strength of solids. *Rep.Progr.Phys.* **12**, 185-232.

* Title missing from original paper.

Brittle Fracture of Rock

Evert Hoek

Chapter 4 in *Rock Mechanics in Engineering Practice*

Edited by K.G. Stagg and O.C. Zienkiewicz

London: J. Wiley, 99 to 124

1968

4.1 Introduction

In chapters 1 and 2 the mechanical properties of rock materials have been discussed in some detail and it has been shown that most rocks exhibit patterns of behaviour which can be usefully employed by the practical engineer. Since most of the conclusions presented in chapters 1 and 2 are based upon empirical studies it is of interest to examine the basic mechanism of brittle failure of rock in order to gain some understanding of the underlying reasons for the behaviour patterns which are observed. Not only does such an examination satisfy the curiosity of the academically inclined but it also provides a basis for meaningful extrapolation from available experimental results.

A comprehensive review of the research effort which has been devoted to the study of the brittle failure of rock has recently been presented by Jaeger (1966). Rather than present yet another review on the theoretical aspects of this subject the author has chosen to present the known physical facts in a form which will be both meaningful and useful to the practical engineer. In order to achieve this end within the limited space available in this chapter, the dynamic aspects of rock fracture have been ignored and the discussion is limited to failure under quasi-static loading conditions such as those which can be expected to occur in rock structures.

4.2 Fracture initiation

A rock material contains a large number of randomly oriented zones of potential failure in the form of grain boundaries. Let us assume that one such grain boundary, illustrated in figure 4.1, contains a number of open flaws and that, in accordance with the concept postulated by Griffith (1921, 1924), these flaws are approximately elliptical in shape. It can be shown that very high tensile stresses occur on the boundary of a suitably oriented elliptical opening, even under compressive stress conditions, and it is assumed that fracture initiates from the boundary of an open flaw when the tensile stress on this boundary exceeds the local tensile strength of the material.

In order to obtain an estimate of the stresses around the boundary of an open elliptical flaw it is necessary to make the following simplifying assumptions:

- a) The ellipse can be treated as a single opening in a semi-infinite elastic medium, i.e. adjacent flaws do not interact and local variations in material properties are ignored.
- b) The ellipse and the stress system which acts upon the material surrounding it can be treated two dimensionally, i.e. the influence of the three-dimensional shape of a flaw and of the stress σ_z in the crack plane can be ignored.

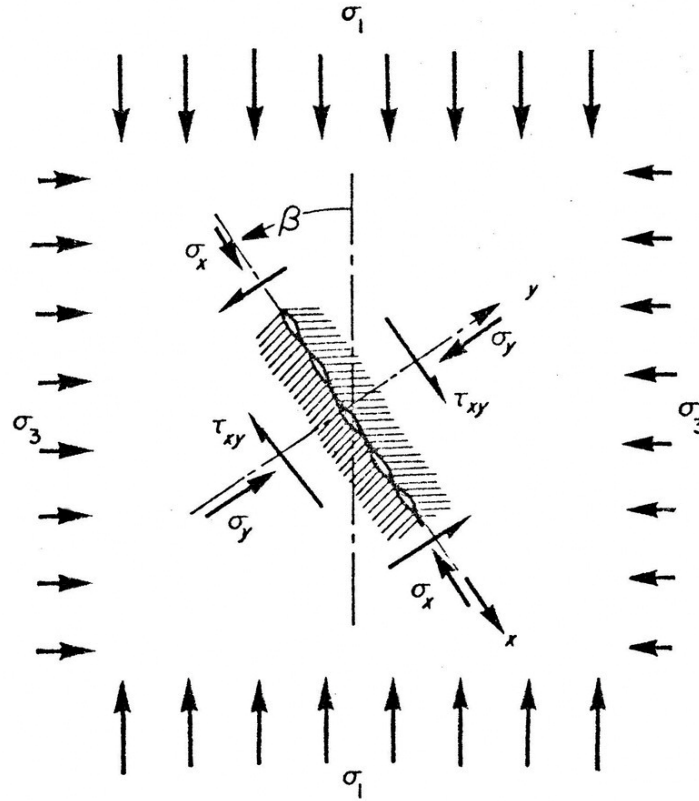


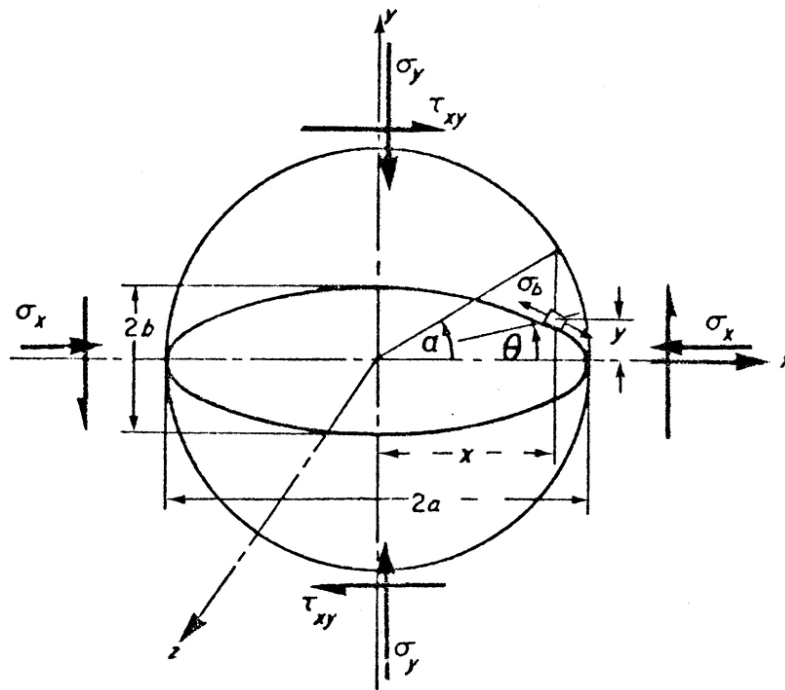
Figure 4.1 Stress system acting on a potential failure plane in rock.

Although these assumptions do introduce certain errors (Jaeger 1966), the magnitude of these errors is estimated to be less than $\pm 10\%$ which is within the order of accuracy aimed at in this analysis.

The stress system acting upon the grain boundary under consideration is shown in Figure 4.1. The convention adopted in this analysis is such that compression is regarded as positive and that $\sigma_1 > \sigma_2 > \sigma_3$ where σ_1, σ_2 and σ_3 are the three principal stresses acting on the rock body. The elliptical flaw is inclined at an angle β to the major stress direction, i.e. the direction of maximum compressive stress. The normal stress σ_y and the shear stress τ_{xy} which act on the material surrounding the elliptical flaw are related to the maximum and minimum principal stresses σ_1 and σ_3 by the following equations:

$$2\sigma_y = (\sigma_1 + \sigma_3) - (\sigma_1 - \sigma_3) \cos 2\beta \quad (4.1)$$

$$2\tau_{xy} = (\sigma_1 - \sigma_3) \sin 2\beta \quad (4.2)$$



Equation of ellipse:

$$x = a \cdot \cos \alpha,$$

$$y = b \cdot \sin \alpha,$$

where α is the eccentric angle;

$$\tan \theta = m \cdot \tan \alpha,$$

where $m = b/a$.

Figure 4.2 Stresses acting on the material surrounding a two-dimensional elliptical flaw.

The stress σ_x which acts parallel to the axis of the elliptical flaw and the intermediate principal stress σ_z which acts in the z direction will be shown to have a negligible influence upon the stresses near the tip of the flaw and can be ignored.

Brittle fracture of rock

In the discussion which follows, the stress system will be discussed in terms of the normal and shear stresses σ_y and τ_{xy} only. The interested reader can revert to the principal stresses σ_1 and σ_3 at any stage of the analysis by substitution of the relations given in equations (4.1) and (4.2).

The parameters which define the boundary of the elliptical flaw are given in Figure 4.2 and, of these, the most important are the ratio of the minor to the major axis of the ellipse $b/a = m$ and the eccentric angle α which defines the position of a point on the boundary of the ellipse. The tangential stress on the boundary of the ellipse σ_b is given by the following equation (Inglis 1913; Denkhaus 1964):

$$\sigma_b = \frac{\sigma_y \{m(m+2)\cos^2 \alpha - \sin^2 \alpha\} + \sigma_x \{(1+2m)\sin^2 \alpha - m^2 \cos^2 \alpha\} - \tau_{xy} \{2(1+m^2)\sin \alpha \cos \alpha\}}{m^2 \cos^2 \alpha + \sin^2 \alpha} \quad (4.3)$$

In a material such as rock it can be assumed that the elliptical flaws will have a very small axis ratio m , i.e. they will be very flat in shape. This means that the maximum tensile stress will occur near the tip of the elliptical flaw, i.e. when the eccentric angle α is very small. When $\alpha \rightarrow 0$, $\sin \alpha \rightarrow \alpha$ and $\cos \alpha \rightarrow 1$. Substitution of these relations into equation (4.3) and neglecting terms of the second order and higher which appear in the numerator gives the following approximate expression for the boundary stress σ_b near the tip of the elliptical flaw:

$$\sigma_b = \frac{2(\sigma_y \cdot m - \tau_{xy} \cdot \alpha)}{m^2 + \alpha^2} \quad (4.4)$$

An important fact which emerges from this simplification is that the stress σ_x , which lies parallel to the major axis of the ellipse, has a negligible influence upon the boundary stress near the tip of the flaw. By analogy the influence of the intermediate principal stress $\sigma_2 = \sigma_z$ can also be ignored.

The maximum tangential stress on the boundary of the elliptical flaw is given when

$$\frac{d\sigma_b}{d\alpha} = 0,$$

i.e. when

Brittle fracture of rock

$$(m^2 + \alpha^2)(-2\tau_{xy}) = 2(\sigma_y \cdot m - \tau_{xy} \cdot \alpha)2\alpha$$

Giving

$$\sigma_b = \frac{-\tau_{xy}}{\alpha}, \quad (4.5)$$

Or, rearranging in terms of $1/\alpha$:

$$\frac{1}{\alpha^2} + \frac{2\sigma_y}{m \cdot \tau_{xy}} \cdot 1 - \frac{1}{m^2} = 0 \quad (4.6)$$

Solving equation (4.6) for $1/\alpha$:

$$\frac{1}{\alpha} = \frac{1}{m \cdot \tau_{xy}} \left\{ \sigma_y \pm \sqrt{(\sigma_y^2 + \tau_{xy}^2)} \right\} \quad (4.7)$$

From equations (4.5) and (4.7)

$$\sigma_b \cdot m = -\sigma_y \pm \sqrt{(\sigma_y^2 + \tau_{xy}^2)} \quad (4.8)$$

The assumed criterion for fracture initiation is that a crack will propagate from the boundary of the elliptical flaw when the tangential stress σ_b reaches a limiting value equal to the tensile strength of the material at that point. Since it is not practical to measure either the local tensile strength of the material surrounding the flaw or the axis ratio m , it is convenient to express the term $\sigma_b \cdot m$ in equation (4.8) in terms of a quantity which can be measured more readily. Such a quantity is the uniaxial tensile strength σ_t of the rock body which contains the flaw under consideration and this is obtained when $\sigma_y = \sigma_t$ and $\tau_{xy} = 0$ giving

$$\sigma_b \cdot m = -2\sigma_t \quad (4.9)$$

Substituting this relation into equation (4.8) and squaring both sides of the resulting equation gives

$$\tau_{xy}^2 = 4\sigma_t(\sigma_t - \sigma_y) \quad (4.10)$$

This equation, which is the equation of a parabola in the $\tau_{xy} - \sigma_y$ plane, defines the

Brittle fracture of rock

relation between the shear and normal stresses τ_{xy} and σ_y at which fracture initiates on the boundary of an open elliptical flaw. Note that, in substituting a numerical value for the uniaxial tensile strength σ_t , it is necessary to include a negative sign in order to satisfy the sign convention adopted in this chapter. Hence a particular rock will have a uniaxial tensile strength of -2000 lb/in^2 .

4.3 Fracture propagation

If it is assumed that the inclination β of the elliptical flaw is such that the boundary stress σ_b is a maximum for any combination of the principal stresses σ_1 and σ_3 then equation (4.10) becomes the equation of an envelope to a number of Mohr circles, one of which is illustrated in Figure 4.3.

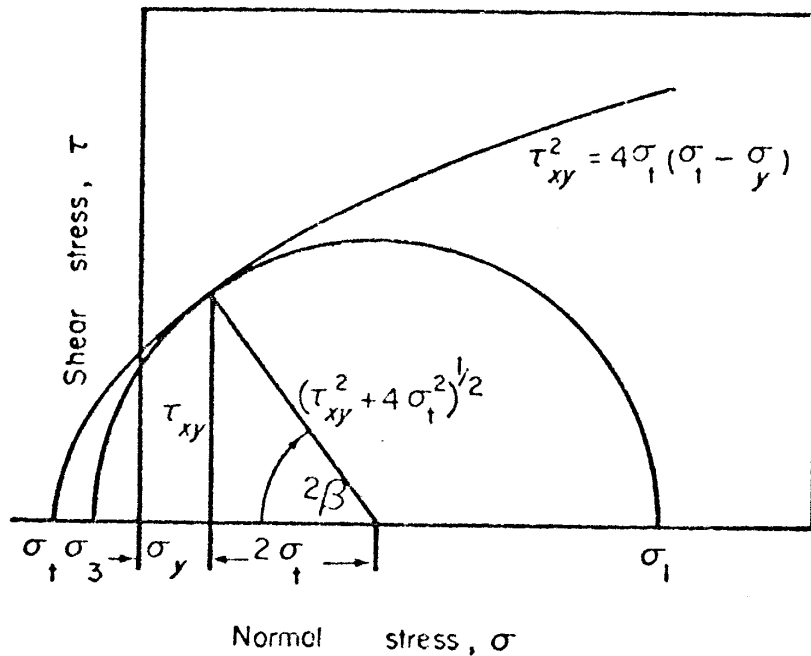


Figure 4.3. Relation between the normal and shear stresses required to initiate tensile fracture from an elliptical flaw.

From the geometry of this circle and from the slope of the normal to the envelope defined by equation (4.10) it follows that

$$\tan 2\beta = \frac{-d\sigma_y}{d\tau_{xy}} = \frac{\tau_{xy}}{2\sigma_t} \quad (4.11)$$

Brittle fracture of rock

From equations (4.5) and (4.9)

$$\sigma_b \cdot m = 2\sigma_t = \frac{-m \cdot \tau_{xy}}{\alpha},$$

hence

$$\alpha = \frac{-m \cdot \tau_{xy}}{2\sigma_t} = -m \cdot \tan 2\beta, \quad (4.12)$$

which defines the relations between the position of the maximum tensile stress on the boundary of the elliptical flaw (α) and the inclination of this flaw (β) to the direction of the minimum principal stress σ_3 .

Since fracture is assumed to occur when the tangential stress on the boundary of the flaw exceeds the local tensile strength of the material, it can be assumed that the crack will propagate in a direction which is normal to the boundary of the ellipse. The normal to the ellipse defined by the equation given in Figure 4.2 is defined by

$$\tan \gamma = \frac{-dx}{dy},$$

where

$$\left. \begin{aligned} dx &= -a \cdot \sin \alpha \cdot d\alpha \\ dy &= ma \cdot \cos \alpha \cdot d\alpha \end{aligned} \right\} \quad (4.13)$$

Hence

$$\tan \gamma = \frac{\tan \alpha}{m} \quad (4.14)$$

But, since α is small, $\tan \alpha \rightarrow \alpha$, hence

$$\tan \gamma = \frac{\alpha}{m} = -\tan 2\beta \quad (4.15)$$

or

$$\gamma = -2\beta \text{ or } (\pi - 2\beta) \quad (4.16)$$

This relation is illustrated in Figure 4.4. From equation (4.11) it can be seen that as soon as $\tau_{xy} > 0$, $\beta > 0$, therefore $\gamma > 0$ and hence the crack which initiates on the boundary of the flaw will tend to propagate out of the plane of the flaw. This is a very important result and it is interesting to investigate the propagation of this crack in greater detail.

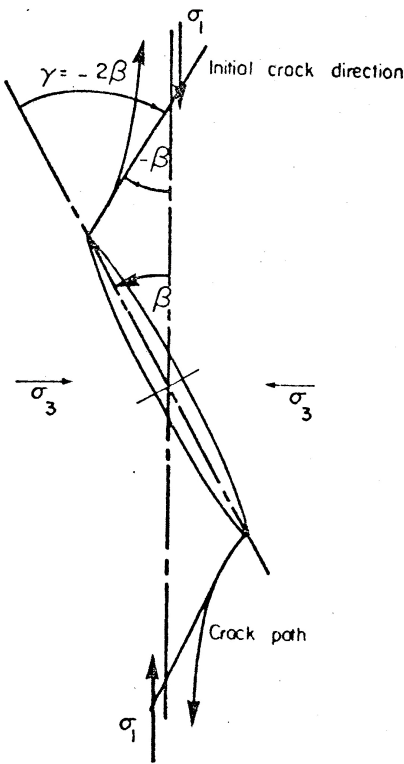


Figure 4.4 Direction of crack propagation from the tip of an elliptical flaw under compressive stress conditions.

4.3.1 Fracture propagation when $\tau_{xy} = 0$

From equations (4.11) and (4.16), when $\tau_{xy} = 0$, $\beta = 0$ and $\lambda = 0$. In other words, under conditions of uniaxial tensile stress to which the crack is perpendicular, a crack is initiated at the tip ($\alpha = 0$) of the elliptical flaw and it will propagate in the plane of the initial flaw.

Substituting $\tau_{xy} = 0$ and $\alpha = 0$ in equation (4.4) gives

$$\sigma_b = \frac{2\sigma_y}{m} = \frac{2\sigma_3}{m} \quad (4.17)$$

If it assumed that the radius of curvature of the propagating crack is of the same order of magnitude as the radius of curvature of the original elliptical flaw, then propagation of this crack has the same effect as decreasing the axis ratio m of the original flaw. From

Brittle fracture of rock

equation (4.17) it will be seen that this results in an increase in the boundary stress σ_b and hence the crack will continue to propagate, even if the applied stresses are decreased.

Under these conditions the propagation of this crack results in tensile rupture¹ of the specimen. An important conclusion which can be drawn from this discussion is that tensile rupture will occur in a plane defined by $\beta=0$, i.e. in a plane which is perpendicular to the direction of the applied tensile stress σ_3 .

4.3.2 Fracture propagation when $\tau_{xy} > 0$

As already discussed, when $\tau_{xy} > 0$, the crack which initiates on the boundary of the elliptical flaw propagates out of the plane of this flaw. It has been demonstrated experimentally (Brace & Bombolakis 1963; Hoek & Bieniawski 1965) and theoretically (Paul & Gangal 1966; Bray, personal communication) that this propagating crack will follow a curved path as indicated in Figure 4.4. This crack path tends to align itself along the direction of the major principal stress σ_1 which, in effect, gives rise to a situation in which the equivalent elliptical flaw is inclined at $\beta=0$ and the stress at the tip of the propagating crack can be approximated from equation (4.17).

When $\sigma_3 > 0$, i.e. when σ_3 is compressive, an entirely different situation occurs in that the stress at the tip of the propagating crack becomes compressive when the crack is aligned in the direction of the major principal stress σ_1 . Under these conditions propagation of the crack will cease and the new flaw so created will be stable under the existing conditions of applied stress.

The length of the crack which propagates from an open elliptical flaw for a given combination of applied stresses has been determined experimentally by Hoek and Bieniawski (1965) and the results of these experiments are plotted in Figure 4.5.

The important conclusion to be drawn from these results is that a single open elliptical flaw cannot cause rupture of a rock specimen under conditions in which that applied stresses (σ_1 and σ_3) are both compressive.

¹ In this discussion the disintegration of the specimen into two or more separate pieces will be termed *rupture*.

4.4 Rock fracture in compression

When the principal stresses σ_1 and σ_3 applied to a rock body containing an open elliptical flaw are both compressive, the crack which is initiated on the boundary of this flaw will only propagate a short distance before it stops and becomes stable (Figure 4.5). In considering the problem of rupture under compressive stress, it is necessary to determine the conditions necessary to propagate the stable crack described above or the conditions necessary to initiate some new failure mode.

Experimental evidence obtained by Hoek and Bieniawski (1965) suggests that propagation of the stable cracks which were initiated from open flaws occurs when the shear resistance of the zone containing these flaws is overcome and shear movement occurs as suggested in Figure 4.6.

The condition for the onset of shear movement may be expressed by the following equation:

$$\tau_{xy} = \tau_o + \mu\sigma_y \quad (4.18)$$

where τ_o is the intrinsic shear resistance of the material, i.e. the shear resistance when the normal stress $\sigma_y = 0$ and which is due to interlocking of asperities and to cohesive forces. The coefficient of internal friction μ is the ratio between the shear stress τ_{xy} required to sustain movement, once the intrinsic shear resistance τ_o has been overcome, and the normal stress σ_y .

The criterion expressed by equation (4.18) is familiar to most engineers and is most commonly associated with the names of Navier, Coulomb and Mohr (see Jaeger's 1966 review for historical details).

Since the condition expressed by equation (4.18) is that required to initiate shear movement, it does not follow automatically that this equation defines the conditions for rupture of the specimen. Consequently it is necessary to consider the events which follow initiation of the shear movement in order to establish whether rupture of the specimen will occur.

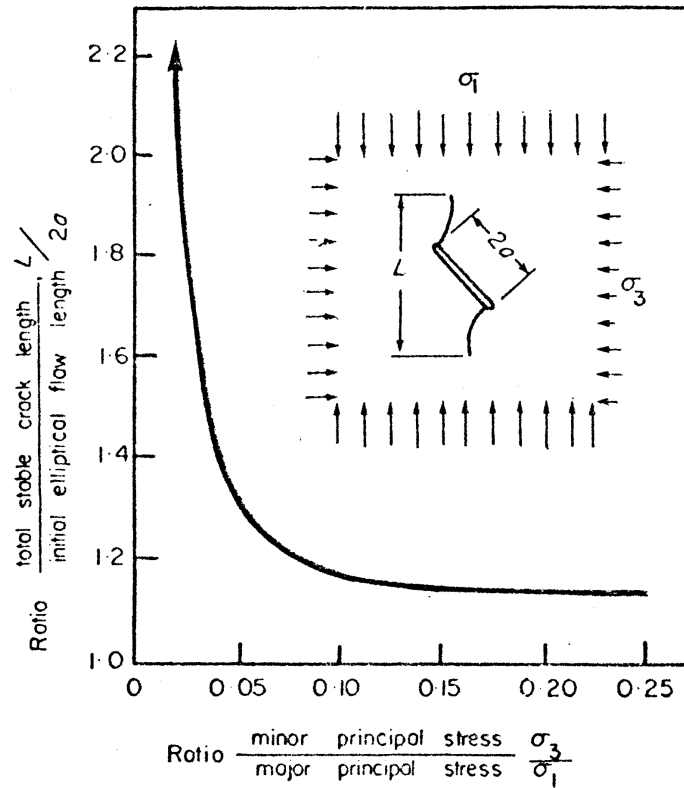


Figure 4.5 Length of stable crack propagated from an elliptical flaw under compressive stress conditions Hoek & Bieniawski 1965

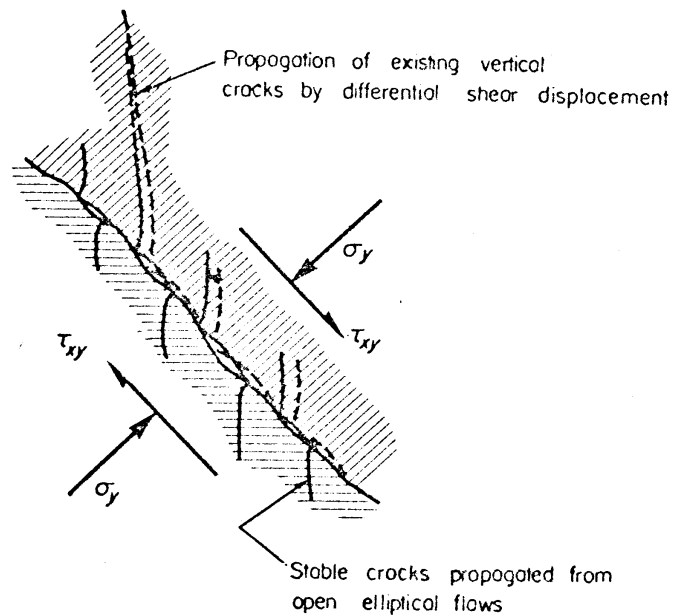


Figure 4.6 Mechanism of fracture propagation caused by displacement on a shear plane

Brittle fracture of rock

In applying the Navier-Coulomb criterion, equation (4.18), to a rock failure problem it is usual to assume that rupture of the specimen takes place as a result of shear movement along a plane inclined at an angle β to the minor principal stress direction as suggested in Figure 4.7(a). The relation between the angle β and the coefficient of internal friction μ can be found by considering the slope of the Mohr envelope as was done earlier in this paper in the case of the Griffith criterion (Figure 4.3):

$$\tan 2\beta = \frac{-d\sigma_y}{d\tau_{xy}} = \frac{-1}{\mu} \quad (4.19)$$

While it is accepted that simultaneous movement on the shear plane is a valid failure mode it is suggested that interlocking of asperities on this plane can also give rise to differential shear movement which results in the propagation of existing vertical cracks, as suggested in Figure 4.6. This would result in the vertical tensile type of rupture illustrated in Figure 4.7(b).

A third possibility is that rupture can occur as a result of some combination of the two modes discussed above, giving a rupture surface which is intermediate between the direction of the major principal stress and the direction of the shear plane which is inclined at an angle β to the major principal stress direction.

A final possibility is that the propagation of either of the above modes could be inhibited by changes in either the stress field or the material properties in the crack path, resulting in a stable crack configuration such as that illustrated in Figure 4.7(c). Propagation of this stable crack system would require a further increase in the applied compressive stress σ_1 .

It will be evident to the reader, from the discussion given above, that the final appearance of a rock specimen which has been tested to rupture under compressive stress conditions will depend upon the size of the specimen and upon the degree of restraint imposed by the testing machine platens. The influence of laboratory test procedures upon the results of rupture tests on rock specimens will be discussed in a later section of this chapter in which the application of such results to practical rock mechanics problems is discussed.

Factors which influence the material 'constants' σ_f , τ_o and μ and the effect of changes in

Brittle fracture of rock

these constants upon the behaviour of the material will also be discussed in a later section of this chapter.

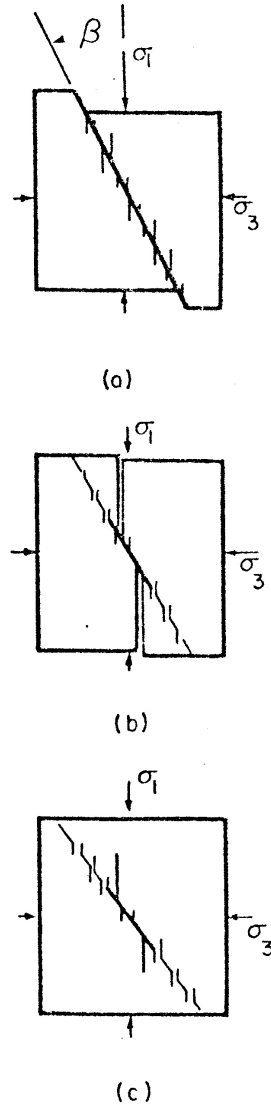


Figure 4.7 Suggested rupture modes under compressive stress conditions, (a) Shear failure; (b) Tensile failure; (c) Stable crack configuration.

4.5 A rupture criterion for brittle rock

In order to obtain the simplest possible rupture criterion for a brittle rock, consider the behaviour of a specimen which contains a large number of randomly oriented flaws of similar size and shape, for example, a carefully selected sample of a homogeneous fine-

Brittle fracture of rock

grained rock, such as Witwatersrand quartzite (Hoek 1966). Such a material will exhibit no significant anisotropy in its strength behaviour and will have a uniaxial compressive strength of approximately ten times its uniaxial tensile strength.

The rupture criterion for such a material can be expected to be a logical extension of the fracture initiation criteria already discussed and the complete rupture criterion is illustrated in Figure 4.8.

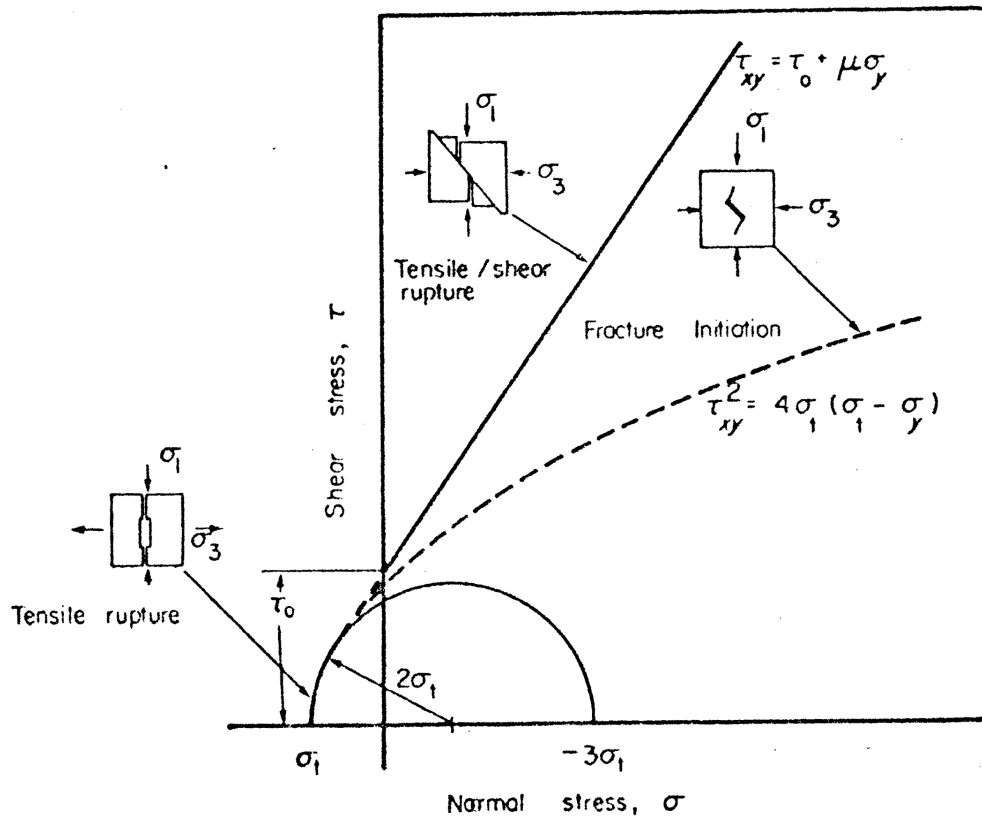


Figure 4.8 A rupture criterion for brittle rock.

In deriving this rupture criterion the following factors were taken into consideration.

(a) The simplest type of tensile rupture occurs when the minor principal stress equals the uniaxial tensile strength of the material, i.e. $\sigma_3 = \sigma_t$. This rupture is caused by the propagation of a crack which initiates at the tip ($\alpha = 0$) of the flaw which is perpendicular to the minor principal stress direction ($\beta = 0$). The conditions under which this type of rupture occurs can be deduced from figure 4.3, from which it can be seen that the radius of curvature of the Mohr envelope at the point of its intersection with the

Brittle fracture of rock

normal stress axis ($\tau_{xy} = 0$) is equal to $2\sigma_t$. Consequently, all Mohr stress circles which fall within this circle of radius $2\sigma_t$ (see Figure 4.8) can only touch the rupture envelope at one point which is defined by $\tau_{xy} = 0$ and $\sigma_3 = \sigma_t$. This implies that pure tensile rupture occurs when $\sigma_1 \leq -3\sigma_3$.

b) Rupture of a rock specimen, when the normal stress acting on the potential shear surface is compressive ($\sigma_y > 0$), is assumed to occur when the shear resistance of this plane is overcome, i.e. when equation (4.18) is satisfied. Shear movement on this plane can induce shear and/or tensile rupture of the specimen as suggested in Figure 4.7.

c) The transition between the conditions which govern pure tensile rupture and the conditions under which rupture is induced as a result of shear displacement cannot be derived directly from the fracture initiation criteria already discussed in this chapter. This difficulty is caused by the fact that the crack which initiates on the boundary of a flaw subjected to a finite shear stress will tend to propagate out of the plane of the flaw (see Figure 4.4). Although this crack will tend to align itself along the major principal stress direction it is not possible to calculate the magnitude of the minor principal stress σ_3 which is required to cause rupture of the specimen. In order to overcome this difficulty it is proposed, on purely phenomenological grounds, that this transition should take the form suggested by the heavy dashed line in Figure 4.8, i.e. it is assumed that the straight-line rupture criterion which defines shear-induced rupture is tangential to the parabolic Mohr envelope which defines fracture initiation from open elliptical flaws.

From the geometry of the rupture diagram presented in Figure 4.8, it is possible to estimate the relation between the intrinsic shear strength τ_o and the uniaxial tensile strength σ_t :

$$\tau_o = -\sigma_t \left(\frac{1}{\mu} + \mu \right) \quad (4.20)$$

The practical significance of this relation is that it enables an estimate of the maximum uniaxial tensile strength of a particular material to be obtained from the value of the intercept τ_o of a Mohr rupture envelope fitted to a number of triaxial compression or shear test results.

Practical experience (Hoek 1966) confirms that the rupture criterion proposed in Figure 4.8 provides an adequate basis for predicting the stresses required to cause rupture of a

brittle rock material under the conditions normally encountered in mining or civil engineering rock mechanics problems². However, from the discussion on the direction of fracture propagation (Figure 4.7), it is evident that no reliable estimate of the angle of rupture of a rock specimen can be made from the Mohr rupture diagram presented in Figure 4.8. In other words, the angle 2β subtended by the normal to the rupture envelope (see Figure 4.3) defines the orientation of the flaw from which fracture initiates or upon which shear displacement occurs but it gives no information on the subsequent path which the fracture will follow. The author believes that the angle of rupture of an element of rock is critically dependent upon the restraints imposed upon it by the testing machine platens, in the case of a laboratory test, or by the surrounding material in the case of a rock structure. A great deal of careful thought and experimentation has still to be devoted to this problem in order to clarify the current confusion which exists in relation to the angle of rupture of rock materials.

4.6 Factors which influence the rupture behaviour of rock

The 'ideal' brittle material upon which the derivation of the fracture initiation and rupture criteria presented above is based cannot be considered representative of the material which would be found in a rock structure, such as a dam foundation or the rock surrounding a mine excavation. Nor can the conditions to which a carefully selected laboratory test specimen is subjected be regarded as representative of the wide variety of conditions which are likely to be encountered in the field.

Obviously, a theoretical rupture criterion which accounts for all possible deviations from the 'ideal' would be far too complex to have any practical value. On the other hand, the 'ideal' would be far too complex to have any practical value if some estimate can be made of the extent to which the rock behaviour is likely to be influenced by deviation from the idealized assumptions.

² Deviations from the linear Mohr envelope defined by equation (4.18) are discussed in a later section of this chapter.

4.6.1 Influence of moisture on the strength of rock

The presence of moisture in a rock body can influence the rupture behaviour of the rock in two important ways:

a) The moisture can reduce the strength of the rock by chemical or physical alternation of its inherent properties. This strength reduction can be very important; for example, the results obtained by Colback and Wiid (Colback & Wiid 1965) for tests on a quartzitic shale (Figure 4.9) show that the strength of specimens which had been dried over calcium chloride for several weeks. This finding emphasizes the need to simulate field conditions as closely as possible in the laboratory and, if in doubt, to assume the worst conditions and to test the specimens in a saturated state.

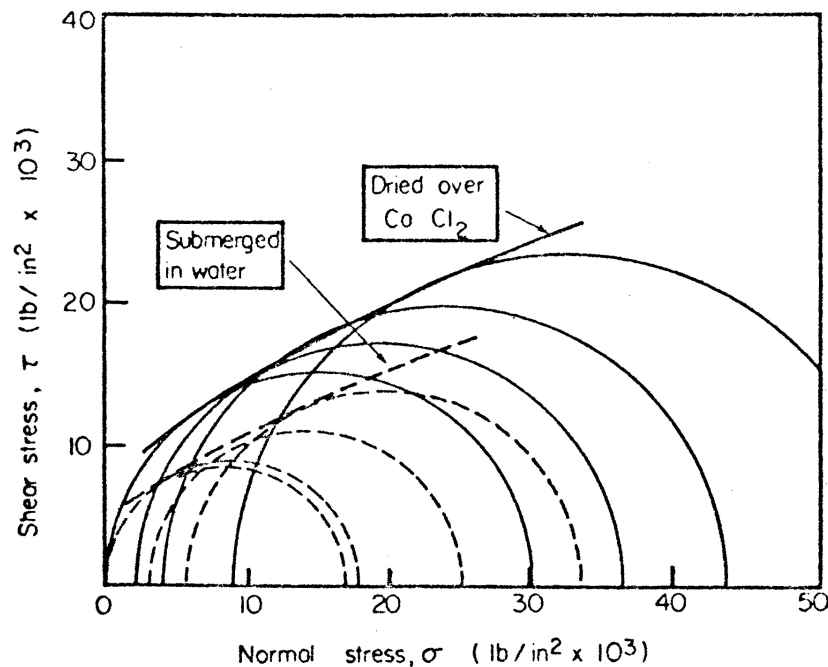


Figure 4.9. Mohr rupture envelopes showing the effect of moisture on the compressive strength of quartzite shale (Colback & Wiid 1965)

(b) If the moisture is present under pressure, the strength of rock is further reduced. Numerous experimental observations (e.g. Murreli 1966 and Byerlee in press) have

Brittle fracture of rock

confirmed the theoretical prediction that the influence of pore pressure can be allowed for in the rupture criteria discussed in this chapter by replacing the normal stress σ_y by an effective stress $(\sigma_y - p)$. Noting that a compressive stress of magnitude p balances the internal pore pressure, it is clear that only the excess $\sigma_y - p$ can be effective in developing tensions. Consequently, equation (4.10) becomes

$$\tau_{xy}^2 = 4\sigma_t \{ \sigma_t - (\sigma_y - p) \} \quad (4.21)$$

while equation (4.18) becomes

$$\tau_{xy} = \tau_o + \mu (\sigma_y - p) \quad (4.22)$$

It is important to note that in any testing involving a study of the influence of moisture or of pore-pressure effects, the rate of loading of the specimen is a critical factor. The discussion presented above is based upon static stress conditions and unless the rate of loading is low enough to permit the pore pressure to distribute itself uniformly throughout the volume of the specimen or, in the case of a drained test, to prevent the build up of dynamic pore pressures, the conclusions presented above will not be valid³.

4.6.2 Influence of the normal stress upon the frictional behaviour of rock

The envelope fitted to a set of Mohr circles obtained from low pressure triaxial compression tests on brittle rocks is usually adequately represented by a straight line as suggested by equation (4.18) (Wuerker 1959). Since many civil and mining engineering applications involve low confining pressures (up to say one-half the uniaxial compressive strength of the rock), the assumption that the coefficient of friction μ is a constant is sufficiently accurate for these applications.

However, in the case of problems involving high confining pressures such as those which may be encountered in deep-level mining or in problems of interest to the geologist, this

³ Professor W. F. Brace of the Massachusetts Institute of Technology, in a personal communication to the author, gives the critical strain rate for the loading of a small specimen (approximately 0.5 inch diameter x 1.5 inches long) of Westerly granite as approximately 10^{-7} in/in/s.

assumption can be seriously in error. The assumption that the coefficient of friction is a constant can also be misleading in the case of 'soft' rocks, such as shales and siltstones, which exhibit non-linear rupture envelopes, even at very low confining pressures.

Experimental evidence obtained by Murrell (1966), Hobbs (1966), Patton (1966) and Byerlee (in press) suggests that the coefficient of internal friction μ in equation (4.18) is not a constant but depends upon the magnitude of the normal compressive stress σ_y . The reason for this breakdown of Amonton's law of friction is associated with the interlocking of the asperities on the shear plane (see Figure 4.6). This interlocking depends upon the intimacy of the contact of the asperities which, in turn, depends upon the magnitude of the normal stress σ_y .

Although a number of theoretical models of this interlocking behaviour have been considered (Murrell 1966; Hobbs 1966; Byerlee in press), the problem has not been adequately solved and, in the author's opinion, a considerable amount of theoretical work is still necessary. However, in the absence of a rigorous theoretical solution, a useful empirical solution can be obtained by assuming that the rupture behaviour of a brittle rock can be characterized by the following equation:

$$\tau_{\max} = \tau_{\max o} + A\sigma_m^b \quad (4.23)$$

where $\tau_{\max} = \frac{1}{2}(\sigma_1 - \sigma_3)$ is the maximum shear stress,

$\sigma_m = \frac{1}{2}(\sigma_1 + \sigma_3)$ is the mean normal stress

and $\tau_{\max o}$ is the intercept of the τ_{\max} versus σ_m plot when $\sigma_m = 0$.

The reasons for the choice of the *maximum* shear stress τ_{\max} and the *mean* normal stress σ_m in place of the shear and normal stresses τ_{xy} and σ_y as suggested by (Murrell 1966) and (Hobbs 1966) are important and are worthy of some consideration.

In analysing the results of conventional triaxial compression tests, we are faced with the problem of determining the values of the shear and normal stresses τ_{xy} and σ_y from the experimentally determined values of the applied axial and lateral stresses σ_1 and σ_3 ($= \sigma_2$). If the inclination β of the plane upon which the shear and normal stresses act is

known, their values can be calculated from equations (4.1) and (4.2). However, as discussed earlier in this chapter, available evidence suggests that the fracture path is a complex one which may have no direct relation to the shear and normal stresses which were responsible for its initiation and propagation (see Figure 4.7b). In addition, current triaxial testing techniques are such that the fracture path is almost certainly influenced by platen effects and by the non-uniformity of the stress distribution in the specimen at the final stages of rupture. Consequently, any attempt to determine the inclination β of the rupture surface from the configuration of a ruptured triaxial specimen must be treated with suspicion.

In order to overcome these difficulties, the author suggests the use of the maximum shear stress and the mean normal stress which can be calculated directly from the axial stress σ_1 and confining pressure σ_3 values obtained from a set of triaxial tests. It will be seen from Figure 4.11 that, for an actual set of experimental results, the τ_{\max} versus σ_y plot is closely related to the τ_{xy} versus σ_y relation which is assumed to be defined by the Mohr envelope. This suggests that the relation proposed in equation (4.23) and a similar relation between τ_{xy} and σ_y proposed by Murrell (1966) and Hobbs (1966) are not contradictory and that the advantage of using equation (4.23) depends solely upon its practical convenience⁴.

In order to evaluate the constants A and b in equation (4.23) for a given material, it is convenient to rewrite the equation in the following form:

$$\log_{10} \frac{\tau_{\max} - \tau_{\max o}}{\sigma_c} = \log_{10} A + b \log_{10} \frac{\sigma_m}{\sigma_c} \quad (4.24)$$

where σ_c is the uniaxial compressive strength of the material.

The advantage of normalizing the experimental results by dividing each measured value by the uniaxial compressive strength of a number of tests on the same plot. This advantage is obvious in Figure 4.10 in which the results of triaxial tests on the eight

⁴ An interesting application of the maximum shear stress versus mean normal stress plot has been described by the author (Hoek 1966) in connection with the analysis of rock fracture around underground excavations by means of photoelastic models

sandstones listed in Table 4.1 are plotted on the same graph. Normalizing the results has the additional advantage of minimizing the influence of testing techniques, specimen sizes and environmental conditions since these conditions are usually common to both numerator and denominator of the dimensionless ratios.

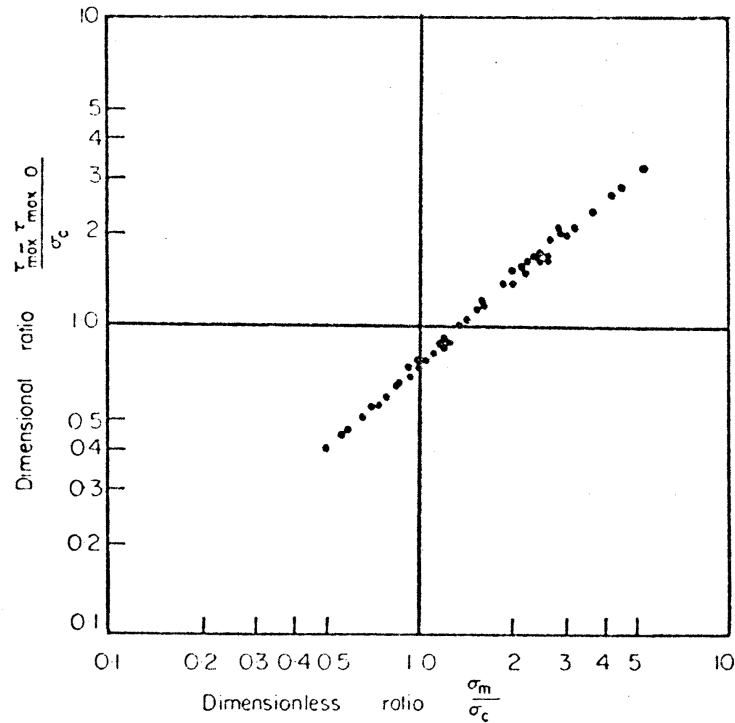


Figure 4.10 Relation between the maximum shear and mean normal stresses at rupture for sandstones

Plotting the experimental results on logarithmic scales permits a direct evaluation of the constants A and b since A is given by the value of $(\tau_{\max} - \tau_0)/\sigma_c$ when $\sigma_m/\sigma_c = 1$, ($\log_{10}(\sigma_m/\sigma_c) = 0$), and the value of b is given by the slope of the straight line through the experimental points. However, complete evaluation of the constants requires that the value of the intercept $\tau_{\max 0}$ be known and, in the absence of experimental values, the author suggests that a reasonable estimate is given by $\tau_{\max 0}/\sigma_c = 0.1$.

Fitting the best straight line to the experimental points plotted in Figure 4.10 by the method of least squares and substitution of the resulting values of A and b into equation (4.23) gives

$$\frac{\tau_{\max}}{\sigma_c} = 0.1 + 0.76 \left(\frac{\sigma_m}{\sigma_c} \right)^{0.85} \quad (4.25)$$

which, as shown in Figure 4.11, adequately defines the rupture behaviour of the sandstones listed in Table 4.1.

Table 4.1 Sandstones included in Figure 4.10

Name	Experimenter	Country	Uniaxial compressive strength	
			lb.in ²	kg/cm ²
---	Jaeger	Australia	9,000	633
Darley Dale 1	Price	England	5,780	406
Pennant	Price	England	22,500	1,582
Rush Springs	Bredthauer	America	25,000	1,758
Iwaki	Horibe and Kobayashi	Japan	1,780	125
----	Everling	Germany	18,500	1,300
Darley Dale II	Murrell	England	11,500	1,300
Warmbaths	Wiid	South Africa	14,750	1,037

In Figure 4.11, a set of idealized Mohr circles and their envelope are shown and it will be noted that, having defined the relation between the maximum shear stress and mean normal stress, the construction of these circles and the fitting of the envelope is reduced to a simple and reliable graphical operation. This is in contrast to the difficulties of fitting an envelope by eye to a set of experimentally determined Mohr circles since such an envelope is invariably fitted to the circles of maximum diameter and does not take into account the scatter of the experimental values⁵.

⁵ The interested reader can easily check this difficulty for himself by constructing a few Mohr circles from the experimental values given in Figure 4.11 and noting the exaggerated curvature of the envelope fitted to the maximum diameter circles.

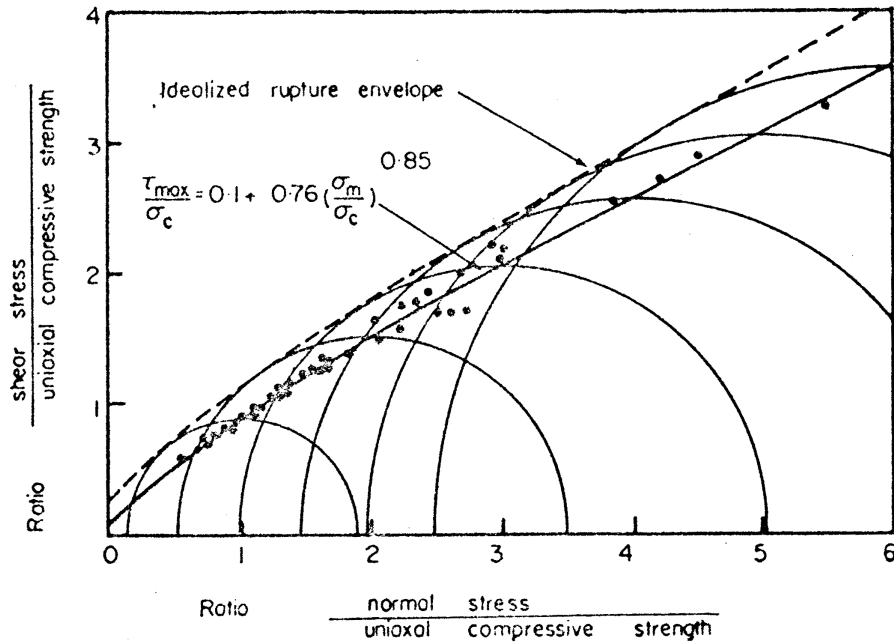


Figure 4.11 Mohr stress diagram for the rupture of sandstone.

Although no attempt is made here to develop the theoretical relation between the Mohr envelope and the τ_{max} versus σ_y plot, it is interesting to examine the relation between the intrinsic shear strength τ_o and the maximum shear stress intercept $\tau_{max o}$. As discussed earlier in this chapter, pure tensile rupture is assumed to occur when $\sigma_1 \leq -3\sigma_3$ which means that all Mohr stress circles within this stress range touch the envelope at one point defined by $\sigma_3 = \sigma_t$ (see Figure 4.8). Rupture under conditions of pure shear, i.e. $\sigma_1 = -\sigma_3$, falls into this category and it can be seen from Figure 4.,8 that the radius of the Mohr circle defining this condition is equal to σ_t and, since this circle defines the maximum shear stress intercept ($\sigma_m = 0$), it follows that

$$\tau_{max o} = \pm\sigma_t \tag{4.26}$$

Comparing equations (4.20) and (4.26) gives

$$\frac{\tau_o}{\tau_{max o}} = \left(\frac{1}{\mu} + \mu \right) \tag{4.27}$$

and substitution of a range of values for μ between 0.5 and 2 shows that a reasonable estimate for the relation between τ_o and $\tau_{max o}$ is given by

$$\tau_o \cong 2\tau_{\max o} \quad (4.28)$$

Although the prime purpose of plotting the triaxial test results for sandstone in Figures 4.10 and 4.11 is to demonstrate the influence of the normal stress upon the frictional behaviour of rock, these figures cannot be left without noting the remarkable similarity in the rupture behaviour of the eight sandstones which, from the information given in Table 4.1, have widely varying geographical locations and geologic materials, any attempt at an explanation of this similarity would be based on pure speculation and would be out of place in this chapter. However, since similar patterns of behaviour have been noted for many other rock types (Hoek & Bieniawski 1965; Hoek 1966), the practical significance of such patterns, even if they can only be defined by empirical relations such as that suggested by Equation (4.23), is important.

Following the thoughts which probably motivated Wuerker (1959) when he prepared his annotated tables of rock strength, it is suggested that the availability of a collection of dimensionless results, such as those presented in figure 4.10, could be of considerable assistance to the practical engineer who may have neither the time nor the facilities to carry out the large number of triaxial tests necessary to define the behaviour of the material with which he is concerned. In order to obtain an estimate of the behaviour of a particular material, it would only be necessary to determine the uniaxial compressive strength σ_c , under the environmental conditions and using the testing technique and size of specimen most appropriate to the particular problem under consideration. Substitution of this value of σ_c into the characteristic equation of that type of material (e.g. equation (4.25) for sandstone) would give a τ_{\max} versus σ_m plot, and if necessary the Mohr circles and envelope, which would be sufficiently accurate for most practical purposes⁶. †

⁶ The author wishes to make it quite clear that he does not advocate the procedure suggested above as a solution to all problems of rock testing. The curve which defines the rupture behaviour of a rock may be an extremely useful tool but it cannot replace the 'feel' of his material which an engineer can only obtain by working with it and observing its behaviour under test conditions. However, since the ever-increasing demands of progress restrict the time which the modern engineer can afford to spend on the luxury of getting to know his material, the suggested procedure, while academically unattractive to the physicist, may still prove very practical in engineering application. In order to implement the ideas outlined above, a research project has been initiated at Imperial College, London, which involves the collection and computer analysis of all available results for triaxial rock tests, using published data and whatever raw data it proves practical to obtain.

4.6.2 Influence of anisotropy on the strength of rock

The ideal brittle rock, upon which most of the discussion presented thus far has been based, is assumed to contain a large number of randomly oriented flaws of equal size. These conditions would very seldom be found in practical rock mechanics problems and, hence, it is necessary to make an estimate of the probable influence of anisotropy would exceed the scope of this chapter and it will suffice to illustrate the main points of practical interest by one example.

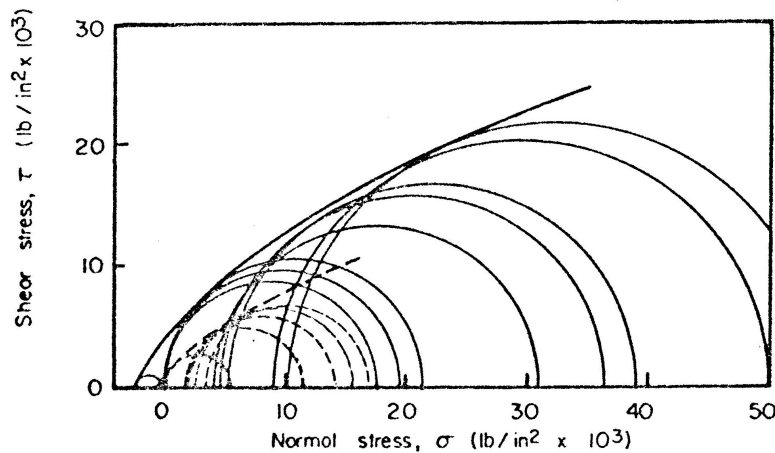


Figure 4.12 Mohr envelopes defining the rupture behaviour of the bedding planes (dashed line) and parent material (solid line) of a South African slate.

Figure 4.12 shows the rupture behaviour of a South African slate (Hoek 1964). The solid line is for tests carried out on specimens in which the bedding planes were oriented in such a way as to minimize their influence ($\beta = 90^\circ$ for tensile tests and $\beta = 90^\circ$ or 0° for compressive tests). The dashed envelope represents the results obtained from specimens in which the bedding planes were oriented to exert their maximum influence $\beta = 0$ for tensile tests and $\beta = \frac{1}{2} \arctan \frac{1}{\mu}$ for compression tests).

It is evident from this figure that the rupture envelope of the slate in its weakest state is merely a scaled down version of the rupture envelope for the strongest state. Plotting these results on dimensionless logarithmic scales as was done in figure 4.29 confirms that the constants A and b (equation 4.23) are not significantly different for these two rupture envelopes but Figure 4.10 shows that the value of the uniaxial compressive strength σ_c

Brittle fracture of rock

varies by a factor of approximately 4, depending upon the orientation of the bedding planes to the principal stress directions.

The practical significance of these findings is that, in problems in which the principal stress directions and major weakness planes in the material are known, the appropriate value of σ_c can be determined and used in analysing the rupture behaviour of the rock. Hence, for example, the analysis of the stability of a slope in which the rock contains well-defined planes of weakness must take the orientation of these planes into account. Note that, in such cases, the weakness planes may contain soft filling material which may reduce the frictional resistance of this plane, i.e. the values of A and b will differ from those of the parent material and must be determined independently.

In cases in which the orientations of the weakness planes in relation to the principal stress directions are not known, it can only be assumed that the rupture behaviour of the material will lie somewhere between the two envelopes representing its weakest and strongest states (e.g. Figure 4.12 for slate). Since this would be the case in many practical rock mechanics problems, it is suggested that, where the stability of a structure is at stake, the only safe course to follow is to use the envelope defining the weakest state of the material.

4.6.4 Influence of laboratory testing techniques upon the rupture of rock

A large proportion of the research effort which has gone into building up the science of rock mechanics has been devoted to the detailed study of laboratory testing techniques. Jaeger (1966) has given an excellent review of this work which includes studies of the influence of specimen geometry, platen friction, rate of loading, size of specimen and of the stiffness of the testing machine upon the behaviour of the rock specimen. No useful purpose would be served by attempting to repeat the details of this review and the following discussion will be confined to certain basic principles of rock testing.

The results of presented in Figures 4.10 and 4.11 suggest that the *shape* of the characteristic curve which defines the rupture behaviour of a rock is largely independent of the method of testing. Consequently, in choosing a testing technique, which determines the *position* of the characteristic curve on the $\tau - \sigma$ plane, it is necessary to consider:

Brittle fracture of rock

a) the basic principles of materials testing which have to be fulfilled and

b) the purpose for which the test results are required.

The most important requirement which must be met in carrying out a test is that it must be possible to determine the stresses acting on the specimen. Since most rocks exhibit some degree of anisotropy and all rock become anisotropic as a point of rupture is approached (Walsh 1965; Brace, Pauling & Scholz 1966), any test specimen in which there are significant stress gradients and for which the stress at rupture has to be calculated on the basis of the theory of elasticity must be treated with suspicion. This applies to specimens tested in bending, torsion and to certain indirect tests which involve high stress gradients, e.g. indentation of the specimen with a steel ball or diamond point. The simplest solution to the problem is to choose a specimen geometry which permits calculation of the applied stresses from a simple load/area relation. However, even when this condition is met, e.g. in the case of a cylindrical specimen subjected to direct compressive stress, it is still necessary to ensure that stress gradients are not induced as a result of poor end conditions (Hoek 1966, Mogi, 1966).

The purpose for which the results of laboratory tests on rock specimens is required can have an important bearing upon the test method chosen. This is particularly true in relation to the direction of the most important failure surface in a ruptured specimen (Figure 4.7). For example, if the results of a set of laboratory tests are to be applied to a slope stability problem in which the shear rupture mode (Figure 4.7a) is of prime importance, an applied stress condition which encourages the development of this shear mode, i.e. a shear-box test, would be a logical choice for the test method.

In the case of the rock surrounding underground mine excavations, both tensile and shear modes may be important. An even more important consideration may be the stress redistribution associated with fracture which may result in the load on an element being relieved if it tends to deform by a large amount in relation to the surrounding rock. An appreciation of this problem has led to the development of 'stiff-machine' testing techniques (Cook and Hojem 1966; Bieniawski in submission) which restrict the strain which takes place in the specimen.

The conclusion to be drawn from the discussion presented above is that, while it is

important to exercise care in preparing and testing rock specimens, it is even more important to give serious consideration to the use to which the results are to be put. Unless the test method chosen bears a direct relation to the problem under consideration, a great deal of effort can be expended on obtaining information which may have little or no practical significance.

References

- Bieniawski, Z.T. Paper submitted. Mechanism of brittle fracture of rock. submitted to *Intern. J. Rock Mech. Mining Sci.*
- Brace, W.F. and E.G. Bombolakis 1963. A note on brittle crack growth in compression, *J. Geophys. Res.*, 68, No. 12, 3709-3713.
- Brace, W.F., Paulding, B.W. and C. Scholz 1966. Dilatancy and fracture of crystalline rocks, *J. Geophys. Res.*, 71, No. 16, 3939-3953.
- Bray, J.W. personal communication.
- Byerlee, J.D. In press. A theory of friction based on brittle fracture, *J. Appl Phys.*
- Byerlee, J.D. In press. The frictional characteristics of granite under high confining pressure, *J. Geophys. Res.*
- Colback, P.S.B. and B. L. Wiid 1965 The influence of moisture content on the compressive strength of rock, *Proc. Symp. Rock Mech.*, 3rd, Toronto.
- Cook, N.G.W. and J.P.M. Hojem, 1966. A rigid 50-ton compression and tension testing machine. *S. African Mech. Engr.*, Nov., 89-92.
- Denkhaus, H.G. 1964. The application of the mathematical theory of elasticity to problems of stress in hard rock at great depth. *Bull. Inst. Mining Met.*, 68, 283-309.
- Donath, F.A. 1964. Strength variation and deformation behaviour in anisotropic rock. In *State of Stress in the Earth's Crust* (Ed. W.R. Judd), Elsevier: New York, pp. 281-298.
- Griffith, A.A. 1924. Theory of rupture, *Intern. Congr. Appl. Mech.*, 1st, Delft, 55-63.
- Griffith, A.A. 1921. The phenomena of rupture and flow in solids. *Phil. Trans. Roy. Soc. London, Series A*, 221, 163-198.
- Hobbs, D.W. 1966. A study of the behaviour of broken rock under triaxial compression,

Brittle fracture of rock

- and its application to mine roadways, *Intern. J. Rock Mech. Mining Sci.*, 3, 11-43.
- Hoek, E. 1964. Fracture of anisotropic rock. *J. S. African Inst. Mining Met.*, 64, 510-518.
- Hoek, E. 1966. A photoelastic technique for the determination of potential fracture zones in rock structures. *Symp. Rock Mech.*, Minnesota, (Proceedings to be published by AIME, 1967).
- Hoek, E. 1966. Rock mechanics - an introduction for the practical engineer. *Mining Mag.* (London), April, June, July issues.
- Hoek, E. and Z. T. Bieniawski 1965. Brittle fracture propagation in rock under compression, *Intern. J. Fracture Mech.*, 1, No. 3, 137-155.
- Inglis, C.E. 1913. Stresses in a plate due to the presence of cracks and sharp corners, *Trans. Inst. Naval Architects*, London, 55, Part I, 219-230.
- Jaeger, J.C. 1966. The brittle fracture of rocks. *Symp. Rock Mech.*, Minnesota, (Proceedings to be published by AIME, 1967).
- K. Mogi 1966. Some precise measurements of fracture strength of rocks under uniform compressive stress, *Rock Mech. Eng. Geol.*, 4, Part 1, 43-55.
- Murrell, S.A.F. 1966. The effect of triaxial stress systems on the strength of rocks at atmospheric temperatures, *Geophys. J.*, 10, No. 3, 231-281.
- Patton, F.D. 1966. Multiple modes of shear failure in rock, *Proc. Intern. Congr. Rock Mech.*, Lisbon, 509-514.
- Paul, B. and M. Gangal 1966. Initial and subsequent fracture curves for biaxial compression of brittle materials, *Symp. Rock Mech.*, Minnesota, 1966 (Proceedings to be published by AIME, 1967).
- Walsh, J. B. and W. F. Brace 1964. A fracture criterion for anisotropic rock. *Geophys. Res.*, 69, No. 16, 3449-3456.
- Walsh, J.B. 1965. The effect of cracks on the compressibility of rock, *Geophys. Res.*, 70, No. 2, 381-389.
- Wuerker, R.D. 1959. Annotated tables of strength of rock, *Trans. AIME (Petrol. Div)*, No. 663-669.



Contents lists available at ScienceDirect

Journal of Rock Mechanics and Geotechnical Engineering

journal homepage: www.rockgeotech.org

Review

Fracture initiation and propagation in intact rock – A review

E. Hoek^a, C.D. Martin^{b,*}^a West Vancouver, British Columbia, V7V 0B3, Canada^b Department of Civil & Environmental Engineering, University of Alberta, Edmonton, Alberta, T6G 2W2, Canada

ARTICLE INFO

Article history:

Received 29 April 2014

Received in revised form

7 June 2014

Accepted 10 June 2014

Available online xxx

Keywords:

Tensile failure

Crack propagation

Griffith theory

Hoek–Brown criterion

Tension cutoff

Crack coalescence

Numerical models

ABSTRACT

The initiation and propagation of failure in intact rock are a matter of fundamental importance in rock engineering. At low confining pressures, tensile fracturing initiates in samples at 40%–60% of the uniaxial compressive strength and as loading continues, and these tensile fractures increase in density, ultimately coalescing and leading to strain localization and macro-scale shear failure of the samples. The Griffith theory of brittle failure provides a simplified model and a useful basis for discussion of this process. The Hoek–Brown failure criterion provides an acceptable estimate of the peak strength for shear failure but a cutoff has been added for tensile conditions. However, neither of these criteria adequately explains the progressive coalition of tensile cracks and the final shearing of the specimens at higher confining stresses. Grain-based numerical models, in which the grain size distributions as well as the physical properties of the component grains of the rock are incorporated, have proved to be very useful in studying these more complex fracture processes.

© 2014 Institute of Rock and Soil Mechanics, Chinese Academy of Sciences. Production and hosting by Elsevier B.V. All rights reserved.

1. Introduction

In order to understand the characteristics of rock and rock masses as engineering materials, it is necessary to start with the behavior of intact rock. From an engineering point of view, this involves studying laboratory-scale samples, such as diamond drill core, with dimensions in the range of 50 mm diameter. For many rock types, the grain size is small enough that samples of this scale can be considered homogeneous and isotropic.

The characteristics that will be discussed in the following text are the strength and deformation characteristics of intact rock. As illustrated in Fig. 1, a number of stress states need to be considered and, as is common in most discussions on this topic, it will be assumed that these stress states can be considered in two dimensions. In other words, it is assumed that the intermediate principal stress σ_2 has a minimal influence on the initiation and

propagation of failure in the samples. While some authors consider this to be an over-simplification, a full three-dimensional treatment of the topic would result in complex text which would defeat the purpose of this presentation which is designed to be as clear and understandable as possible.

2. Theoretical fracture initiation: background

2.1. Griffith tensile theory

Griffith (1921) proposed that tensile failure in brittle materials such as glass initiates at the tips of minute defects which he represented by flat elliptical cracks. His original work dealt with fracture in material subjected to tensile stress but later he extended this concept to include biaxial compression loading (Griffith, 1924). The equation governing tensile failure initiation in a biaxial compressive stress field is

$$\sigma_1 = \frac{-8\sigma_t \left(1 + \frac{\sigma_3}{\sigma_1}\right)}{(1 - \sigma_3/\sigma_1)^2} \quad (1)$$

where σ_t is the uniaxial tensile strength of the material. Note that tensile stresses are negative.

Murrell (1958) proposed the application of Griffith theory to rock. In the 1960s, Griffith's two-dimensional theory was extended to three dimensions by a number of authors including Murrell (1958), Sack and Kouznetsov whose work was summarized in books on brittle failure of rock materials by Andrieu (1995) and

* Corresponding author.

E-mail addresses: ehoek@xsmail.com (E. Hoek), derek.martin@ualberta.ca (C.D. Martin).

Peer review under responsibility of Institute of Rock and Soil Mechanics, Chinese Academy of Sciences.



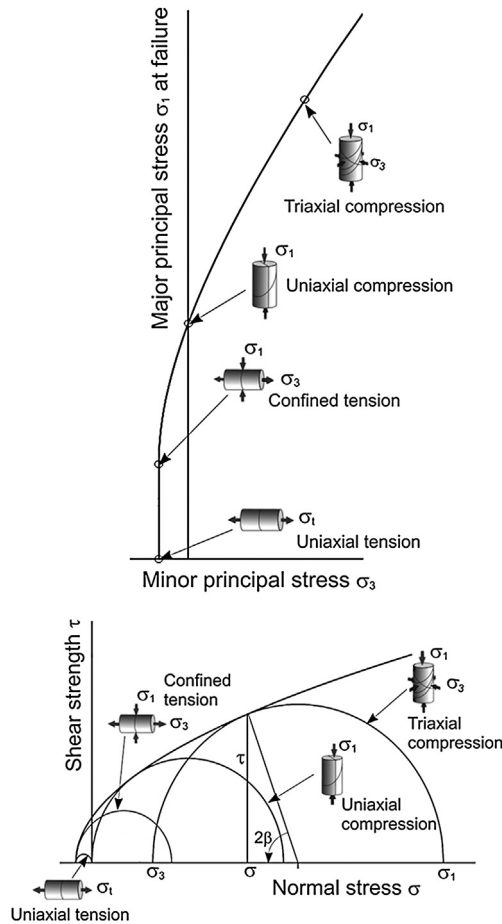


Fig. 1. Typical failure characteristics of intact rock plotted in terms of major and minor principal stresses and Mohr circles and envelope.

Paterson and Wong (2005). These extensions involve examining the stresses induced around open penny-shaped cracks in a semi-infinite body subjected to triaxial compressive stresses σ_1 , σ_2 and σ_3 . It was shown that the intermediate principal stress σ_2 has no significant influence on the crack tip stresses inducing tensile failure initiation. Hence, this criterion is essentially equivalent to loading a penny-shaped crack in a biaxial stress field, as shown in Fig. 2.

The equation governing tensile failure initiation is

$$\sigma_1 = \frac{-12\sigma_t \left(1 + 2\frac{\sigma_3}{\sigma_1}\right)}{\left(1 - \sigma_3/\sigma_1\right)^2} \quad (2)$$

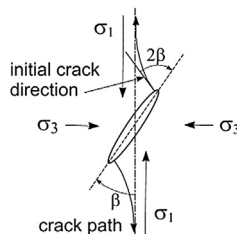


Fig. 2. Tensile crack propagation from an inclined elliptical Griffith crack in a biaxial compressive stress field.

Note that, whereas the original Griffith theory predicts a ratio of compressive to tensile strength $\sigma_c/|\sigma_t| = 8$, the penny-shaped crack version predicts $\sigma_c/|\sigma_t| = 12$. The corresponding Mohr envelope for the penny-shaped crack version is

$$\tau^2 = |\sigma_t|(|\sigma_t| + \sigma) \left(\sqrt{\frac{\sigma_c}{|\sigma_t|} + 1} - 1 \right)^2 \quad (3)$$

where σ_c is the uniaxial compressive strength of the material.

The Griffith theory deals only with the initiation of tensile failure. It cannot be extended to deal with failure propagation and eventual shear failure in compression. However, under certain conditions when tensile stresses exceed the tensile strength, tensile failure initiation can lead to crack propagation. In these cases the tensile cracks propagate along the major principal stress (σ_1) trajectory as shown in Fig. 2.

2.2. Modifications to Griffith theory for closed cracks

The original Griffith theory was derived from analyses of crack initiation at or near the tips of open elliptical cracks. In the case of rocks, most of the defects from which tensile cracks originate are grain boundaries which are usually cemented and have to be considered as closed cracks. McClintock and Walsh (1962) proposed that tensile fracture from closed Griffith cracks can be predicted on the basis of the conventional Mohr–Coulomb equation: where ϕ is the angle of friction and τ_0 is the shear strength at zero normal stress.

$$\tau = \tau_0 + \sigma \tan \phi \quad (4)$$

Hoek (1965) discussed the transition from the Griffith theory for open cracks, which applies for confining stresses $\sigma_3 < 0$, and the modified theory for closed cracks which applies for compressive confining stresses. For the principal stress plot, this transition occurs at $\sigma_3 = 0$, while for the Mohr envelope, the transition occurs at the tangent points on the Mohr circle representing the uniaxial compressive strength σ_c of the intact rock. The transition is illustrated in Fig. 3 in which the principal stress plots are shown for friction angles of 35°, 45° and 55°.

A much more comprehensive discussion on this topic is given in Paterson and Wong (2005) but the plotted results are essentially the same as those shown in Fig. 3. Hence, for the purpose of this discussion, Eq. (4) above is adequate.

Zuo et al. (2008) examined the growth of microcracks in rock-like materials on the basis of fracture mechanics considerations. They assumed a sliding-crack model which generates wing cracks, similar to those shown in Fig. 2, from close to the crack tips when the frictional strength of the sliding surfaces is overcome. They found that the failure initiation criterion can be expressed by the following equation:

$$\sigma_1 = \sigma_3 + \sqrt{\frac{\mu}{\kappa} \frac{\sigma_c}{|\sigma_t|} \sigma_c \sigma_3 + \sigma_c^2} \quad (5)$$

where μ is the coefficient of friction which is equal to the tangent of the friction angle, i.e. $\mu = \tan \phi$.

The coefficient κ is used for mixed mode fracture and it can be derived from various approximations based on a maximum stress criterion or a maximum energy release criterion (Zuo et al., 2008). Plots for Eq. (5), when $\mu = 0.7, 1$ and 1.43 ($\phi = 35^\circ, 45^\circ$ and 55°), $\kappa = 1$ and $\sigma_c/|\sigma_t| = 12$, are included in Fig. 3. Note that the same transition from open to closed crack behavior has been assumed as for the Mohr–Coulomb criterion (Eq. (4)) discussed above.

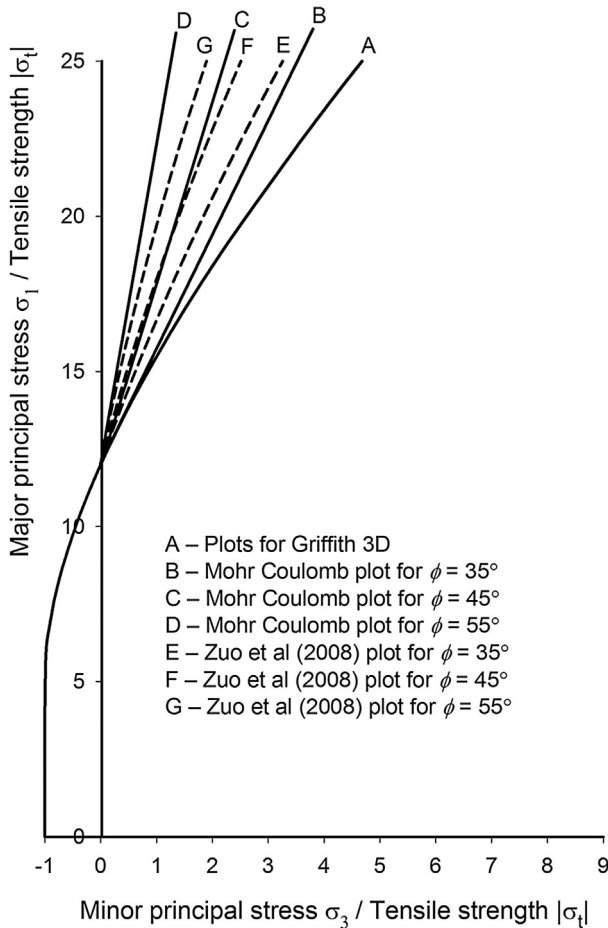


Fig. 3. Principal stress plots for various criteria for tensile failure initiation from closed cracks in brittle materials such as rock.

2.3. Length of induced tensile cracks

Hoek (1965) carried out experiments in which flat open “cracks” were machined ultrasonically into annealed glass plates which were then loaded biaxially. The initiation of tensile cracks from near the tips of these simulated cracks, as predicted by Griffith’s original theory, was confirmed. However, it was found that the length of the tensile cracks was limited by the ratio of the applied biaxial stresses σ_3/σ_1 . As reported by Cho et al. (2007), theoretical studies on closed cracks have been carried out by several authors including Ashby and Hallam (1986), Kemeny and Cook (1987), Germanovich and Dyskin (1988), Martin (1997) and Cai et al. (1998). These studies, the results of which are plotted in Fig. 4, confirm the importance of confinement in limiting the length of induced tensile cracks from pre-existing flaws in brittle materials subjected to compressive loading. Fig. 5 summarizes some of this information in a different form and shows a principal stress plot and Mohr’s diagram for open penny-shaped cracks subjected to different biaxial compressive stress loadings.

2.4. Summary

Griffith theory of brittle fracture initiation and its modifications have been discussed in hundreds of technical papers. A particularly useful review was presented by Fairhurst (1972) which is recommended reading for anyone interested in pursuing this topic in greater depth. While there can be no dispute that this is very important background material for an understanding of the

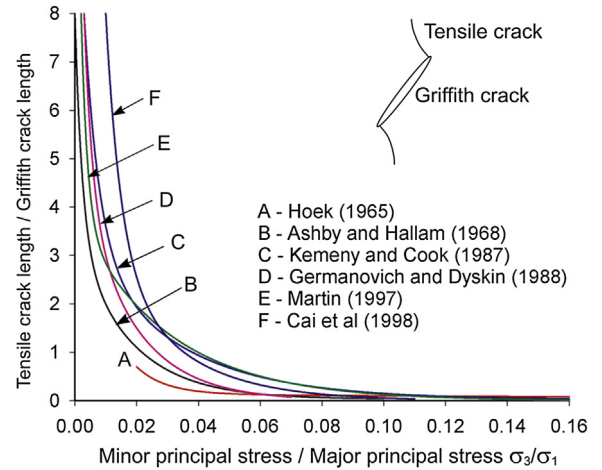


Fig. 4. Dependence of length of tensile cracks on principal stress ratio σ_3/σ_1 .

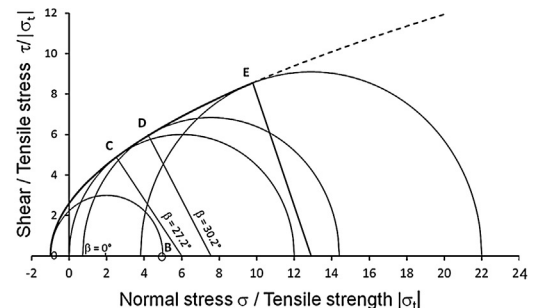
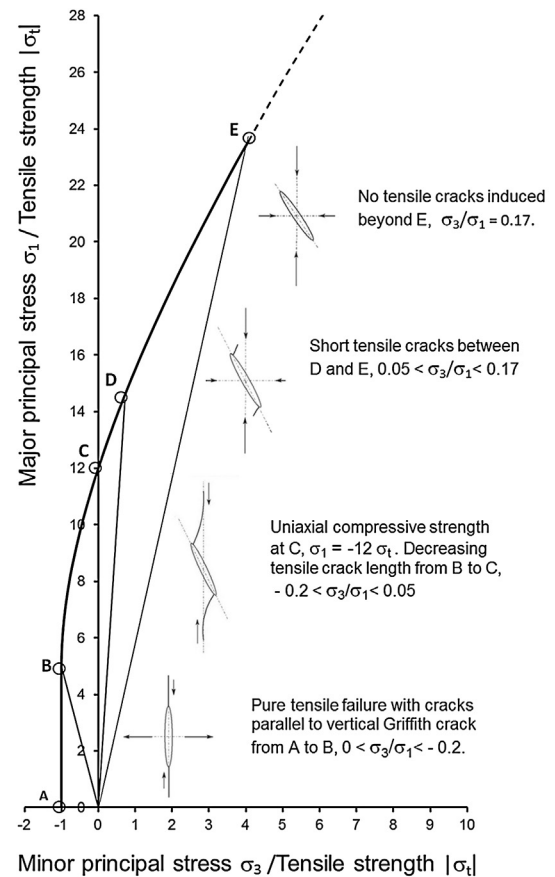


Fig. 5. Plots of principal stresses defining tensile failure initiation from open penny-shaped cracks in a homogeneous isotropic elastic solid loaded biaxially.

mechanics of brittle failure initiation, it is of limited practical value in the field of rock engineering.

This is because an isolated Griffith crack in a semi-infinite plate is an inadequate model of the grain boundary network in which tensile failure originates and propagates in intact rock as shown in Fig. 6. This photograph shows that, while it would always be possible to find a critically oriented grain boundary from which tensile failure could initiate, it is unlikely that the induced crack would follow the path suggested in Fig. 2 for homogeneous isotropic materials. Rather, the tensile crack path would follow a path dictated by grain boundaries with only isolated cracks running across intact grains. This means that we have to explore other more complicated models in order to fully understand the fracture process in rock.

Before leaving the topic of Griffith theory and its modifications, it is worth summarizing what we have learned from the discussion given earlier since the same or similar issues will apply to the numerical analysis of fracture initiation and propagation:

- (1) The brittle failure process initiates and is, to a very large extent, controlled by the tensile strength of intact rock or of its component grains.
- (2) The initiation of tensile cracks at or near the tip of a Griffith crack, whether this crack is open or closed, depends upon the orientation of the Griffith crack in relation to the applied stresses. Fracture will initiate at or close to the tip of a critically oriented crack when the conditions defined by Eqs. (1)–(5) are satisfied, depending upon the assumptions made in deriving these equations.



Fig. 6. Crack path in a specimen of Witwatersrand Quartzite from a deep gold mine in South Africa, sectioned after uniaxial compressive loading to about 75% of the uniaxial compressive strength.

Photograph reproduced from Hoek and Bieniawski (1965).

- (3) This process is extremely sensitive to the degree of confinement and the extent of failure reduces quickly as the minor principal stress (σ_3) increases from $\sigma_3 = \sigma_t$ to $\sigma_3 > 0$, as shown in Figs. 1 and 5.
- (4) At some level of confinement, in the range of $\sigma_3/\sigma_1 \approx 0.2$, tensile failure can be suppressed completely and the peak strength of the intact rock is controlled by shear failure for higher confinement.
- (5) For applications to confined rock materials, the closed Griffith crack model (Eqs. (4) and (5)) is the most appropriate. The shear strength of the confined defects (typically grain boundaries) is a controlling parameter in the initiation and propagation of the tensile failure.
- (6) The ratio of uniaxial compressive to tensile strength ($\sigma_c/|\sigma_t|$) is an important parameter in understanding the failure of rock and similar brittle materials.

3. Fracture initiation and propagation: laboratory tests

3.1. Peak strength and the Hoek–Brown criterion

Hoek and Brown (1980) and Hoek (1983) described the development of the Hoek–Brown failure criterion as a trial-and-error process using the Griffith theory as a starting point. They were seeking an empirical relationship that fitted observed shear failure conditions for brittle rock subjected to triaxial compressive stresses. The equation chosen to represent the failure of intact rock was

$$\sigma_1 = \sigma_3 + \sigma_c \sqrt{m_i \frac{\sigma_3}{\sigma_c} + 1} \quad (6)$$

where m_i is a material constant.

Zuo et al. (2008) pointed out that the substitution of $(\mu/\kappa)(\sigma_c/|\sigma_t|) = m_i$ in their failure criterion (Eq. (5)) leads to the Hoek–Brown criterion for intact rock (Eq. (6)). They suggested that the constant m_i is not simply an empirical constant but that it has real physical meaning.

During the 1970s, when the Hoek–Brown criterion was developed, there was little interest in the tensile strength of rock and, in fact, it was frequently assumed to be zero. The emphasis was on confined shear failure which was assumed to control the stability of the relatively small slopes and shallow tunnels that were constructed at the time. However, with the increase in depth of excavations in civil and mining engineering projects and the depth of boreholes in oil exploration and recovery, the issue of the tensile strength of rock became increasingly important. In particular, the process of brittle fracture which results in splitting, popping, spalling and rockbursting in pillars and tunnels, and “breakouts” in boreholes is a tensile failure process which is not adequately dealt with by the Hoek–Brown failure criterion. Simply projecting the Hoek–Brown equation (Eq. (6)) back to its σ_3 intercept with $\sigma_1 = 0$ does not give an acceptable value for the tensile strength of the rock.

Ramsey and Chester (2004) and Bobich (2005) have investigated this issue in a series of experiments in which they used dogbone-shaped specimens as shown in Fig. 7. By choosing appropriate diameters for the ends and center of the specimen and by adjusting the values of the confining pressure P_c and the axial stress P_a , a range of values of σ_3 and σ_1 can be generated in the test section.

The results of tests on Carrara marble are reproduced in Fig. 8. The Hoek–Brown criterion (Eq. (6)) has been fitted to the shear data obtained in these tests and the resulting curve has been projected back to give an intercept of $\sigma_3 = -17.2$ MPa for $\sigma_1 = 0$. As can be seen in Fig. 8, this does not correspond to the tensile failure data

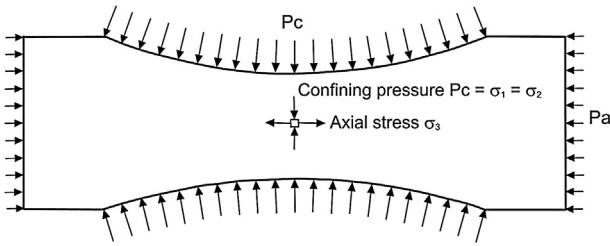


Fig. 7. Dogbone-shaped specimen used by Ramsey and Chester (2004) to investigate tensile failure of Carrara marble.

which gives an average tensile strength $\sigma_3 = -7.75$ MPa. In other words, the Hoek–Brown criterion has no provision for predicting the tensile strength shown in Fig. 8, and highlighted by the “Tension cutoff”.

3.2. Fairhurst’s generalized Griffith fracture criterion

Fairhurst (1964) proposed that the Griffith failure criterion, discussed in Section 2 of this paper, could be generalized in terms of the ratio of compressive to tensile strength $\sigma_c/|\sigma_t|$ as follows (a detailed derivation is given in the Appendix):

- (1) If $w(w - 2) \sigma_3 + \sigma_1 \leq 0$, failure occurs when $\sigma_3 = \sigma_t$;
- (2) If $w(w - 2) \sigma_3 + \sigma_1 > 0$, failure occurs when

$$\sigma_1 = \frac{(2\sigma_3 - A\sigma_t) + \sqrt{(A\sigma_t - 2\sigma_3)^2 - 4(\sigma_3^2 + A\sigma_t\sigma_3 + 2AB\sigma_t^2)}}{2} \tag{7}$$

$$\left. \begin{aligned} A &= 2(w - 1)^2 \\ B &= [(w - 1)/2]^2 - 1 \\ w &= \sqrt{\sigma_c/|\sigma_t| + 1} \end{aligned} \right\} \tag{8}$$

Fitting Eq. (7) to the results plotted in Fig. 8 gives the combined plot shown in Fig. 9.

Reliable direct tensile test data on rock are very rare and the authors have only been able to assemble the limited number of results included in Table 1. However, by fitting both Hoek–Brown and Fairhurst curves to these data, as shown in Fig. 9, it has been possible to arrive at a preliminary relationship between the Fairhurst tension cutoff (defined by $\sigma_c/|\sigma_t|$) and the Hoek–Brown parameter m_i plotted in Fig. 10. While more work remains to be done on this topic, particularly more tests of the type carried out by Ramsey and Chester (2004) and Bobich (2005), the authors suggest that Fig. 10 provides a useful practical tool for estimating a tensile cutoff for the Hoek–Brown criterion.

Examination of Table 1 shows that, for low m_i values, the Hoek–Brown criterion over-estimates the tensile strength compared with the Fairhurst criterion. However, for $m_i > 25$ the Hoek–Brown criterion under-estimates the tensile strength by an amount that is generally small enough to be ignored for most engineering applications.

Hoek (1965) assembled a significant quantity of laboratory triaxial test data for a variety of rock types and concrete and these results (peak strength values) are plotted in a dimensionless form in Fig. 11. It can be seen that individual data sets plot on parabolic curves and that a family of such curves, covering all of the shear data collected, can be generated for different values of the Hoek–Brown constant m_i . The constant m_i is an indicator of the brittleness of the rock with weaker and more ductile rocks having low m_i values while stronger and more brittle rocks have high m_i values. A few data points for $\sigma_3 < 0$ are included in Fig. 11 and these are dealt with adequately by the tension cutoff discussed above.

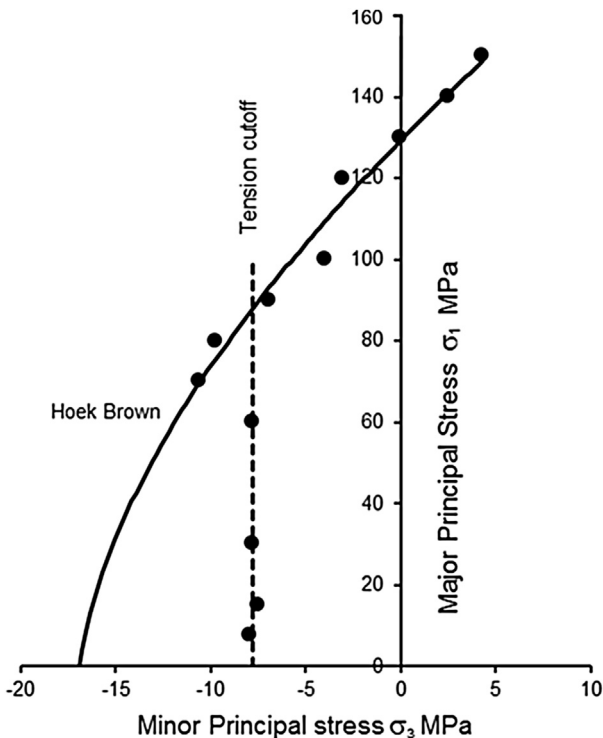


Fig. 8. Results from confined extension tests and triaxial compression tests by Ramsey and Chester (2004).

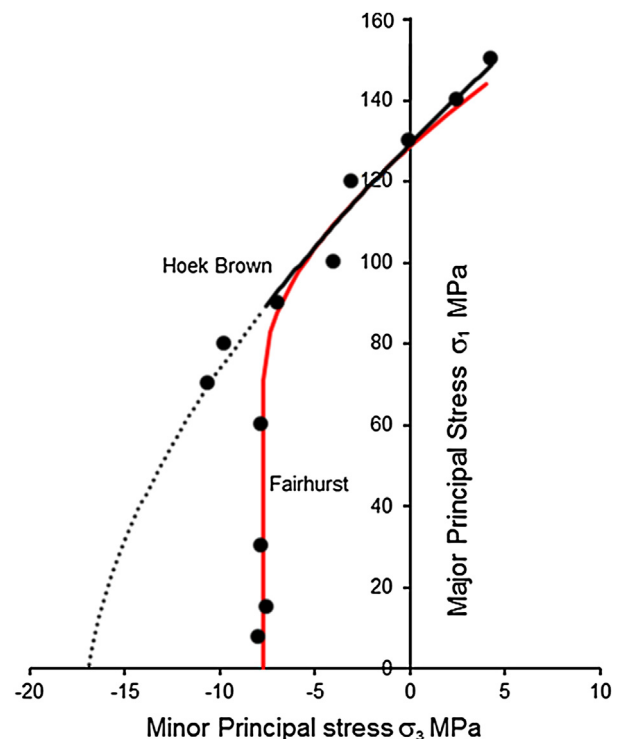


Fig. 9. Combined plot of Hoek–Brown and Fairhurst failure criteria with tension cutoff.

Table 1
Analysis of data containing reliable tensile values.

Fairhurst ($\sigma_t \leq 2$ MPa)			Hoek–Brown (shear data)			Data set and reference
σ_c (MPa)	σ_t (MPa)	$\sigma_c/ \sigma_t $	σ_c (MPa)	σ_t (MPa)	m_i	
128.5	-7.74	16.6	129	-15.6	8.25	Carrara marble (Ramsey and Chester, 2004)
516.5	-33.72	13.9	557	-65.9	8.45	Blair dolomite (Brace, 1964)
95.5	-6.41	14.9	102	-10.6	9.65	Berea sandstone (Bobich, 2005)
125.5	-8.72	14.4	131	-12.4	10.60	Webtuck dolomite (Brace, 1964)
614.0	-25.5	24.1	592	-28.7	20.65	Granite aplite (Hoek, 1965)
220	-7.06	31.1	227	-6.01	32.4	Lac du Bonnet granite (Lau and Gorski, 1992)

3.3. Interpretation of laboratory triaxial tests

In order to understand the application of the Hoek–Brown failure criterion to intact rock behavior, it is useful to consider a practical example which involves uniaxial and triaxial tests on specimens of Lac du Bonnet granite from the site of the Atomic Energy of Canada Limited Underground Research Laboratory at Pinawa in Manitoba, Canada (Read and Martin, 1991). The specimen preparation and testing were carried out by the CANMET Mining and Mineral Sciences Laboratories in Ottawa, Canada, which has a long-standing international reputation for high quality testing services.

Using strain and acoustic emission measurements, Lau and Gorski (1992) determined the crack initiation, onset of strain localization and peak strengths for each confining pressure in a series of triaxial tests carried out in a servo-controlled stiff testing machine, based on the procedure summarized in Fig. 12 (Martin and Chandler, 1994). The results of these tests are plotted in Fig. 13. The Hoek–Brown failure criterion (Eq. (6)) has been fitted to each data set and the fitted parameters are included in Table 2. Note that, because the m_i value for the peak strength is 32.4, no correction has been made for the measured tensile strength, as discussed above.

It is clear from Figs. 12 and 13 that fracturing in laboratory samples is a complex process and that simply measuring the peak stress does not capture this fracturing process. However, it is also clear from Fig. 13 that we can define the boundaries for this process, i.e. fracture initiation, onset of fracture localization and collapse

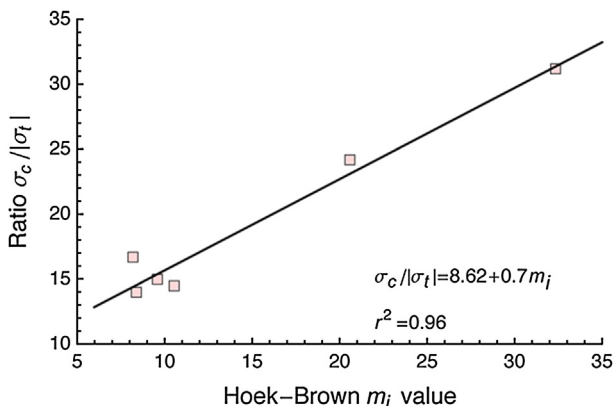


Fig. 10. Relationship between $\sigma_c/|\sigma_t|$ and m_i from Table 1.

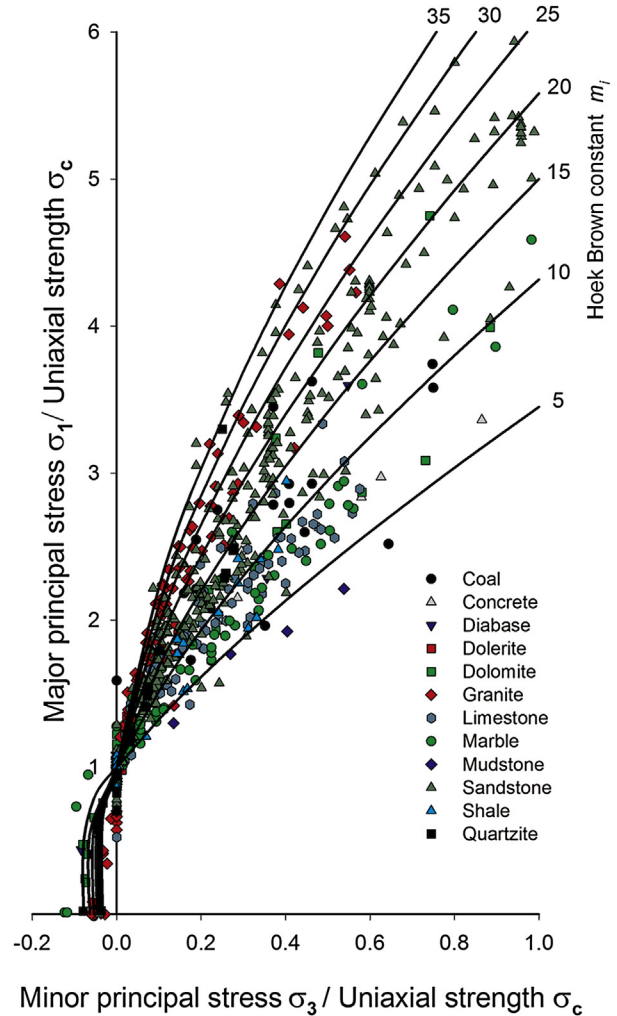


Fig. 11. Dimensionless plot of triaxial test results from laboratory tests on samples from a wide range of rock types and concrete.

peak stress. In the next section, a numerical approach that can simulate this process is examined.

3.4. Numerical approaches

Since the early 1980s, there has been an exponential growth in the sophistication and power of numerical programs which have been increasingly applied to the study of failure initiation and propagation processes in soil, rock and concrete. Fig. 14 illustrates two phenomenological approaches that are typically used to replicate the failure process numerically. The early approaches often used the sliding-crack model to capture many of the elements discussed in the earlier section on Griffith theory. More recently, there has been an increasing focus on the force-chain crack model using discrete element formulations (Fig. 14). A small selection of some of the more significant papers in this latter field includes: Cundall and Strack (1979), Diederichs (1999, 2003), Potyondy and Cundall (2004), Pierce et al. (2007), Lorig (2007), Cho et al. (2007), Cundall et al. (2008), Lan et al. (2010), Potyondy (2012) and Scholtès and Donzé (2013).

Potyondy and Cundall (2004) pointed out that systems composed of many simple objects commonly exhibit behavior that is much more complicated than that of the constituents. They listed the following characteristics that need to be considered in developing a rock mass model:

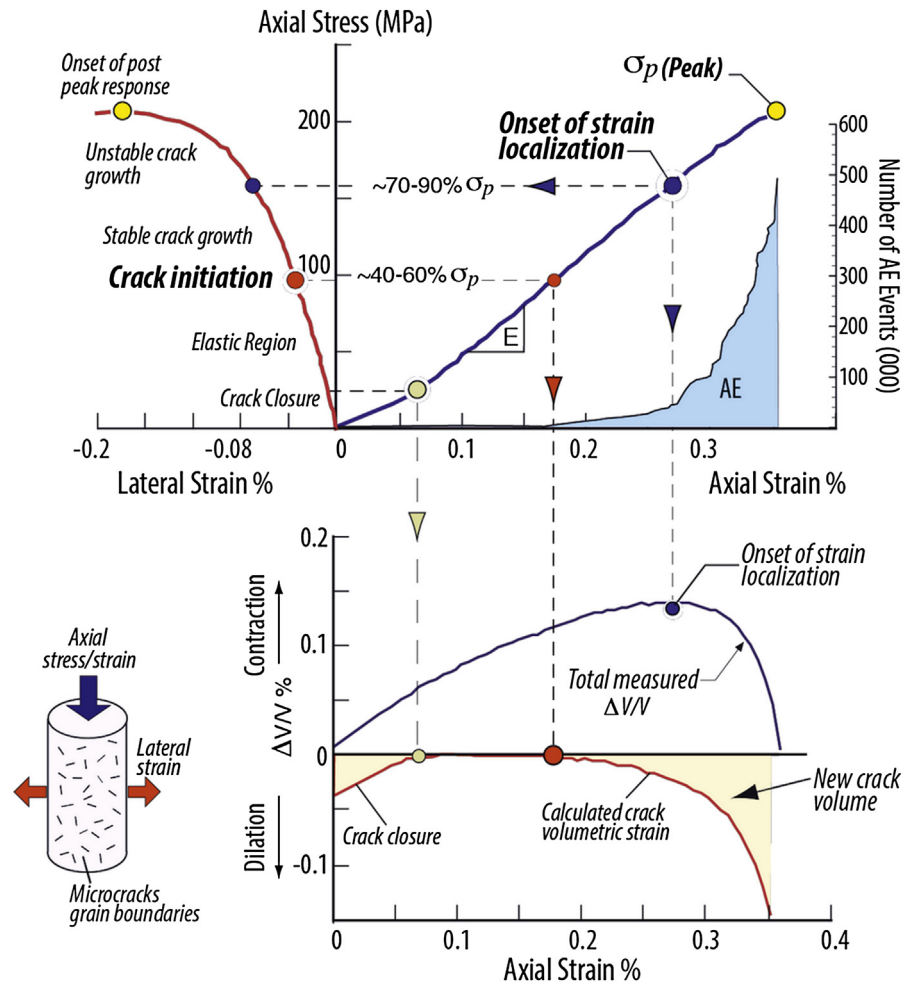


Fig. 12. Stages in the progressive failure of intact rock specimens subjected to compressive loading. Modified from Martin and Christiansson (2009).

- (1) Continuously nonlinear stress–strain response, with ultimate yield, followed by softening or hardening.
- (2) Behavior that changes in character, according to stress state; for example, crack patterns quite different in tensile, unconfined- and confined-compressive regimes.
- (3) Memory of previous stress or strain excursions, in both magnitude and direction.
- (4) Dilatancy that depends on history, mean stress and initial state.
- (5) Hysteresis at all levels of cyclic loading/unloading.
- (6) Transition from brittle to ductile shear response as the mean stress is increased.
- (7) Dependence of incremental stiffness on mean stress and history.
- (8) Induced anisotropy of stiffness and strength with stress and strain path.
- (9) Nonlinear envelope of strength.
- (10) Spontaneous appearance of microcracks and localized macro fractures.
- (11) Spontaneous emission of acoustic energy.

Within the limitations of this document, it is clearly not feasible to present a summary of the many approaches that have been adopted in the numerical modeling of intact rock fracture initiation

and propagation. Nor it is possible to judge the extent to which the requirements outlined above by Potyondy and Cundall (2004) have been met in these studies. A most useful DEM (discrete element method) approach is considered to be that given by Lan et al. (2010) who presented results of a study of fracture initiation and propagation in Äspö diorite and Lac du Bonnet granite. The mineral grain structures for these two crystalline rocks are shown in Fig. 15.

The program UDEC (Itasca, 2013) was used in this study and a Voronoi tessellation scheme was employed to create polygonal structures which closely simulated the mineral grain structures shown in Fig. 15. Each grain has a unique identity, location and material type and the average grain size distribution has also been simulated in these models. The properties of the principal grain minerals (plagioclase, K-feldspar and quartz with biotite in the Lac du Bonnet granite and with chlorite in the Äspö diorite) were exported to an ASCII file which was then imported into the UDEC model using the FISH internal macro-language. The model geometry is then created automatically in UDEC and the grains are made deformable by discretizing, each polygon using triangular zones. These deformable grains, which were unbreakable in the Lan et al. (2010) study, are then cemented together along their adjoining sides as shown in Fig. 16.

Fig. 17 shows the results of two uniaxial compression tests carried out by Lan et al. (2010) on UDEC models of Äspö diorite and

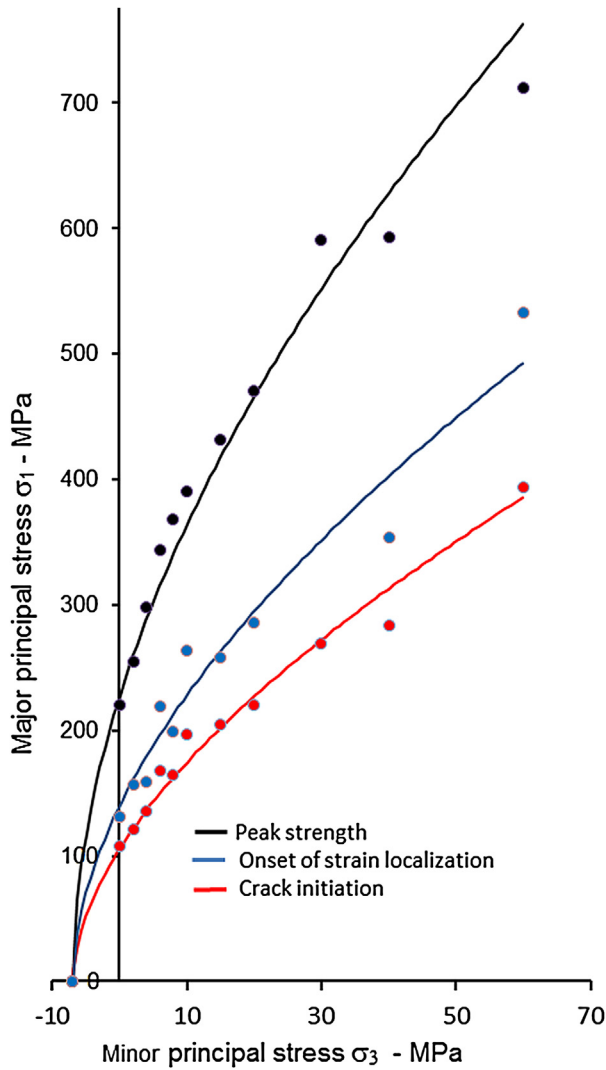


Fig. 13. Tensile crack initiation, strain localization and peak strength for Lac du Bonnet granite from tests by Lau and Gorski (1992).

Lac du Bonnet granite. The stress–strain response, the crack initiation stress (σ_{ci}), the crack damage stress σ_{cd} and the peak stress σ_f show excellent agreement with those defined from laboratory tests on Åspö diorite by Staub and Andersson (2004) and on Lac du Bonnet granite by Martin and Chandler (1994).

Table 2
Results of triaxial tests on Lac du Bonnet granite.

Confining stress (MPa)	Crack initiation (MPa)	Strain localization (MPa)	Peak strength (MPa)	Average tensile strength (direct tension) (MPa)
0	131	108	220	–7
2	157	121	255	
4	159	136	298	
6	219	168	344	
8	199	165	368	
10	264	197	391	
15	258	205	432	
20	286	220	471	
30	–	269	591	
40	354	284	593	
60	533	394	712	
Hoek–Brown parameters used	$\sigma_c = 106$ MPa, $m_i = 15$	$\sigma_c = 140$ MPa, $m_i = 20$	$\sigma_c = 227$ MPa, $m_i = 32.4$	

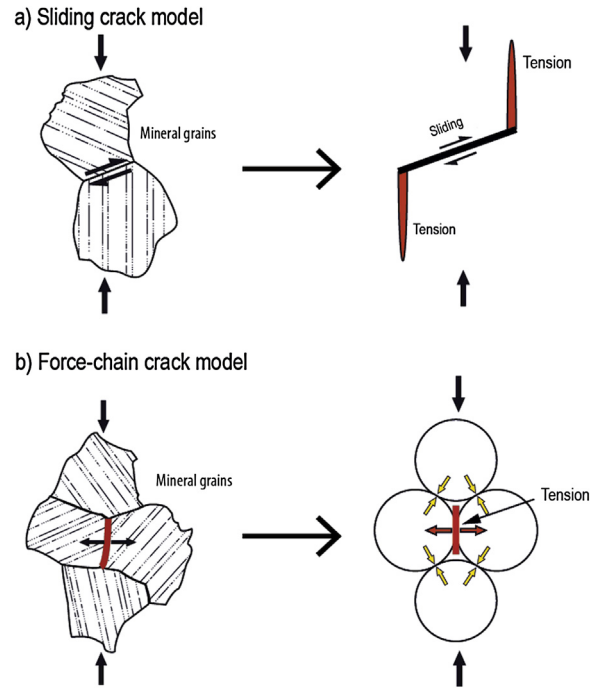


Fig. 14. Two models commonly used to simulate cracking observed in heterogeneous assemblages of polygonal shaped minerals. Modified from Nicksiar and Martin (2013).

The paper by Lan et al. (2010) is a good example of the application of numerical modeling to the study of fracture initiation and propagation in intact rock and is recommended reading for anyone interested in this field. Much more work is required to bring this approach to maturity.

Professor E.T. Brown, in a foreword to the scoping study for the application of numerical methods to mass mining wrote: “In my opinion, the development of the bonded particle model based on the PFC and PFC3D distinct element codes by Dr. Peter Cundall and his co-workers at Itasca represents one of the most significant contributions made to modern rock mechanics research. It is now well established that this model has the ability to reproduce the essential, and some more subtle, features of the initiation and propagation of fracturing in rocks and rock masses.” Numerical modeling has now progressed beyond the original bonded particle models developed by Itasca but Brown’s comments remain valid as we look ahead to the research that remains to be done on these

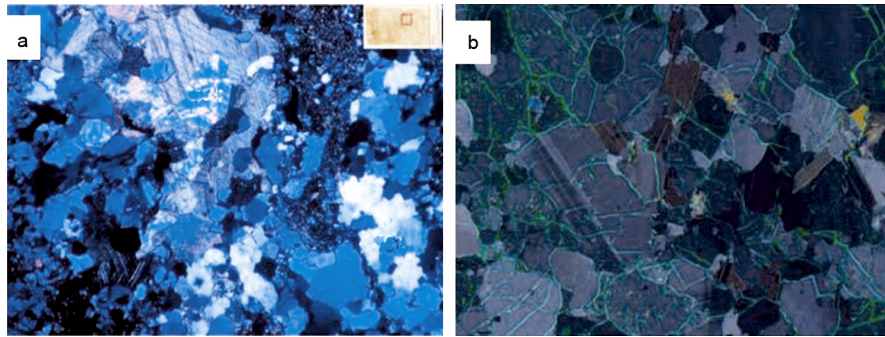


Fig. 15. Example of mineral grain structure observed in polarized light thin section. (a) Åspö diorite. Width of the image is 4 mm (modified from [Lampinen \(2006\)](#)). (b) Lac du Bonnet granite. Combined polarized and fluorescent microscope image of specimen from Underground Research Laboratory in Canada. Width of image is 4 mm (modified from [Åkesson \(2008\)](#)).

Images reproduced from [Lan et al. \(2010\)](#).

complex fundamental processes of failure initiation and propagation.

A word of warning. In the rush to get into print, many authors have published papers on numerical modeling in which pictures of fracture propagation in Brazilian disk tests or uniaxial compression tests have been included as a demonstration of the validity of the numerical approach used. It is relatively easy to produce results which appear to be credible for these tests but, unfortunately, in many cases the numerical methods used are immature and fail when applied to more complex problems.

In the following section, we briefly consider two approaches that may be used to evaluate fracture initiation and propagation in situ. The process is commonly referred to as spalling.

4. Fracture initiation and propagation in situ: spalling

There are two practical issues associated with spalling: (1) identifying the conditions that will initiate spalling, and (2) defining the extent and depth of spalling. The results from two well-documented in situ experiments in crystalline rock are used to examine these practical issues.

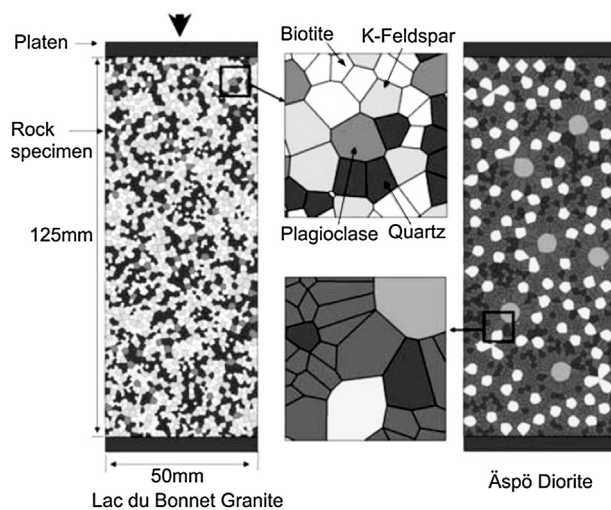


Fig. 16. Layout for an unconfined compression test for a Lac du Bonnet granite sample and an Åspö diorite sample using the UDEC model. The different gray scales indicate the degree of mineral grain strength. Higher strength grains have a darker color. Reproduced from [Lan et al. \(2010\)](#).

4.1. Test tunnel of the URL Mine-by experiment

[Martin et al. \(1997\)](#) have described spalling observed in a test tunnel ([Fig. 18](#)) in massive Lac du Bonnet granite at a depth of 420 m below surface in the Underground Research Laboratory. The intent of the experiment was to study the damage resulting from stress redistribution associated with the full-face mining of 3.5 m diameter tunnel. The mining was carried out using line drilling and rock splitters to avoid the potential for blasting-induced damage. This technique allowed full-face 1-m advance increments.

An extensive program of in situ stress measurements was carried out at this site and the rock mass surrounding the test tunnel. The in situ rock mass stresses at this location were a sub-vertical stress $\sigma_v = 11$ MPa and a sub-horizontal stress of $k\sigma_v = 60$ MPa, inclined at 11° to the horizontal, with an intermediate sub-horizontal stress of 44 MPa.

The spalling which occurred after excavation of the test tunnel is illustrated in [Fig. 19](#). This spalling occurred as a relatively gentle fracture process during the excavation advance. The full extent of

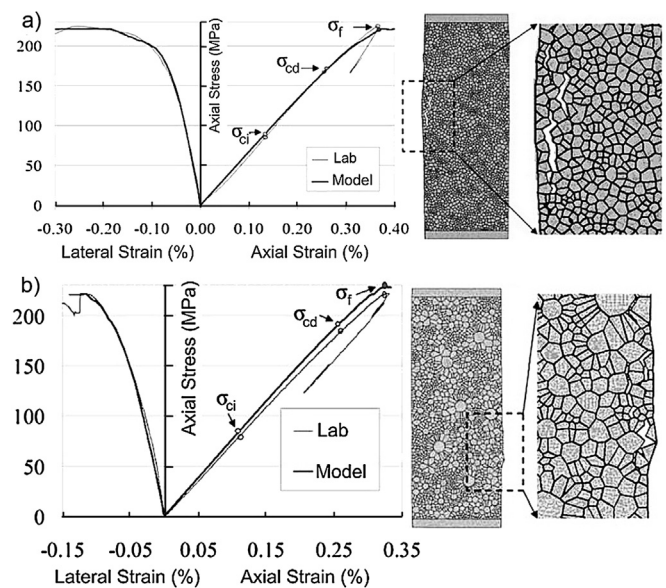


Fig. 17. Calibrated stress–strain response with laboratory data for (a) Åspö diorite and (b) Lac du Bonnet granite. The drawings at the right show the damage pattern of the specimen.

Images reproduced from [Lan et al. \(2010\)](#).

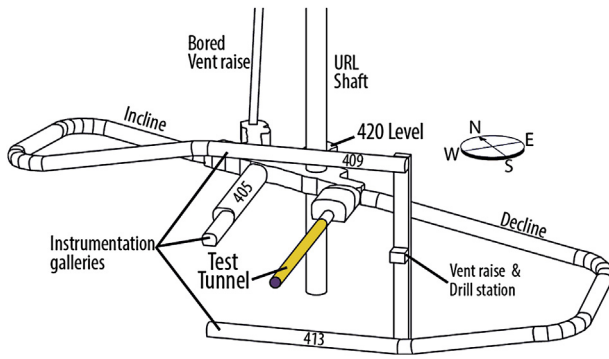


Fig. 18. Layout of the Mine-by experiment at the 420 m level of the Underground Research Laboratory. Modified from Martin and Read (1996).

the spalling was only evident once the tunnel had been cleaned and loose spall remnants removed by scaling. When these remnants were removed in the floor, it was sufficient to trigger minor amounts of new spalling, suggesting the important role of small confining stress in controlling the spalling process.

Fig. 20 shows the zone of potential spalling for the Lac du Bonnet granite in which the test tunnel was mined as well as the stress changes associated with the tunnel excavation. The measured in situ stresses, denoted by point A in Fig. 20, are equal to the principal stresses $\sigma_1 = 60$ MPa and $\sigma_3 = 11$ MPa in the rock before the tunnel was mined. The 11° inclination of the stress field can be ignored in the discussion which follows. After excavation, the minor principal stress in the tunnel wall is reduced to $\sigma_3 = 0$. The maximum principal stress on the tunnel roof and floor is given by

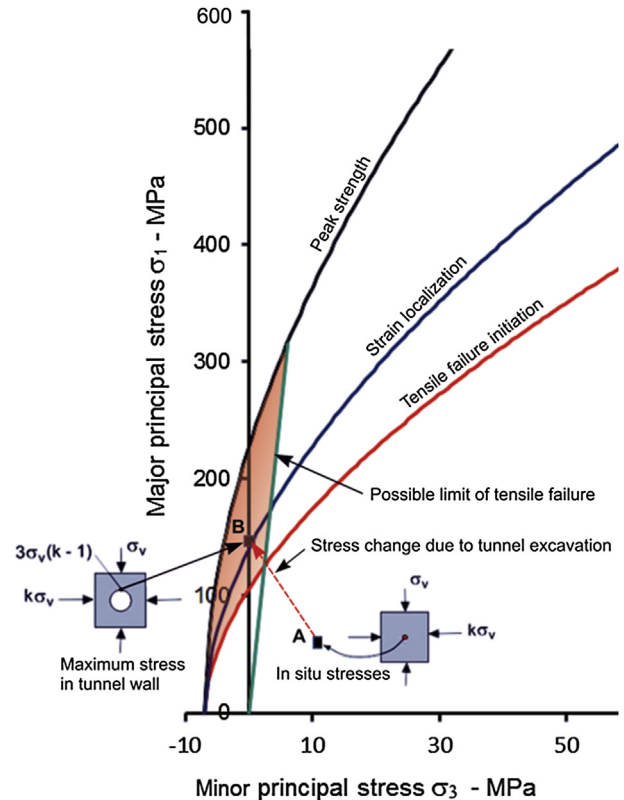


Fig. 20. Definition of the zone of potential spalling in massive Lac du Bonnet granite, from Fig. 13. The changes in the stresses in the rock surrounding the tunnel are also shown as points A and B in this plot.

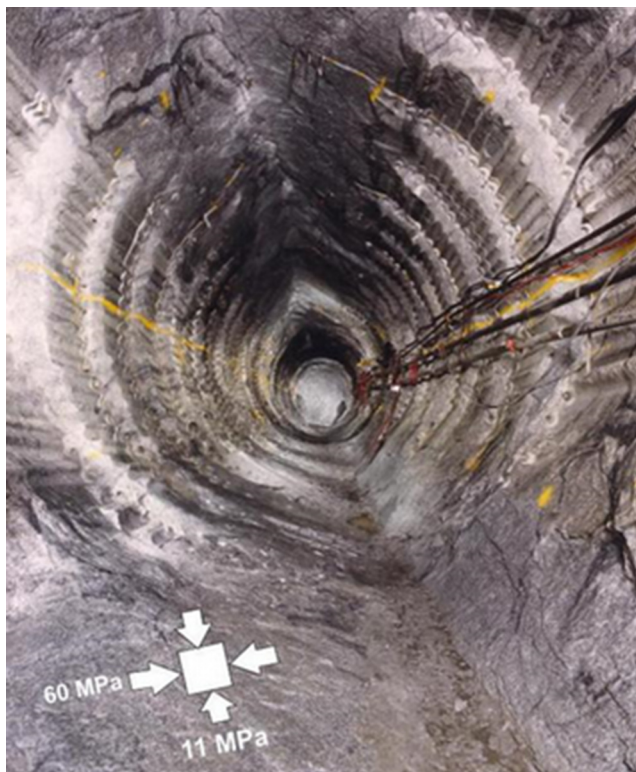


Fig. 19. Spalling in the roof and floor of a circular test tunnel in the Underground Research Laboratory at Pinawa in Manitoba, Canada. Photo courtesy of AECL.

$\sigma_{\max} = 3\sigma_v(k - 1) = 169$ MPa. These stresses are plotted as point B in Fig. 20.

These roof and floor stresses fall just above the curve defining strain localization and well above the tensile failure initiation curve. Martin and Christiansson (2009) concluded that in the absence of in situ results, the laboratory crack initiation stress (see Fig. 13) could be taken as a lower bound for the spalling strength. More recently, Nicksiar and Martin (2013) compiled the crack initiation stress for a range of rock types. The results are illustrated in Fig. 21 and demonstrate the consistency of tensile crack initiation observed in laboratory tests. Using a spalling initiation criterion based on this approach is a useful first step and supported by recent experience. Diederichs et al. (2010) implemented this approach in a continuum model with good success.

Knowing that spalling may occur, the next step is to establish the severity of the failure. The depth of the notch created by spalling is dependent upon the ratio of the maximum boundary stress to the uniaxial compressive strength (peak) or σ_{\max}/σ_c as shown in Fig. 22 (Martin et al., 1999). In the case of the test tunnel under discussion here, this ratio is $169/227 = 0.74$ and hence the notch depth is approximately 0.3–0.4 times the tunnel radius according to Fig. 22.

Experience with the application of the trend line in Fig. 22 indicates that the uniaxial compressive strength should be the mean uniaxial compressive strength value (Rojat et al., 2009). Determining the mean uniaxial compressive strength may appear straightforward. The scatter in the values for 13 samples of Lac du Bonnet granite is shown in Fig. 23. Notice that the mean value of 211 MPa is less than the σ_c value of 227 MPa given in Table 2 using the Hoek–Brown equations. This is a typical finding and in this case reflects the effect of the microcracks common in Lac du Bonnet

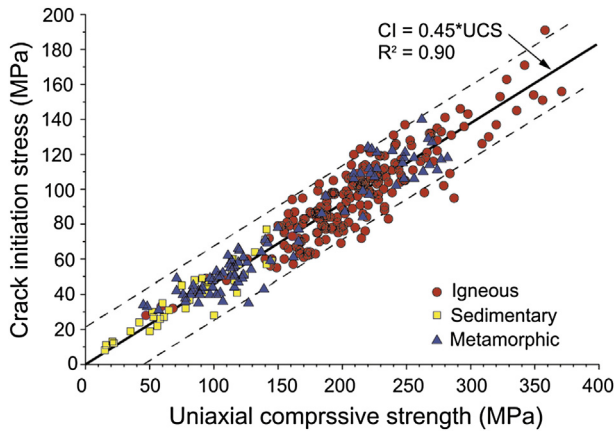


Fig. 21. Tensile crack initiation in various rocks. Modified from Nicksiar and Martin (2013).

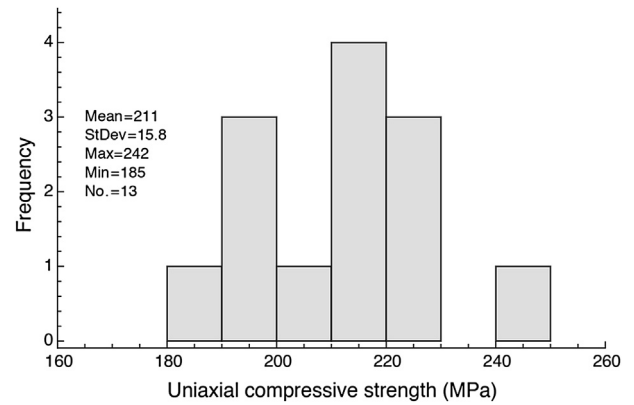


Fig. 23. Example of the distribution of uniaxial compressive strength for 13 samples of Lac du Bonnet granite.

granite. Despite the suggestions in the ISRM Suggested Methods, conducting uniaxial tests requires significant care in order to reduce the effect of uneven and/or misaligned sample ends. Simply conducting a large number of tests is no substitute for properly preparing the samples, and in many cases can be misleading as the mean value often decreases as the number of samples increases, due to poor quality control with sample preparation.

Figs. 24 and 25 show examples of mild spalling and severe rockbursting in underground excavations, representing the extremes of the process under discussion here. Practical experience suggests that shallow spalls are generally associated with pure tensile failure which causes thin slivers or plates of rock to peel the tunnel surface. These occur with little “popping” and, once the maximum depth of the spall has been achieved, they remain stable provided that there are no changes in the surrounding stress field due, for example, to excavation of adjacent openings.

Deeper spalls, such as that in the Mine-by tunnel described above, are somewhat more complicated in that shear failure probably becomes involved as the notch tip moves away from the excavation boundary. Numerical analyses of this failure process have proved to be extremely challenging and it has to be said that much work remains to be done before the complex interaction of



Fig. 24. Mild spalling in the sidewalls of a vertical raise bored shaft in an underground mine.

tensile and shear processes associated with deep spall notches can be predicted with any degree of confidence.

Rockbursts, such as that illustrated in Fig. 25, are probably associated with conditions in which the maximum induced boundary stress approaches the uniaxial compressive strength of the surrounding massive rock. These events involve implosion of the rock into the tunnel with the release of significant amounts of

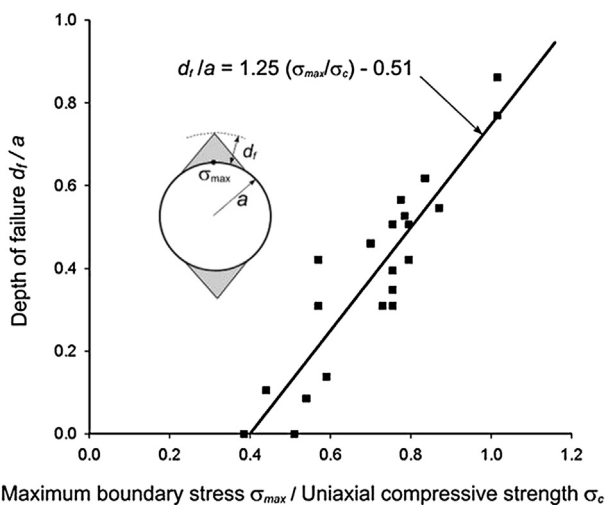


Fig. 22. Observed spalling notch depths plotted against the ratio of maximum boundary stress to uniaxial compressive strength (Martin et al., 1999).

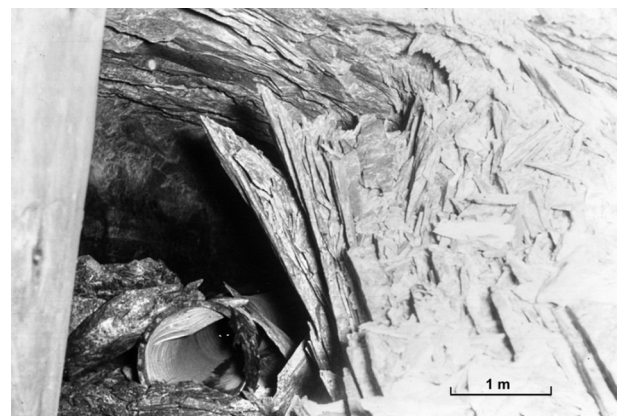


Fig. 25. Severe rockbursting in an access tunnel in a deep level gold mine in South Africa.

energy. The authors are not aware of any currently available numerical tools that offer any credible means of explaining or predicting the rockburst process.

4.2. Numerical simulation of spalling

The approach described above to estimate the onset and depth of spalling is a reasonable first step. But to make progress in the support interaction needed for tunnel design, proper numerical approaches are needed. While this is still an on-going research topic, one approach that goes from the laboratory calibration to spall prediction is described briefly below.

The nuclear industry in Finland and Sweden is preparing for the construction of a geological repository for used nuclear fuel at a depth of about 450 m. Their concept requires excavation of 1.75-m-diameter 8-m-deep boreholes and spalling is a design issue that must be addressed. Andersson et al. (2009) described and reported the results of a full-scale experiment (APSE) that examined the development of spalling around two of the large diameter boreholes. The APSE experiment was carried out at the 450-m level of the Äspö Hard Rock Laboratory in southern Sweden. Lan et al. (2013) described how the UDEC modeling work originally described by Lan et al. (2010) was used to model the spalling process. Fig. 26 shows the model configuration and the grain-scale geometry. The approach and the properties of the grains and the contacts were exactly the same as that given in Lan et al. (2010).

The APSE experiment was unique because the magnitude of the stresses on the boundary of the large boreholes was controlled by excavation-induced and thermally induced stresses. The experiment demonstrated that in situ experiments could follow the same

loading conditions and control that are normally associated with laboratory tests.

The configuration of the experiment allowed the boundary stresses to be applied gradually. This facilitated observing the spalling process at different stages. Fig. 27 provides comparison of the results from the UDEC model with the visual observations at two loading stages. An important conclusion from the APSE work is that the findings related to fracture initiation and propagation that were observed in the Mine-by test tunnel in massive un-fractured granite were applicable to the fractured water-bearing rock mass of the APSE experiment.

The approach described by Lan et al. (2010, 2013) demonstrated that the properties of the laboratory tests can be used to evaluate the in situ spalling process when coupled with numerical approaches that capture all stages of brittle failure, i.e. from fracture initiation through to fracture propagation. While this approach holds much promise, it is still limited to two dimensions, and much work needs to be done before this approach becomes state of practice.

5. Conclusions

Our understanding of initiation and propagation of fracturing in intact rock has resulted from detailed analysis of the stress–strain data from laboratory-scale samples with dimensions in the range of 50 mm diameter. At low confining pressures, tensile fracturing initiates in these samples at 40%–60% of the uniaxial compressive strength and as loading continues, these tensile fractures increase in density and ultimately coalesce, leading to strain localization and macro-scale shear failure of the sample. The Griffith theory of brittle failure provides a simplified model assuming that all

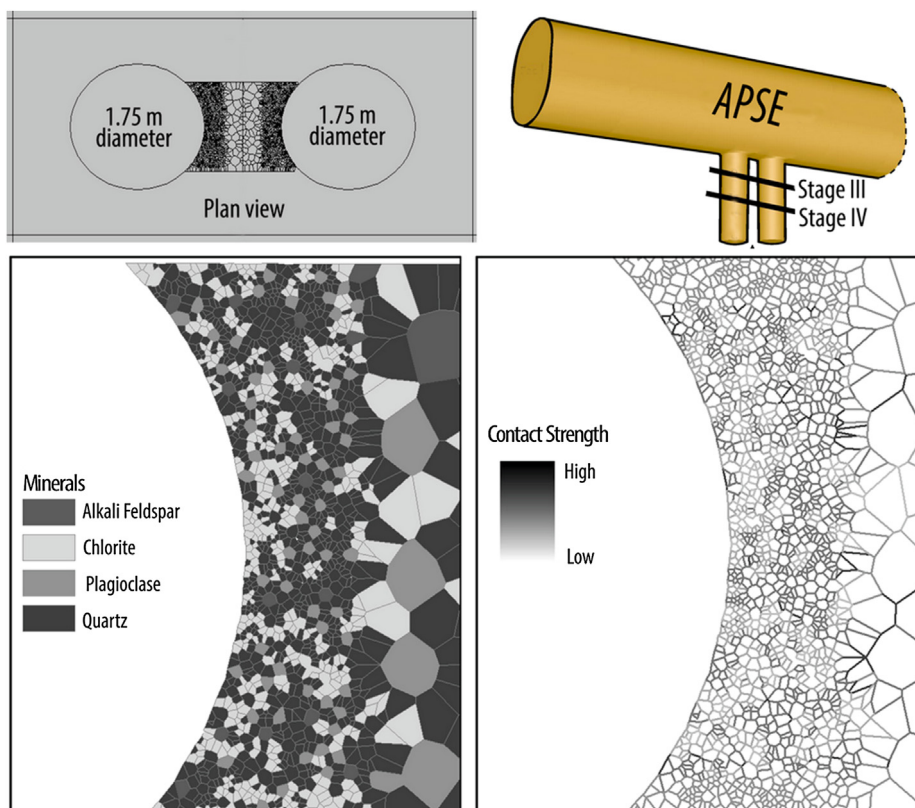


Fig. 26. Grain-based UDEC model developed by Lan et al. (2010) and used to simulate the spalling process observed by Andersson et al. (2009). Modified from Lan et al. (2013).

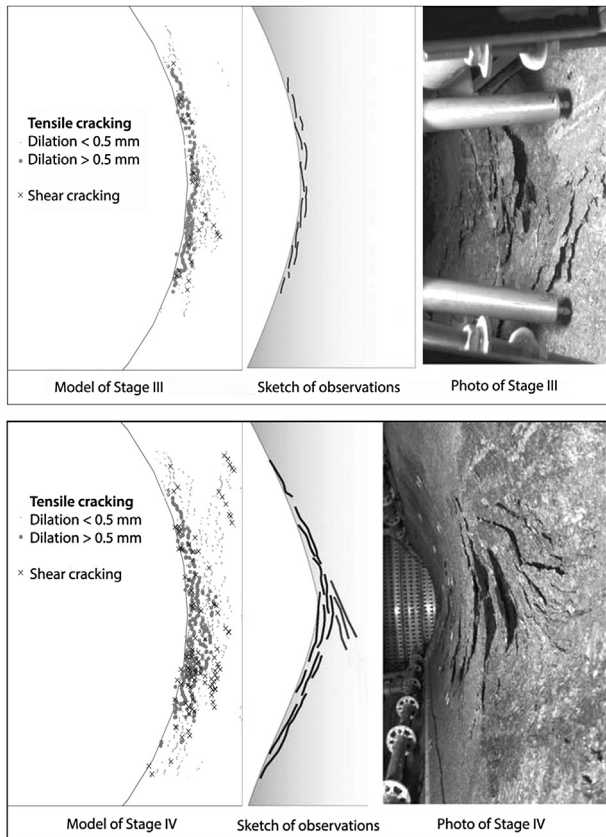


Fig. 27. Modeled damage at stages III and IV compared with observation. Modeling result shows the distribution of tensile cracking and shear cracking at different damage stages.

The photograph and illustration are modified from Lan et al. (2013).

fractures initiate from the tips of inclined flaws, namely grain boundaries in the sliding-crack model. The Hoek–Brown failure envelope is used to capture the collapse load associated with this localized macro-scale shear fracture. However, it has been necessary to add a tension cutoff, based on a generalized fracture theory proposed by Fairhurst (1964) in order to accommodate the tensile failure observed in detailed laboratory tests.

Fracture initiation while tensile in nature is more difficult to be modeled. With the improvements in computing power, the discrete element codes have shown that the force-chain crack model is a viable alternative to explain the tensile fracture initiation coalition of tensile cracks and the final shearing of the specimens at higher confining stresses. Grain-based numerical models, based on the discrete element formulation, in which the grain size distributions as well as the physical properties of the component grains of the rock are incorporated, have proved to be very useful in studying these complex processes. They have also demonstrated that the approach based on laboratory processes is useful for capturing spalling, the in situ process of fracture initiation and coalescence. While this approach holds much promise, the current grain-based models are still limited to two dimensions, and much research needs to be carried out before this approach becomes state of practice.

Conflict of interest

The authors wish to confirm that there are no known conflicts of interest associated with this publication and there has been no

significant financial support for this work that could have influenced its outcome.

Acknowledgments

The contribution of Dr. Connor Langford in deriving the solution to the generalized fracture criterion proposed by Fairhurst (1964) is gratefully acknowledged. This derivation is presented in the Appendix.

Professor Ted Brown reviewed the final manuscript and offered a number of valuable comments, which are also acknowledged.

Appendix

According to the generalized Fairhurst criterion:

- (1) If $w(w - 2)\sigma_3 + \sigma_1 \leq 0$, failure occurs when $\sigma_3 = \sigma_1$;
- (2) If $w(w - 2)\sigma_3 + \sigma_1 \leq 0$, failure occurs when

$$\frac{(\sigma_1 - \sigma_3)^2}{(\sigma_1 + \sigma_3)} = -2\sigma_t(w - 1)^2 \left\{ 1 + \frac{2\sigma_t}{\sigma_1 + \sigma_3} \left[\left(\frac{w - 1}{2} \right)^2 - 1 \right] \right\} \quad (\text{A1})$$

where

$$w = \sqrt{\frac{\sigma_c}{|\sigma_t|} + 1} \quad (\text{A2})$$

Let $A = 2(w - 1)^2$ and $B = [(w - 1)/2]^2 - 1$, and rearrange Fairhurst's equation:

$$\sigma_1^2 + \sigma_1(A\sigma_t - 2\sigma_3) + (\sigma_3^2 + A\sigma_t\sigma_3 + 2AB\sigma_t^2) = 0 \quad (\text{A3})$$

σ_1 can be written by

$$\sigma_1 = \frac{(2\sigma_3 - A\sigma_t) + \sqrt{(A\sigma_t - 2\sigma_3)^2 - 4(\sigma_3^2 + A\sigma_t\sigma_3 + 2AB\sigma_t^2)}}{2} \quad (\text{A4})$$

References

- Åkesson U. Characterization of micro cracks using core diskings. SKB Report P-08-103. Stockholm: Swedish Nuclear Fuel and Waste Manage Co.; 2008. p. 43.
- Andersson J, Martin CD, Stille H. The Åspö pillar stability experiment: Part II-rock mass response to coupled excavation-induced and thermal-induced stresses. *International Journal of Rock Mechanics & Mining Sciences* 2009;46(5):879–95.
- Andrieu GE. Brittle failure of rock materials. Rotterdam: A. A. Balkema; 1995.
- Ashby MF, Hallam D. The failure of brittle solids containing small cracks under compressive stress. *Acta Metallurgica* 1986;34(3):497–510.
- Bobich JK. Experimental analysis of the extension to shear fracture transition in Berea sandstone [MS Thesis]. Texas, USA: Texas A&M University; 2005.
- Brace WF. Brittle fracture of rocks. In: Judd WR, editor. *State of stress in the earth's crust*. New York: American Elsevier; 1964. pp. 111–80.
- Cai M, Kaiser PK, Martin CD. A tensile model for the interpretation of microseismic events near underground openings. *Pure and Applied Geophysics* 1998;153: 67–92.
- Cho N, Martin CD, Sego DS. A clumped particle model for rock. *International Journal of Rock Mechanics and Mining Sciences* 2007;44(7):997–1010.
- Cundall PA, Strack O. A discrete numerical model for granular assemblies. *Geotechnique* 1979;29(1):47–65.
- Cundall PA, Pierce ME, Mas Ivars D. Quantifying the size effect of rock mass strength. In: Potvin Y, Carter J, Dyskin A, Jeffrey R, editors. *Proceedings of the 1st southern hemisphere international rock mechanics symposium*. Nedlands, Western Australia: Australian Centre for Geomechanics; 2008. pp. 3–15.
- Diederichs MS, Carter T, Martin CD. Practical rock spall prediction in tunnels. In: *Proceedings of ITA World Tunnel Congress*; 2010. pp. 1–8. Vancouver, (CD-ROM).

- Diederichs MS. Instability of hard rockmasses: the role of tensile damage and relaxation [PhD Thesis]. Waterloo, Canada: University of Waterloo; 1999.
- Diederichs MS. Rock fracture and collapse under low confinement conditions. *Rock Mechanics and Rock Engineering* 2003;36(5):339–81.
- Fairhurst C. On the validity of the “Brazilian” test for brittle materials. *International Journal of Rock Mechanics and Mining Sciences & Geomechanics Abstracts* 1964;1(4):535–46.
- Fairhurst C. Fundamental considerations relating to the strength of rock. In: *Colloquium on rock fracture*. Bochum, Germany: Ruhr Universitat; 1972. www.itascacg.com. Updated in 2004 and available from:.
- Germanovich JN, Dyskin AV. A model of brittle failure for material with cracks in uniaxial loading. *Mechanics of Solids* 1988;23(2):111–23.
- Griffith AA. The phenomena of rupture and flow in solids. *The Philosophical Transactions of the Royal Society London (Series A)* 1921;221:163–98.
- Griffith AA. Theory of rupture. In: *Proceedings of the 1st international Congress of applied mechanics*. Delft: Tech. Boekhandel en Drukkerij J Walter Jr; 1924. pp. 55–63.
- Hoek E. Rock fracture under static stress conditions. Pretoria, South Africa: Council for Scientific and Industrial Research Report MEG 383; 1965.
- Hoek E, Bieniawski ZT. Brittle fracture propagation in rock under compression. *International Journal of Rock Mechanics* 1965;1(3):137–55.
- Hoek E, Brown ET. Empirical strength criterion for rock masses. *Journal of the Geotechnical Engineering Division, ASCE* 1980;106(9):1013–35.
- Hoek E. The strength of jointed rock masses. *Geotechnique* 1983;33(3):187–223.
- Itasca. UDEC 5.00 software reference manual. Minneapolis: Itasca; 2013.
- Kemeny JM, Cook NGW. Crack models for the failure of rock under compression. In: Desai CS, Krempf E, Kiousis PD, Kundu T, editors. *Proceedings of the 2nd international conference constitutive laws for engineering materials, theory and applications*, vol. 1. London: Elsevier Science Publishing Co; 1987. pp. 879–87.
- Lampinen H. Äspö Pillar Stability Experiment. Detailed geological mapping of pillar blocks. SKB Report IPR-05-24. Stockholm, Sweden: Swedish Nuclear Fuel and Waste Manage. Co.; 2006. p. 67.
- Lan H, Martin CD, Andersson JC. Evolution of in situ rock mass damage induced by mechanical-thermal loading. *Rock Mechanics and Rock Engineering* 2013;46(1):153–68.
- Lan H, Martin CD, Hu B. Effect of heterogeneity of brittle rock on micromechanical extensile behavior during compression loading. *Journal of Geophysical Research* 2010;115:B01202. <http://dx.doi.org/10.1029/2009JB006496>.
- Lau JSO, Gorski B. Uniaxial and triaxial compression tests on URL rock samples from boreholes 207-045-GC3 and 209-069-PH3. CANMET Divisional Report MRL 92 – 025 (TR); 1992. p. 46.
- Lorig IJ. Using numbers from geology. In: *Proceedings of the 11th Congress of the international society for rock mechanics*. London: Taylor and Francis; 2007. pp. 1369–77.
- Martin CD, Chandler NA. The progressive fracture of Lac du Bonnet granite. *International Journal of Rock Mechanics and Mining Sciences & Geomechanics Abstracts* 1994;31(6):643–59.
- Martin CD, Read RS. AECL’s Mine-by experiment: a test tunnel in brittle rock. In: Aubertin M, Hassani F, Mitri H, editors. *Proceedings of the 2nd North American rock mechanics symposium*, vol. 1. Rotterdam: A.A. Balkema; 1996. pp. 13–24.
- Martin CD, Read RS, Martino JB. Observations of brittle failure around a circular test tunnel. *International Journal of Rock Mechanics and Mining Sciences* 1997;34(7):1065–73.
- Martin CD. The effect of cohesion loss and stress path on brittle rock strength. *Canadian Geotechnical Journal* 1997;34(5):698–725.
- Martin CD, Kaiser PK, McCreath DR. Hoek-Brown parameters for predicting the depth of brittle failure around tunnels. *Canadian Geotechnical Journal* 1999;36(1):136–51.
- Martin CD, Christiansson R. Estimating the potential for spalling around a deep nuclear waste repository in crystalline rock. *International Journal of Rock Mechanics and Mining Sciences* 2009;46(2):219–28.
- McClintock FA, Walsh JB. Friction on Griffith cracks in rock under pressure. In: *Proceedings of the 4th US national Congress on applied mechanics*, vol. 2. New York: Am. Soc. Mech. Eng.; 1962. pp. 1015–21.
- Murrell SAF. The strength of coal under tri-axial compression. In: Walton WH, editor. *Mechanical properties of non-metallic brittle materials*. London: Butterworth Scientific Publications; 1958. pp. 123–45.
- Nicksiar M, Martin CD. Crack initiation stress in low porosity crystalline and sedimentary rocks. *Engineering Geology* 2013;154:64–76.
- Paterson MS, Wong TF. *Experimental rock deformation – the brittle field*. 2nd ed. New York: Springer-Verlag; 2005.
- Pierce M, Mas Ivars D, Cundall P, Potyondy D. A synthetic rock mass model for jointed rock. In: Eberhardt E, Stead D, Morrison T, editors. *Proceedings of Canada-U.S. rock mechanics symposium*, vol. 1. London: Taylor & Francis Group; 2007. pp. 341–9.
- Potyondy DO, Cundall PA. A bonded particle model for rock. *International Journal of Rock Mechanics and Mining Sciences* 2004;41(8):1329–64.
- Potyondy DO. The bonded-particle model as a tool for rock mechanics research and application: current trends and future directions. In: *Proceedings of the 7th Asian rock mechanics symposium, ARMS7*. Seoul: ARMS; 2012. pp. 1–33.
- Ramsey J, Chester F. Hybrid fracture and the transition from extension fracture to shear fracture. *Nature* 2004;428:63–6.
- Read RS, Martin CD. The underground research laboratory Mine-by experiment – a research perspective on tunnel design. *Canadian Tunnelling* 1991:75–88.
- Rojat F, Labiouse V, Kaiser PK, Descoedres F. Brittle rock failure in the Steg Lateral Adit of the Lötschberg base tunnel. *Rock Mechanics and Rock Engineering* 2009;42(2):341–59.
- Scholtès L, Donzé FV. A DEM model for soft and hard rocks role of grain interlocking on strength. *Journal of the Mechanics and Physics of Solids* 2013;61(2):352–69.
- Staub I, Andersson JC. Äspö pillar stability experiment geology and mechanical properties of the rock in TASQ. SKB Report R-04-0. Stockholm: SvenskaKärnbränslehantering AB; 2004.
- Zuo JP, Li HT, Xie HP, Ju Y, Peng SP. A nonlinear strength criterion for rock-like materials based on fracture mechanics. *International Journal of Rock Mechanics and Mining Sciences* 2008;45(4):594–9.



Evert Hoek graduated with a BSc and MSc in mechanical engineering from the University of Cape Town (1955 and 1958) and became involved in the young science of rock mechanics in 1958 when he started working in research on the problems of brittle fracture associated with rockbursts in very deep mines in South Africa. His degrees include a PhD from the University of Cape Town, a DSc (Eng.) from the University of London and honorary doctorates from the Universities of Waterloo and Toronto in Canada. He has been elected as a Fellow of the Royal Academy of Engineering (UK), a Foreign Associate of the US National Academy of Engineering and a Fellow of the Canadian Academy of Engineering. He was Reader and then Professor of Rock Mechanics at the Imperial College of Science and Technology in London (1966–1975), a Principal of Golder Associates in Vancouver (1975–1987), Industrial Research Professor of Rock Engineering at the University of Toronto in Canada (1987–1993) and an independent consulting engineer based in Vancouver, Canada (1993–2013). He retired in 2013. His consulting work included major civil and mining projects in 35 countries around the world and has involved rock slopes, dam foundations, hydroelectric projects, underground caverns and tunnels excavated conventionally and by TBM.